2014-01-01

Mechanisms To Mitigate Neurodegeneration By Maintaining Mitochondrial Health

Parijat Kabiraj
University of Texas at El Paso, pkabiraj@miners.utep.edu

MECHANISMS TO MITIGATE NEURODEGENERATION BY MAINTAINING MITOCHONDRIAL HEALTH

PARIJAT KABIRAJ

Department of Chemistry

APPROVED:

_____

Mahesh Narayan, Ph.D.

_____

Jorge Gardea-Torresdey, Ph.D.

_____

Ricardo A. Bernal, Ph.D.

_____

Manuel Miranda-Arango, Ph.D.

_____

Charles H. Ambler, Ph.D.

Dean of the Graduate School

MECHANISMS TO MITIGATE NEURODEGENERATION BY MAINTAINING MITOCHONDRIAL HEALTH

By

PARIJAT KABIRAJ, B.V.Sc., M.V.Sc.

DISSERTATION

Presented to the Faculty of the Graduate School of

The University of Texas at El Paso

in Partial Fulfillment

of the Requirements

for the Degree of

DOCTOR OF PHILOSOPHY

Department of Chemistry

THE UNIVERSITY OF TEXAS AT EL PASO

December 2014

Dedication

I want to dedicate my doctoral dissertation to my mother Mrs. Prova Kabiraj and my father Mr. Parimal Kumar Kabiraj for their relentless support, hard work and for seeding the dream of higher education in me since my childhood. Their unconditional love, care and prayer allowed me to reach this stage in my life. They have my eternal gratitude.

Acknowledgements

I would like to express my sincere admiration to my dissertation advisor, Dr Mahesh Narayan. I want to thank for the faith you have shown in me since slecting me as part of your research group till today. Your vision, guidance, suggestions and support for my doctoral work are absolutely invaluable and truly indispensible. His endless patience, encouragement, trusts, and accommodation for free and open discussion not only helped shape and strengthen my research but also promoted my personal growth. I feel so lucky and privileged to have had the opportunity to work with Dr. Narayan on various projects that we are both very passionate about. Finally it has been a immense pleasure to work with you.

I would also like to express my sincere thanks to all of my committee members, Drs. Jorge Gardea-Torresdey, Manuel Miranda, and Ricardo Bernal for providing helpful comments whenever it was needed. Your valuable suggestions have been appreciated. I am also grateful to Dr.Armando Varela, Dr. Marc B. Cox, for their generous help during my collaborative work with them.

I would also like to take this opportunity to acknowledge all my laboratory members, past and present. Special thanks to Dr. Rituraj Pal for helping me through the experiments. Similarly I appreciate the thoughtful advice of Veronica Gonzalez during the earlier days; Marisol Romero, Emmanuel Zubia, Mahmood Helal, Jose Marin and Lois Mendez for being great friends and for helping me in different projects and to understand the local colloquialisms unique to local cultures. I also thank my many supportive friends Dr. Debarshi Roy, Dr. Jorge Sierra, and all those who have made my stay lovely and enjoyable in El Paso.

Last but by no means, my deepest gratitude goes towards my father Mr. Parimal Kumar Kabiraj, mother Mrs. Prova Kabiraj, my elder sister Mrs. Priyanka Sarkar, my younger brother Mr. Parikshit Kabiraj and my uncle Mr. Sujoy Mondal. Their enduring love and support have been the greatest gift I could ever receive. Last but not the least, I also would like express my sincere thank to the most important person in my life, my lovely wife, Mrs. Suparna Maiti for her unconditional encouragement, love, care and giving the feeling of home.

Abstract

Cerebral accumulation of amyloidogenic protein aggregates is most frequently observed in the pathogenesis of neurodegenerative diseases. Recent studies showed prion like spreading of beta amyloid (Aβ) in Alzheimer's disease (AD) and α-synuclein protein in Parkinson's disease (PD) brain. Failure or compromise to the chaperone activity of protein disulfide isomerase (PDI) is also been reported as a major factor of aggregate formation. Nitrosative stress mediated S-nitrosylation (SNO) of protein disulfide isomerase (PDI), a housekeeping oxidoreductase, has been implicated in the pathogenesis of sporadic PD and AD. Mitochondrial dysfunction, leading to elevated levels of reactive oxygen species (ROS), is associated with the pathogenesis of neurodegenerative disorders and neuronal cell death. Rotenone and MPTP has traditionally been employed as mitochondrial stressor to induce ROS insult in cell line experiments. In this study, we have monitored the aggregation of green-fluorescent protein (GFP)-tagged synphilin-1 (a Parkinsonin biomarker) as a function of rotenone insult. We report that the innate ketone body, Na-D-β-hydroxybutyrate (NaβHB) reduces markedly the incidence of synphilin-1 aggregation. Furthermore, both rotenone and MPTP induce caspase-9 and caspase-3 activation leading to proteolytic cleavage of substrate nuclear poly (ADP-ribose) polymerase (PARP). PARP cleavage is directly related to apoptotic cell death. Our data reveal that NaβHB also prevents rotenone-induced caspase-activated apoptotic cell death in dopaminergic SH-SY5Y cells.

Interaction of Aβ (1-42) and α-synuclein has also been speculated in previous studies. However, the mechanism behind the alleged interaction is not clear. Beta amyloid (25-35) fragment can induce toxicity as of Aβ (1-42) peptide fragment, and is capable of forming beta sheet stacked fibril. We hypothesized whether the 25-35 mer can induce α-synuclein and promotes the interaction between Aβ (25-35) and α-synuclein in SH-SY5Y cell. We found that

the addition of beta amyloid (25-35) promotes intracellular accumulation of Lewy body (LB)-like inclusions (synphilin-1: α-synuclein). We have also found the Aβ (25-35) induces S-nitrosylation of PDI, and subsequent increase in Aβ (25-35) and PDI co-localization in SH-SY5Y. Together, these results strongly suggest that Aβ (25-35) oligomers aggravate the formation of LB-like inclusions through posttranslational modification of PDI, highlighting PDI as a potential therapeutic target of neurodegenerative diseases.

Previous cell line studies have indicated that SNO-PDI formation provokes synphilin-1 aggregation, the minor Parkinsonian biomarker protein. Yet no work exists investigating whether SNO-PDI induces α-synuclein aggregation, the major Lewy body constituent associated with Parkinson's pathogenesis. Here, we report that SNO-PDI formation is linked to the aggregation of α-synuclein and also provokes α-synuclein:synphilin-1 deposits (Lewy body-like debris) normally found in the PD brain. Furthermore, we have examined the ability of a small molecule, 2,3,7,8-Tetrahydroxy-chromeno[5,4,3-cde]chromene-5,10-dione (ellagic acid; EA) to scavenge NOx radicals and to protect cells from SNO-PDI formation via rotenone insult both, cell-based and cell-independent *in vitro* experiments. Furthermore, EA not only mitigates nitrosative-stress-induced aggregation of synphilin-1 but also α-synuclein and α-synuclein:synphilin-1 composites (Lewy-like neurites) in PC12 cells. Mechanistic analyses of the neuroprotective phenomena revealed that EA lowered rotenone-instigated reactive oxygen species (ROS) and reactive nitrogen species (RNS) in PC12 cells, imparted anti-apoptotic tributes and directly interfered with SNO-PDI formation. Lastly, we demonstrate that EA can bind human serum albumin (HSA). Together these results collectively indicate that small molecules can provide a therapeutic foothold for overcoming Parkinson's through a prophylactic approach.

Table of Contents

List of Tables

List of Figures

Chapter 1

Abbreviations:

PD, Parkinson's disease; AD, Alzheimer's disease; PC12, Pheochromocytoma cell; EA, Ellagic acid; RT, Rotenone; GFP, Green fluorescent protein; PDI, Protein disulfide isomerase; LBVAD, Lewy Body Variant of Alzheimer's Disease; ROS, Reactive oxygen species; RNS, Reactive nitrogen species; PARP, Poly (ADP-ribose) polymerase; HSP70, Heat shock protein 70; HSA, Human serum albumin; TNM, Tetranitromethane; SNO, S-nitrosylated; Aβ (25-35), Beta Amyloid (25-35); (snph-1), Synphilin-1; (α-syn), α-synuclein; LB, Lewy-body; SNO, S-nitrosylation.

CHAPTER 1:

Introduction

1.1 Frequency and distribution of neurodegenerative disease

Deeper understanding of nature through science gave us ability to increase the average life expectancy rate. As a result, demographics of the older population have been accelerating dramatically in past few decades. Forty million people aged 65 and over in the United States, accounted for 13 percent of the total population in 2010. In 2030, the older population is projected to be twice as large as in 2000, growing from 35 million to 72 million, and representing nearly 20 percent of the total U.S. population[1]. Diseases like dementia are of particular concern among elderly people because the nature of the pathological symptoms that characterize this condition lead to a loss of independent function, this has a severe impact on society. Alzheimer's disease (AD) and Parkinson's disease (PD) are the most common among all types of dementia in America[2]. It is estimated that 5.4 million Americans of all ages had Alzheimer's disease in 2012, 5.2 million of these aged 65 and older[3] and 200,000 under age 65 who have younger-onset Alzheimer's[4]. The Aging, Demographics, and Memory Study (ADAMS) in 2007 estimated that among 13.9 percent of dementia patients (among people aged 71 or older in America) near about 9.7 percent affected with AD[2] and 1.5 million diagnosed as PD[5].

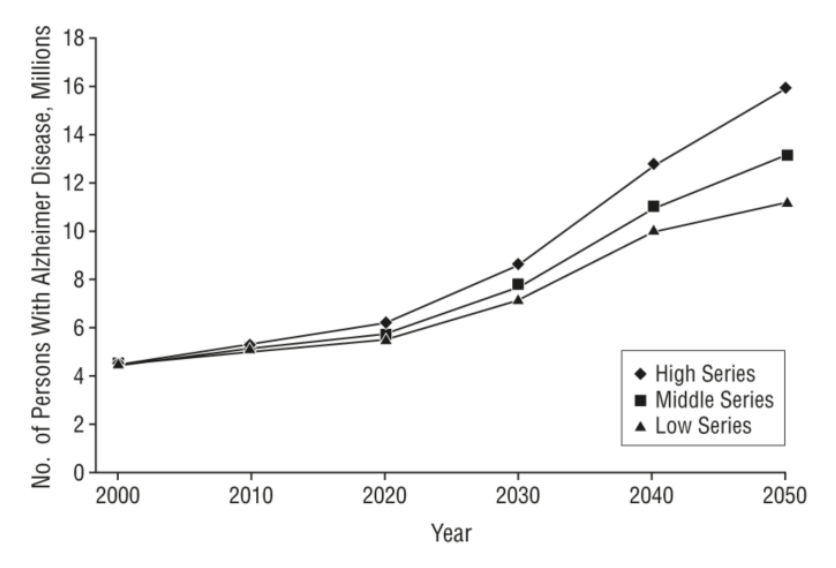

Fig. 1.1. Projected number of persons in US population with Alzheimer disease using the 2000 US Census Bureau middle-series estimates of population growth, bounded by high- and low-series[3].

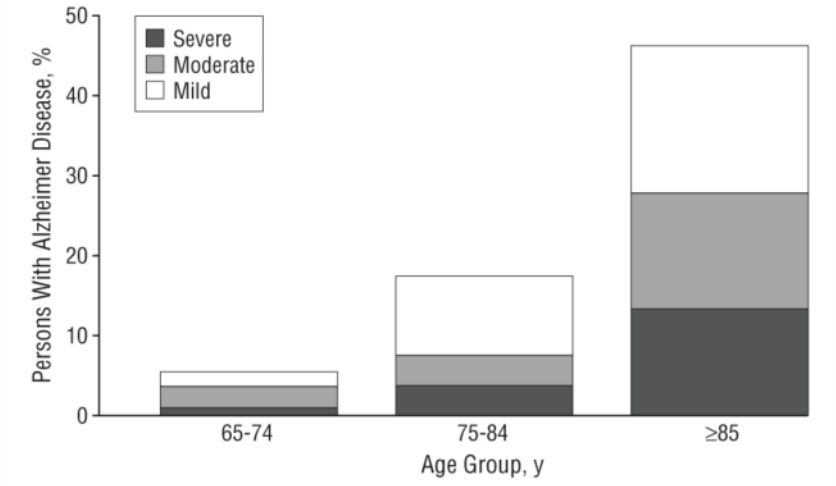

Fig. 1.2. Prevalence of severe (Mini-Mental State Examination score, ≤9), moderate (10-17), and mild (≥18) Alzheimer's disease, in each of three age groups, in the community population providing data for these estimates[3].

Current and Projected Number of Persons With Alzheimer Disease (in Millions) Older Than 65 Years in the US Population by 3 Age Subgroups*

Year and Series	Age Group, y			Total
	65-74	75-84	≥85	
2000	0.3	2.4	1.8	**4.5**
2010				
Low	0.3	2.4	2.4	**5.1**
Middle	0.3	2.4	2.4	**5.1**
High	0.3	2.5	2.5	**5.3**
2020				
Low	0.3	2.5	2.7	**5.5**
Middle	0.3	2.6	2.8	**5.7**
High	0.4	2.7	3.1	**6.2**
2030				
Low	0.4	3.6	3.2	**7.2**
Middle	0.5	3.8	3.5	**7.7†**
High	0.5	4.1	4.0	**8.6**
2040				
Low	0.4	4.6	5.0	**10.0**
Middle	0.4	5.0	5.6	**11.0**
High	0.5	5.6	6.7	**12.8**
2050				
Low	0.4	4.2	6.7	**11.3**
Middle	0.4	4.8	8.0	**13.2**
High	0.5	5.6	9.9	**16.0**

*Estimates are projected by the low-, middle-, and high-series estimates of population growth of the US Census Bureau based on the 2000 US census.
†Value does not total precisely because of rounding.

Table 1.1 Current and Projected Number of Persons with Alzheimer Disease (in Millions) Older Than 65 Years in the US Population by three Age Subgroups*

1.2 Proteins associated with Alzheimer's disease

Alzheimer's disease, an irreversible form of dementia characterized by slow decline of cognitive function, currently affects around 27 million people worldwide. Presently, in the United States, AD is the sixth leading cause of death which on an average, occurs nine years after diagnosis[6]. Pathological findings of human brain's afflicted with AD confirm the involvement of extracellular beta-amyloid (Aβ) plaques and hyperphosphorylated intracellular tau tangles[7-12]. Alzheimer's disease can have early or late onset depending on whether it has a

familial or sporadic nature, respectively. Mutation of the amyloid precursor protein (APP), presenelin1&2 (PSEN1 and PSEN2)[13,14] and duplication of APP gene[15] lead to early onset of AD. Whereas the etiology behind late onset of AD is attributed to the failure of Aβ-degrading enzymes and reduced clearance efficiency due to genetic variation in apolipoprotein E (APOE), PICALM, CR1 and CLU gene[16,17].

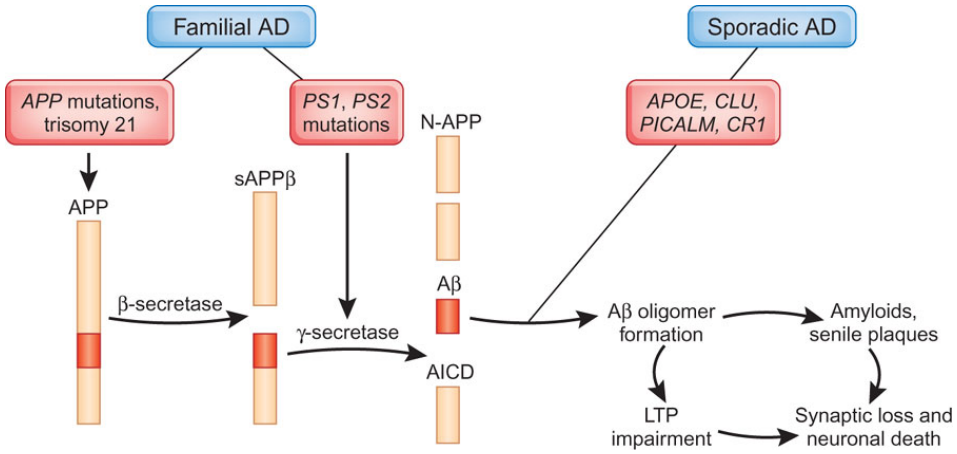

Fig. 1.3. Balance between APP processing and clearance in a model of AD pathogenesis[17].

Beta-amyloid (Aβ)

Cell surface receptor protein APP is the precursor of Aβ as a result of β-secretase and γ-secretase activity[18]. α-secretase and γ-secretase cleave the APP to give rise to the neuroprotective p3 fragment[19]. γ-secretase can cut the Aβ amino acid after 38th, 40th or 42nd position and give rise to less pathological Aβ38 or Aβ40 and neurotoxic Aβ42 isoform[19,20]. According to the amyloid cascade hypothesis, increase in the Aβ42/ Aβ40 ratio alter the ionic homeostasis and oxidative stress, leading to: hyperphosphorylation of tau, tangle formation which ultimately causes axonal dysfunction, and neuronal cell death[21,22].

Tau protein

Microtubule associated protein tau is a highly soluble cytoplasmic protein. Tau binds to tubulin protein during its polymerization into microtubules and gives strength to the neuronal structure. Hyperphosphorylated tau released from the microtubule results in the collapse of the neuronal structure and the formation of NFTs, a hallmark histopathological characteristic in AD patients[23-25].

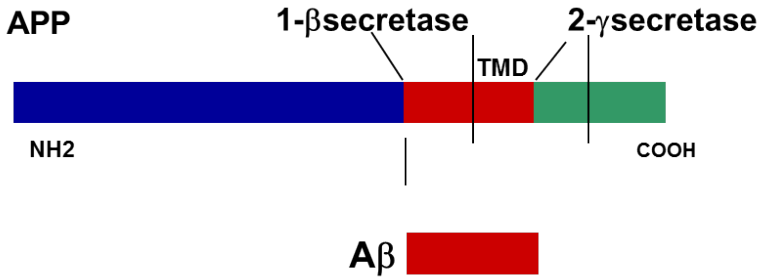

Fig. 1.4. Amyloidogenic Processing Pathway

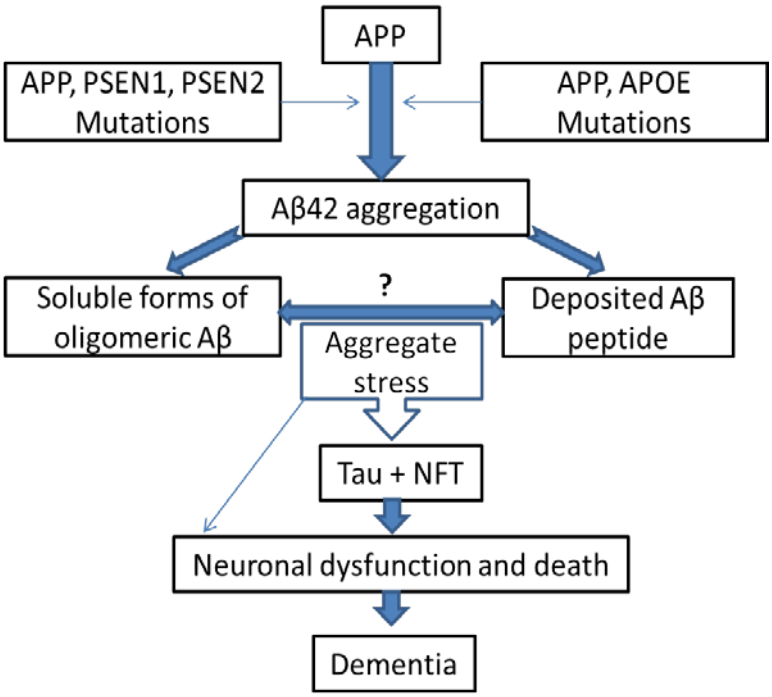

Fig. 1.5. The Amyloid Cascade Hypothesis[26,27]

1.3 Protein associated with Parkinson's disease

Parkinson's disease (PD) is the second most common form of dementia in elderly people, after AD. The central pathological feature of PD is characterized by progressive and profound loss of dopaminergic neurons in the substantia nigra pars compacta (SNpc), with deposition of intraneuronal cytoplasmic inclusions termed as Lewy bodies (LB)[28]. Molecular pathways responsible for the onset of this disease are still obscure and a matter of debate. It is believed that PD may result from an environmental factor, a genetic cause, or a combination of the two. Familial autosomal-dominant type PD is caused by mutations (A53T or A30P) in the gene SNCA (encoding pre-synaptic protein called α-synuclein)[29-31]. Neuro-pathological findings of patients with sporadic PD suggest that α-synuclein found in Lewy bodies may be involved in the pathogenesis of PD[32,33]. Synphilin-1 protein, associated with synaptic vesicle[34], also interacts with α-synuclein and might have role play in Lewy body and Lewy neurite (LN) formation[35-37].

PARK1 (α-Synuclein)

α-Synuclein (α-syn), a natively unfolded protein of 140 amino acid residues, is important for the recycling and size regulation of synaptic vesicle[38]. Structurally, α-syn consists of an N-terminal amphipathic region, a hydrophobic middle region known as non-amyloid-b component (NAC) domain, and C-terminal acidic region. PARK1 is the most prevalent among 12 other locus associated with PD[39] because of the hydrophobic NAC domain which tends to aggregate.

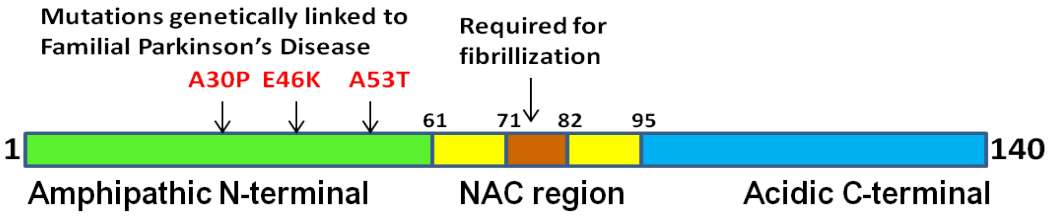

Fig. 1.6. Schematic representation of α-synuclein protein.

Three missense mutations (A53T, A30P and E46K) have been identified so far in α-syn gene[40-42]. The importance of alpha-synuclein residues 71-82 in the formation of aggregates and oligomeric species has been proven in flies, whereas the truncated version of α-syn containing the NAC domain also increased aggregation into large inclusion bodies enhancing dopaminergic neurotoxicity[43]. Mechanisms involving abnormal processing and aggregation of α-syn which disrupts cellular homeostasis, leading towards dopaminergic neurodegeneration, are highly debated. α-syn aggregates block the normal trafficking between the endoplasmic reticulum (ER) to the golgi vesicular system leading to ER stress [44]. Continuous decrease in dopamine level is a hallmark sign of PD patients. Results from α-syn knockout mice suggest that α-syn inhibits dopamine biosynthesis[45] and negatively regulates dopaminergic neurotransmission[46]. These pathophysiological aspects are detrimental to normal functioning of dopaminergic neurons and provide implications for disease pathogenesis in α-synuclein-induced PD[47].

Synphilin-1

Synphilin-1 is a protein of 919 amino acid residues found in the presynaptic terminal, suggesting its involvement in neuronal signal transmission[48]. Synphilin-1 contains six ankyrin (ANK) repeats (Swiss Protein Database number Q9Y6H5), a coiled-coil domain, and an ATP/GTP-binding site[49]. Several research groups showed the involvement of synphilin-1 in Lewy bodies of PD patients along with α-syn[48-50]. When synphilin-1 cotransfected with the NAC portion of α-syn, the formation of eosinophilic inclusion bodies in cultured cells[51] was observed; the interaction between synphilin-1 and α-syn has been confirmed by several groups[52-54]. Ubiquitinated synphilin-1 has also been shown to interact with Parkin protein trough ankyrin repeat domain[55].

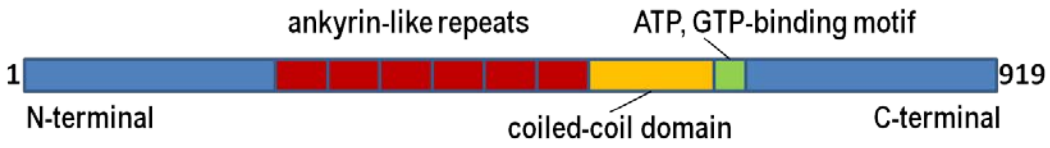

Fig. 1.7. Schematic diagram of synphilin-1

Co-expression of synphilin-1, α-synuclein, and Parkin elicits formation of ubiquitin-positive cytoplasmic inclusions that resemble LBs, suggesting that synphilin-1 might link -synuclein and Parkin to a common pathogenic mechanism[55]. A recent report demonstrated that Dorfin, an E3 for mutant superoxide dismutase-1, also interacts with and ubiquitinates synphilin-1[56].

1.4 Mitochondrial dysfunction and free radicals

Free radicals are chemically very reactive molecules capable of oxidizing different cellular biomolecules like protein, lipid etc. They are continuously being produced inside cells at a low concentration due to: the mitochondrial respiratory chain, phagocytosis, ovulation, fertilization, arachidonic acid synthesis, and many other naturally occurring physiological processes. Although free radicals are produced in our body for certain functions, high levels of free radicals can be detrimental to cellular homeostasis. Free radicals can be categorized into two broad classes: reactive oxygen species (ROS) and reactive nitrogen species (RNS). Ubiquinone in the mitochondrial electron transfer chain can readily transfer unpaired electrons to oxygen, which may give rise to superoxide radicals[57]. Alongside, excessive activation of NMDA type receptors lead to high release of calcium (Ca^{2+}) ion inside the neuronal cell. At a resting condition, the Ca^{2+} ion level is around 100nM, whereas at excitatory state the level can raise above 1000 nM[57]. An excessive Ca^{2+} ion surge activate production the free radicals (e.g., NO* and ROS), contributing to cell death. Intracellular Ca^{2+} triggers overexpression of neural nitric oxide synthase protein in a Ca^{2+}calmodulin (CaM)-dependent manner[58].

Chronic stimulation of excitatory receptors leads to apoptosis or other forms of cell death[58]. Increased levels of neuronal Ca^{2+} ion can induce the activation of the superoxide dismutase (SOD) and nitric oxide synthase (NOS) gene leading to subsequent generation of ROS and RNS [58]. The NO* radical plays some vital role in important signal transduction; however, it also can react with free superoxide radical to form very toxic peroxynitrite ($ONOO^-$). Peroxynitrite can react with body fluids to form nitrotyrosines, which may lead to neuronal cell damage and death[58]. In brain, glial cells and macrophages are the major sources of nitric oxide (NO_2)[57]. Activation of glial cell and macrophages in neurodegeneration is also an indication towards the pathogenesis of reactive species. Different diseases as result of increased free radical production are depicted in Fig. 1.8.

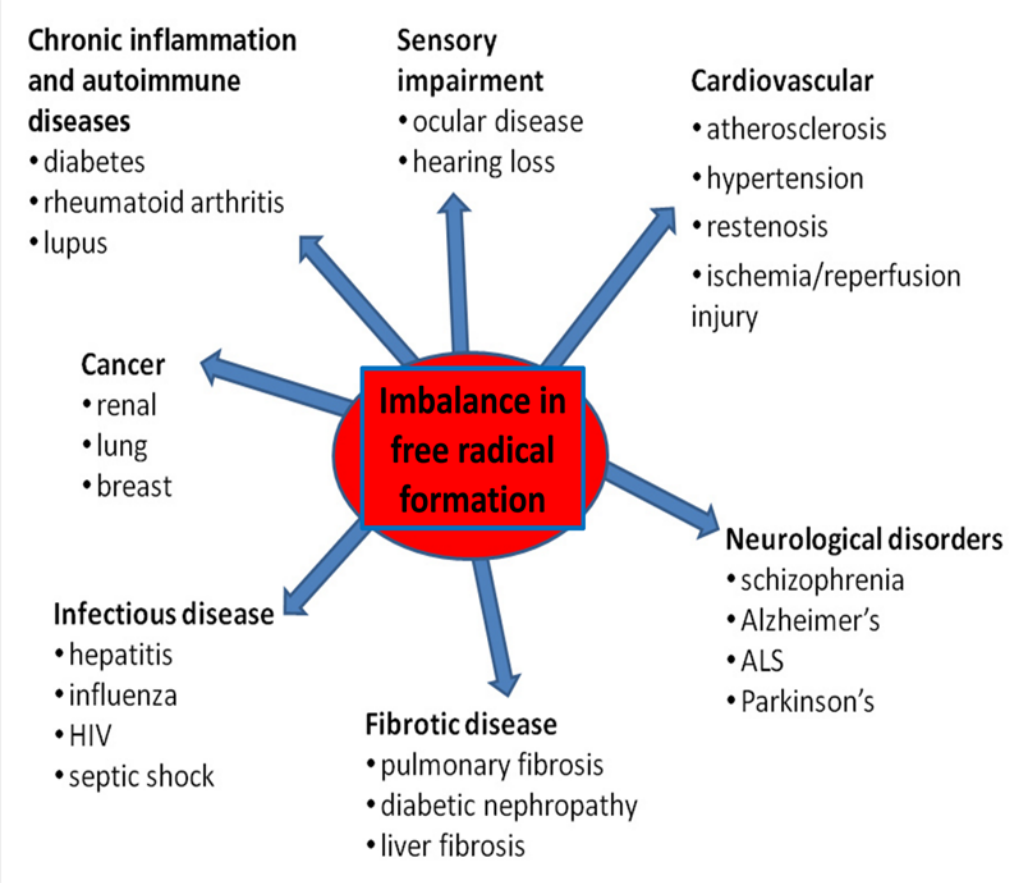

Fig. 1.8. Pathogenesis due to imbalance in free radical formation

Among the plethora of known factors associated with the etiology of apoptotic cell death, nitrosative stress induced cell death by the excessive generation of NO species has been demonstrated with high importance in recent studies. However, the mechanism underlying this fact is still unclear. Inhibition of the mitochondrial respiratory chain by rotenone has been widely used to study the role of the mitochondrial respiratory chain in apoptosis[57].

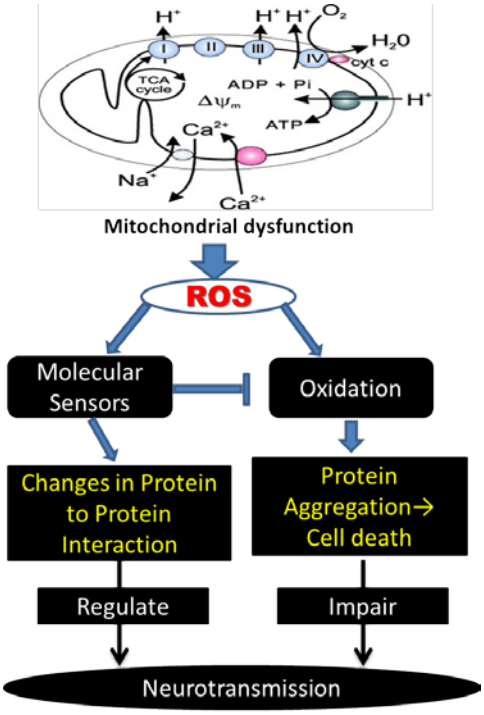

Fig. 1.9. ROS mediated loss of neurotransmission due to mitochondrial dysfunction

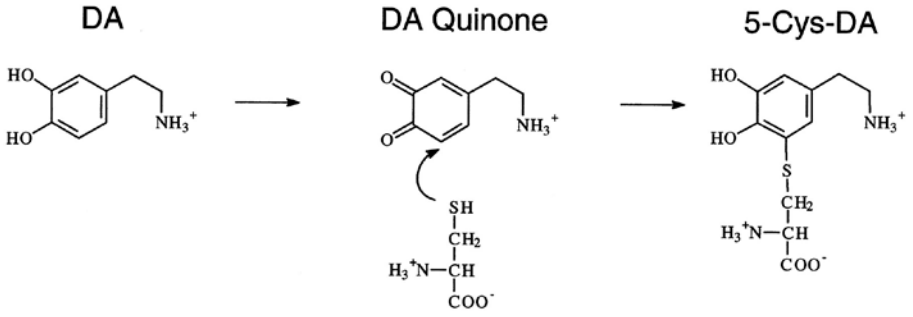

Fig. 1.10. Toxicity of dopamine due to oxidative stress. Schematic showing conversion of dopamine to toxic DA Quinone.

Recent studies showed evidence that rotenone and MPTP, both mitochondrial respiratory chain complex I inhibitors, could induce cell death in a variety of cell types[59-63]. Since it is been well established that ROS and RNS play an important role in apoptosis, the molecules that stimulate formation of these reactive species can result in apoptosis[64,65] and a process that can be inhibited by antioxidants[66,67]. The mitochondrial derived ROS are vital not only because mitochondrial respiratory chain components are present in almost all eukaryotic cells, but also because the ROS produced in mitochondria can readily influence mitochondrial function without having to cope with long diffusion times from the cytosol. Earlier studies have shown the mechanism of rotenone-induced apoptosis; rotenone can induce mitochondrial ROS production and that rotenone-induced mitochondrial ROS production is closely related to rotenone induced apoptosis[68,69]. Upon rotenone exposure, the activation of NOX gene has also been speculated[58]. Both ROS and RNS are believed to block the complex III, IV and V of mitochondrial electron transfer chain and thus, inhibit the ATP production process[70]. In these circumstances the mitochondria looses its integrity and releases cytochrome c as a signal to initiate the apoptotic cycle[68-71]. Release of cytochrome c from the mitochondrial inner membrane space into the cytosol triggers the autocatalytic processing of procaspase-9 by interacting with Apaf-1. Caspase-3 gets activated along with other effector caspases by caspase-9, resulting in the proteolytic cleavage of substrate nuclear poly (ADP-ribose) polymerase (PARP)[70]. Importantly, PARP cleavage is directly related to nitrosative stress-mediated cell death along with variety of apoptotic responses[71]. In case of chronic rotenone/ MPTP exposure, the consequences on neuronal cells is lethal and an often found symptom of PD pathogenesis[58].

1.5 Protein disulfide isomerase (PDI) structure, function and posttranslational modification

Implication of Protein Disulfide Isomerase (PDI; Molecular weight approximately 57kDa), an endoplasmic reticulum resident protein, in maintaining neuronal cell homeostasis is gaining popularity among the scientific community[72]. The ubiquitous presence of PDI in all types of cell is indicative of the importance in folding maturation of newly synthesized proteins that are destined to transit via the secretory pathway. PDI is part of the thioredoxin super family and the PDI family of proteins[73]. Proper perception of PDI function in maintaining disulfide mediated protein folding is an urgent need for understanding neurodegenerative disease.

PDI is a multi-domain thioredoxin-like (TRX) protein and the active domain composed of two –CGHC- sequences (Fig. 1.10). There are two "a" type and two "b" type domains in PDI. The "a" type domains serve as an oxidoreductase catalytic motif whereas the "b" type domains are implicated for the chaperone-like activity (Fig. 1.10)[74].

Structure and function of PDI

Edman and co-workers in 1985 first determined the full amino acid sequence of PDI. The primary sequence consists of 508 amino acids with a molecular weight of about 57kDa[74]. At the N terminal end of PDI sequence there are 19 hydrophobic amino acids, characteristic of a signal sequence for endoplasmic reticulum localization[74]. Domain a (7 to 117) and domain a'(348 to 462) show 40% sequence homology whereas b (119-220) and b'(221-332) domain share only 28% of sequence homology (Fig.1.10).

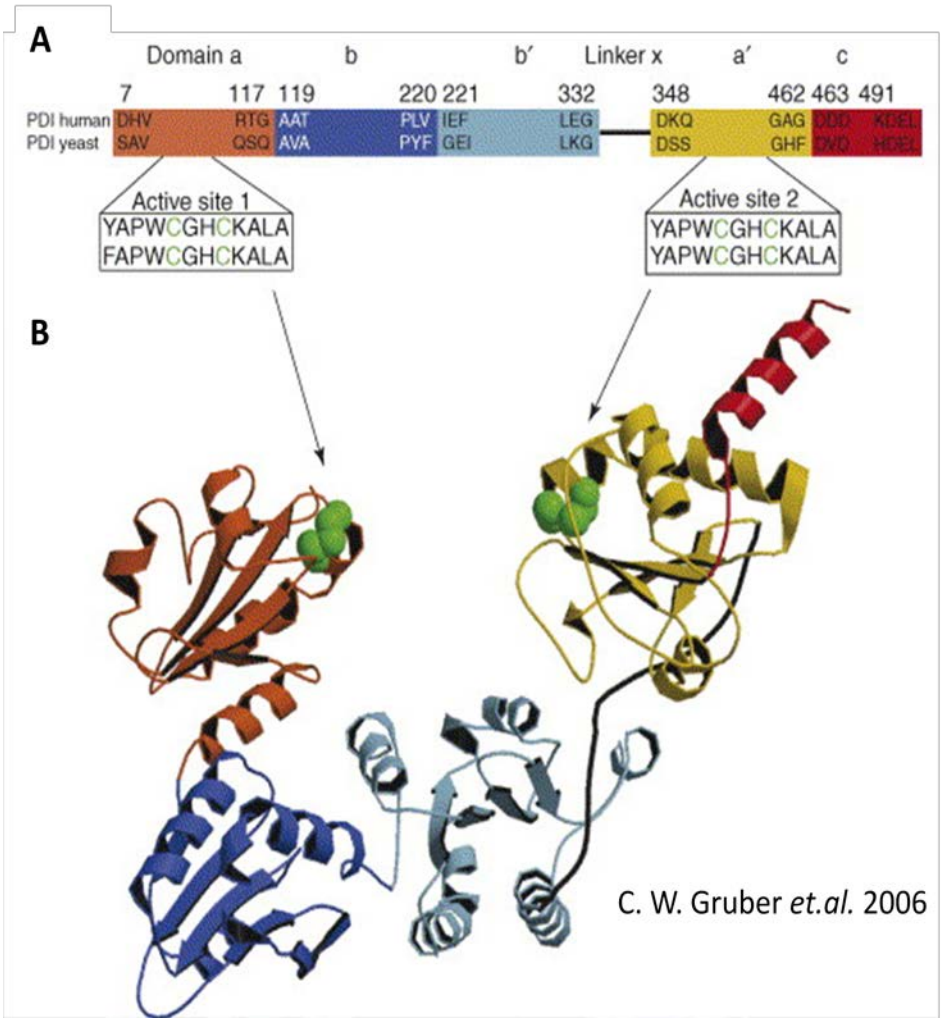

Fig. 1.11. Schematic diagram of Protein Disulfide Isomerase (PDI). Human and yeast primary sequence of PDI is compared (A). Catalytic domain "a" represent the oxidoreductase motif and domain "b" represents the chaperonin motif (B).

PDI is highly abundant in mammalian cells due to the large demand imposed by proteins that need to attain their functional native structure before being secreted[75]. In mammalian cells, PDI is mostly in a reduced state due to the need for disulfide bond shuffling of secreted proteins[75]. PDI has two major functions: oxidation of proteins and isomerization of mismatched

disulfide bonds that can be carried out by PDI because of its own reduced and oxidized states[75]. It also participates in protein degradation[75].

Oxidation and Isomerization

Correct folding of proteins is essential for functionality; otherwise it can be problematic to the cellular homeostasis. All the secreted proteins have to go through the ER system for posttranslational modification. Oxidized PDI transfers its disulfide equivalents to create new disulfide connection to thiol-containing newly synthesized proteins[76]. Then the reduced PDI is recycled by another ER-resident protein, Ero1, which oxidizes the PDI, thereby recycles the enzyme for another cycle[76]. PDI functions as an oxidative enzyme, this is illustrated in Fig. 1.11.

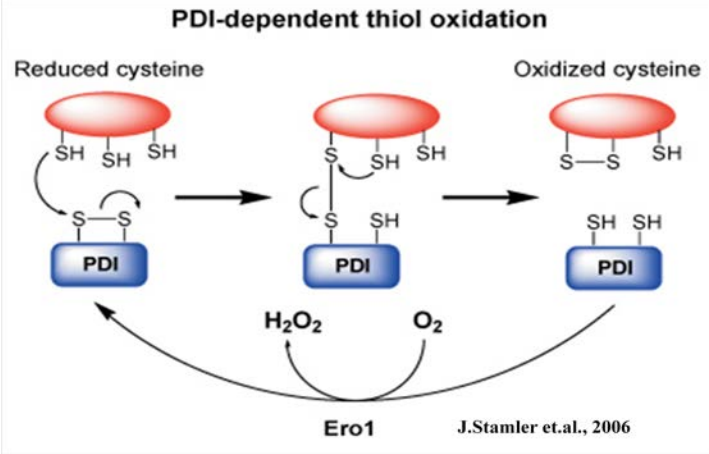

Figure 1.12. Schematic diagram of PDI dependent thiol oxidation

Isomerization is another important function of PDI. It can isomerize disulfides by shuffling existing disulfide bonds of substrates and thereby allowing proteins to acquire their native diulfide bond. In nascent proteins, the disulfide bond formation can be erroneous: incorrect disulfide bonds must be broken and corrected for acquiring the native structure[76]. PDI can

accelerate the shuffling of disulfide bonds to attain a thermodynamically favorable conformation in a timely manner[76]. This mechanism is depicted in Fig. 1.12.

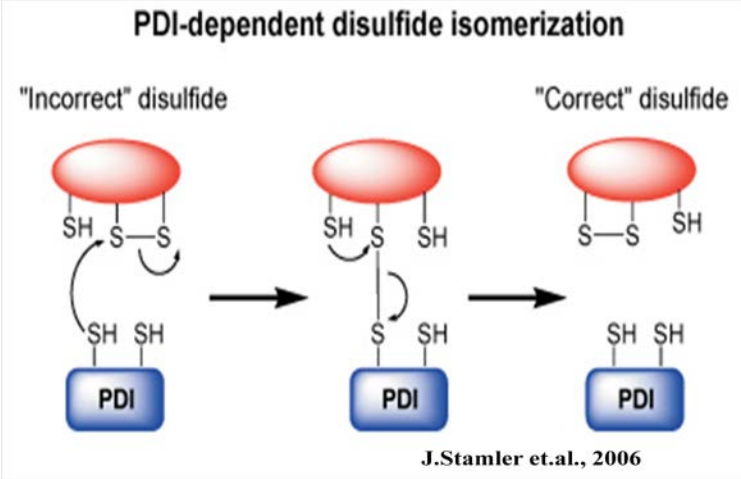

Fig. 1.13. Schematic diagram of PDI dependent thiol isomerization.

1.6 Free-radical stress mediated chemical modification of PDI

So far, we discussed that inhibition of mitochondrial electron transfer chain can trigger excess production of nitrogen species (NO*) and reactive oxygen species. In the presence of oxygen and ferrous ions, generation of hydroxyl radicals via the Fenton reaction (Fe^{2+} + $H_2O_2 \rightarrow Fe^{3+}$ +*OH + $^-$OH), can result in oxidative stress[77,78]. Reactive nitrogen species (RNS) also can also react with superoxide to from highly toxic peroxynitrite ($ONOO^-$)[57,58]. The discovery of ROS and RNS as a major transducer molecule in cell help to change our perception in the field of free radical research. It is now well accepted that free radicals and superoxides play an important role in cellular homeostasis and ER stress[58,78].

Overproduction of ROS and RNS can trigger redox-mediated signaling cascade inside the cell through the posttranslational modification of free thiols including s-nitrosylation and s-glutationylation. This free radical-induced stress can result in posttranslational modification of

the active cysteine residue of PDI[78]. Cysteine residues (Cys) in PDI are labile to protein oxidation, as they easily can react with NO* and *OH free radicals[78]. Deprotonated Cys of thiol group generates the thiolate anion to increase its nucleophilicity and therefore reactivity towards free radicals[77,78]. Due to the attack of NO* and *OH free radicals, the thiolate group (SH) of PDI is converted into inactive S-nitrosylated (S-NO) and (S-OH) group[78]. Chronic exposure to these harmful free redicals can jeopardize the posttranslational process of to be secreted proteins due to reduced PDI functionality. Aggregation of proteins and ER stress have been linked to the s-nitrosylation of PDI[58,77,78].

1.7 Ubiquitin protease system (UPS)

The importance of ubiquitin in tagging misfolded, denatured, unfolded, damaged or improperly translated proteins was very recently realized. Ubiquitinated proteins are destined for the proteosomal dedragation system. The whole cycle of events is known as Ubiquitin Protease System (UPS).

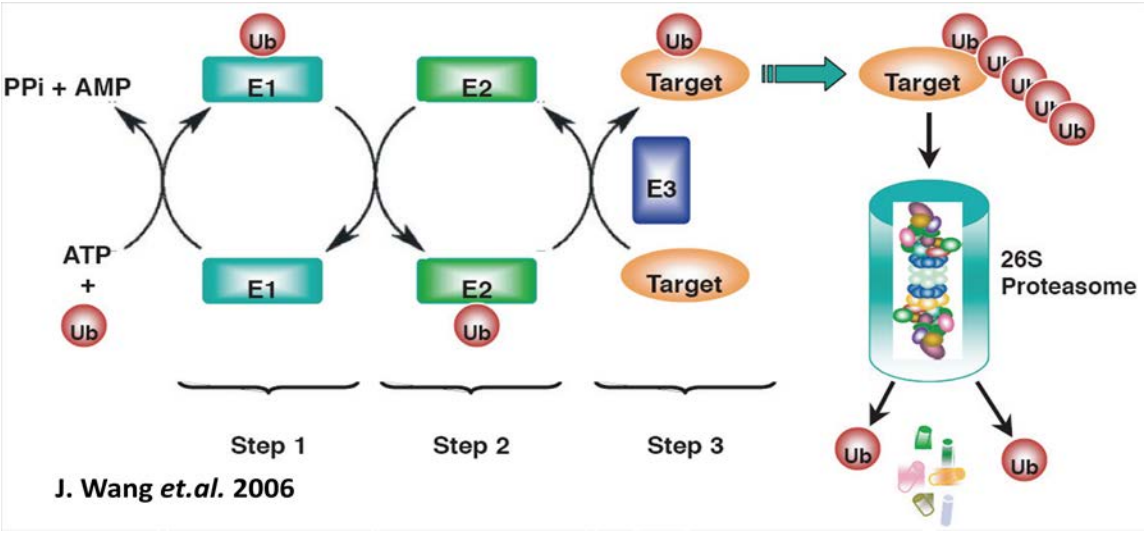

Fig. 1.14. Schematic of Ubiquitin Proteosome System (UPS).

Ubiquitin, a 76 amino acids long protein, needs ATP for activation. Ubiquitination of targated protein starts with the help of three enzymes, i.e. E1, E2 and E3 (Fig. 1.13)[58]. Of the previously mentioned enzymes, E1 activates the ubiquitin protein then, E2 prepare the ubiquitin for attachment whereas E3 helps to recognize the proper substrate for ubiquitin to bind with[52,55]. The ubiqutinated substrate is targeted for degradation by a proteosome, the major component of UPS[52,58]. The 26S proteosome is composed of 20S (functional domain) and a 19S subunit (regulatory domain). After degradation of tagged proteins, the proteosome recycles the ubiquitin for its next use[58].

The UPS system helps to maintain the amino acid pool by recycling the amino acid from degraded proteins. Increased accumulation of ubiquitinated proteins is an indication of stress response and that often leads to activation of the apoptotic pathway[55]. Abnormality in the UPS system is often related with several pathologies like: autoimmune disease, cancer, diabetes, stroke, AD, ALS, PD, multiple sclerosis etc.[52,55].

1.8 Prion like propagation

Prion protein (PrP^{C}) isoforms control various biological functions including, the immune response, long-term memory storage, and translation termination[79-81]. PrP^{C} is a glycosyl-phosphatidylinositol-anchored glycosylated protein attached to the outer leaflet of the cell membrane. An abnormal isoform of prion protein (PrP^{Sc}) is the causative agent of a fatal neurodegenerative disorder, known as prion disease, which affects both humans and animals[81-83]. Importantly, PrP^{Sc} is infectious and transmits experimentally or naturally among the same species or even across different species. Alternatively, folded PrP (PrP^{Sc}) acts as a template that self-propagates by inducing the misfolding of normal prion protein (PrP^{C}) into a structured PrP^{Sc} polymer, ultimately leading to aggregation and neurodegeneration[84].

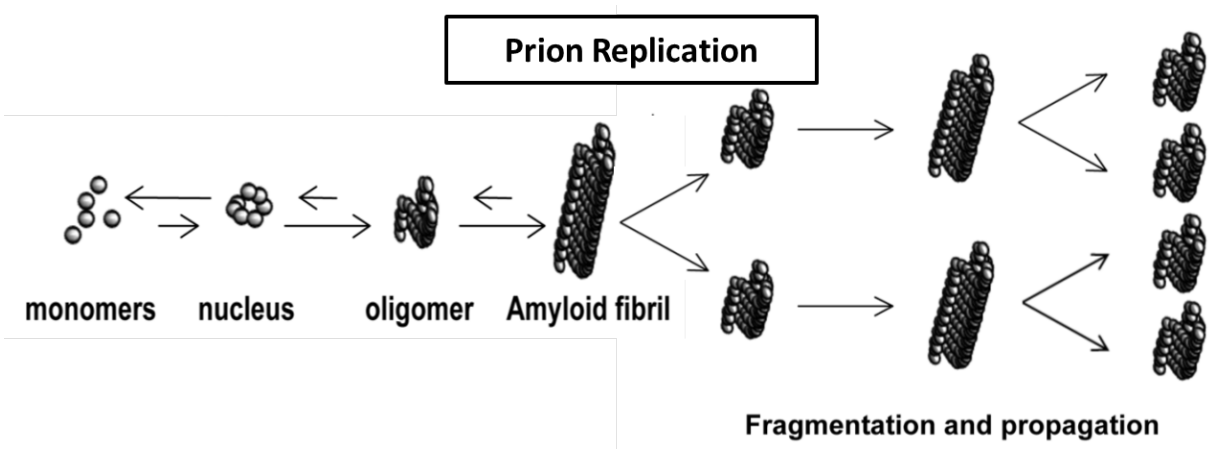

Fig. 1.15. Schematic representation of amyloid and prion formation.

Late onset characteristics of AD, despite the presence of the mutation from birth, gave rise to speculation of prion like self-propagating Aβ protein aggregates throughout the brain[80,81]. Several evidence argues that Aβ is a prion[82,83]. There is direct evidence for the existence of Aβ prions, defined as Aβ assemblies capable of self-propagation within the brain[84]. Though it is not clear what accounts for the different potencies of the brain-derived and synthetic beta-amyloid. Failure of the ubiquitin-proteasome system that normally degrades misfolded proteins leads to the formation of so-called aggresomes, pericentriolar inclusions[85,86]. These proteinaceous aggregates can induce cytosolic assembly of aggregation-prone soluble proteins through a seeding-like mechanism that shares similarities with prion propagation[87-90]. It is also speculated that Aβ (1-42) fragment can also induce the aggregation in other amyloidogenic proteins (Fig. 1.15).

In the case of functional prion protein, the secondary structure is α-helix dominated whereas the abnormal PrP^{SC} is β-sheet dominated (Fig. 1.16). The same trend can be noticed in amyloidogenic proteins like α-synuclein, amyloid beta etc[80]. All these features gave rise to the speculation of prion-like propagation of amyloidogenic proteins[91].

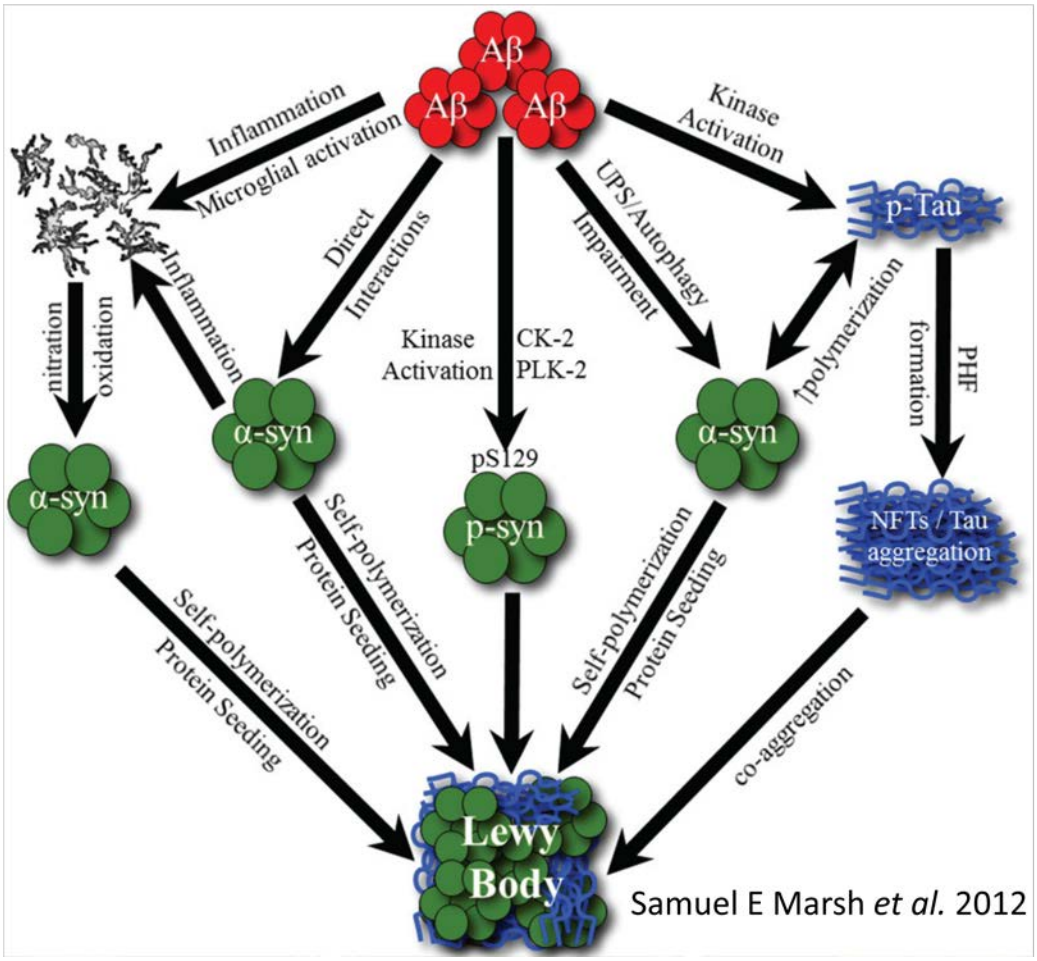

Fig. 1.16. Probable mechanisms behind β-amyloid and α-synuclein cross reactivity. **S**everal postulated mechanisms by which α-synuclein (α-syn) and β-amyloid (Aβ) may interact to form Lewy body. Such mechanisms include (left to right): chronic inflammation and microglial activation induced by both Aβ and α-syn; direct interactions and hybrid oligomerization of Aβ and α-syn; Aβ-induced kinase activation and α-syn phosphorylation; impairment of proteasome and autophagy degradation pathways; and Aβ-induced phosphorylation of tau leading to tau-mediated enhancement of α-syn aggregation. (CK-2, casein kinase 2; PLK-2, polo-like kinase 2; PHF, paired helical fi laments; NFT, neurofi brillary tangle; p-Tau, phosphorylated tau; pS129,

phosphorylated at serine 129; p-syn, phosphorylated α-synuclein; UPS, ubiquitin–proteasome system). (Adapted from S.E. Marsh *et. al.* 2012)

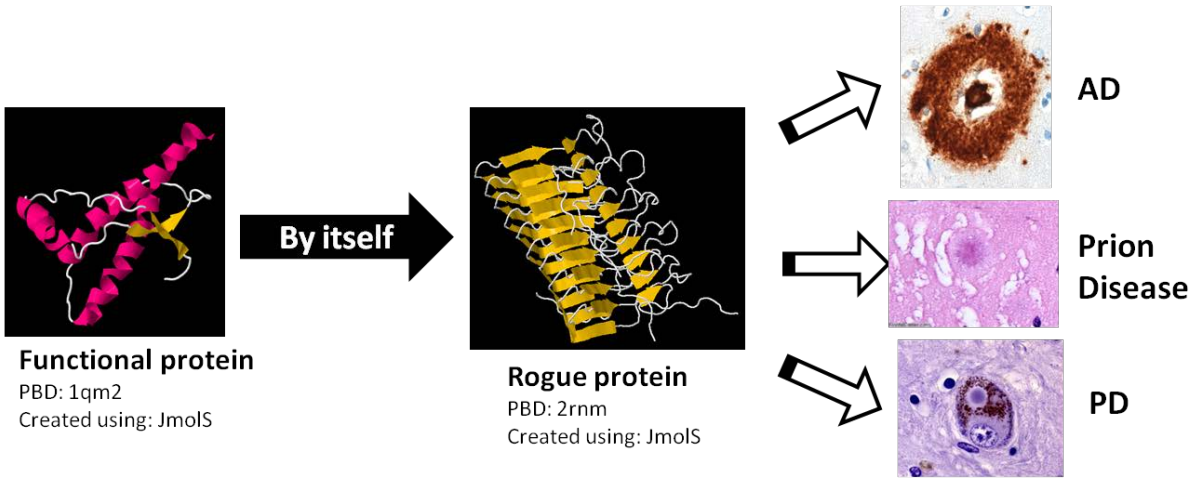

Fig. 1.17. Change from α-helix dominated functional protein structure to non-functional β-sheet dominated aggregated protein striking a common ground between AD, PD and Prion disese.

1.9 Polyphenolic compounds and intrinsic metabolites as potential drug therapies

Diphenyl difluoroketone (EF24)

The present investigation studied to determine the, Diphenyl difluoroketone, (EF24, Fig.1.18.A) a curcumin analog, against the rotenone induced nitrosative stress. Curcumin is a turmeric (*Curcuma Longa*) spice which has already been used clinically and is approved by the FDA to scavenge excess ROS and protect PDI function under conditions of nitrosative stress. However curcumin's low bioavailability and efficacy profile in vivo hinders its clinical development[92]. Currently, EF24 is being used as an anticancer drug and found that EF24 is more efficacious and considerably a less toxic, commonly used chemotherapeutic agent[93]. In this

study, I assessed the free radical scavenging property of EF24 to prevent the protein misfolding leading towards apoptotic cell death.

Na-D-β-Hydroxybutyrate (NaβHB; $C_4H_7NaO_3$)

NaβHB (Fig.1.18.B) is a ketone body produced by hepatocytes and serves as an alternative source of energy in the brain during starvation[94,95]. Neuronal damage induced by glucose deprivation and mitochondrial poisoning is prevented by NaβHB[96,97]. Ketone bodies decrease the need for glycolysis[98], bypass the blockade of the pyruvate dehydrogenase multi-enzyme complex, and reduce the mitochondrial [NAD+]/ [NADH] ratio (Fig. 1.17)[99,100].

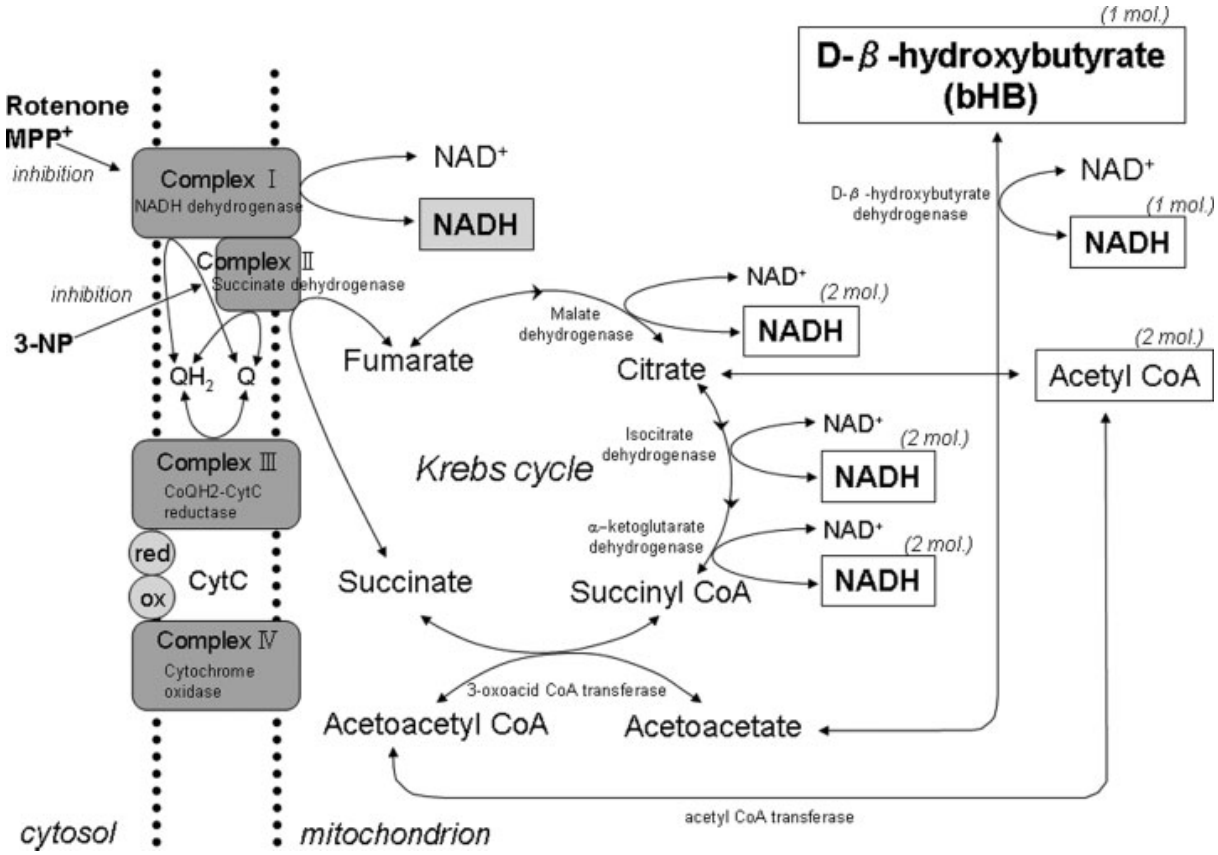

Fig. 1.18. Hypothesized effects of βHB on mitochondrial inhibition by rotenone.

In this study, I have investigated the neuroprotective effect of NaβHB against rotenone induced caspase-activated apoptosis by using SH-SY5Y dopaminergic neuroblastoma cells. Furthermore, the aggregation of overexpressed green-fluorescent protein tagged synphilin-1 in SH-SY5Y cells was monitored. This work can open avenues for the design and development of more effective prophylactics against nitrosative-stress linked PD.

Piperine

Piperine (Fig.1.18.C; C17H19NO3), the alkaloid is found in *P. nigrum L. and P. longum L* is traditionally used as an Indian spice[101]. Piperine, popularly known as black pepper is believed to have the antidepressant effect and cognitive enhancing effect during entire treatment duration in mice[102]. Most interestingly, piperine was found to have antioxidant and anti-apoptotic properties and anti-apoptotic property[103,104]. Some research groups claimed to observe increased bioavailability of different test drugs in blood vessels when administered along with piperine[105-108].

Ellagic Acid

Ellagic acid (EA)- 2,3,7,8-tetrahydroxy-chromeno (Fig. 1.18.D; $C_{14}H_6O_8$) a plant polyphenol, present in fruits and berries such as pomegranates, strawberries, raspberries and blackberries, exerts strong antioxidative, anticarcinogenic, and antifibrosis properties[109-112]. Antioxidants are compounds that can delay, inhibit or prevent the oxidation of compounds by trapping free radicals and reducing oxidative stress. In various commercial products, the presence of ellagic acid as antioxidant has also been reported. These molecules can also act as inhibitors of human immunodeficiency virus (HIV)[113,114]. The polyphenolic ring is suggestive of its antioxidant property as well as, it can be predicted from the structure, it’s ability to scavenge reactive

nitrogen specie. In this study, we want to investigate the efficacy of ellagic acid along with previously mentioned small molecules.

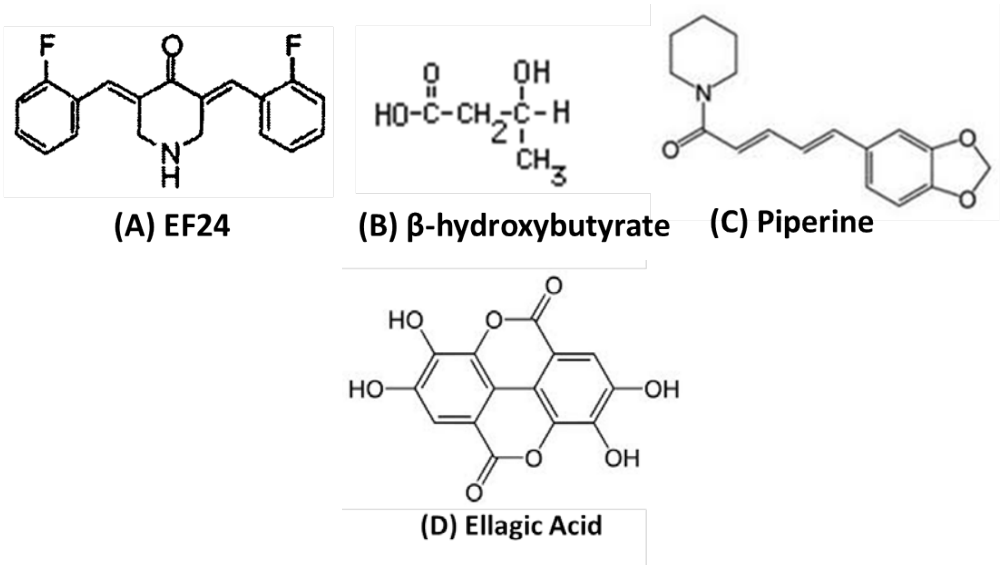

Fig. 1.19. Schematic of polyphenolic compounds and intrinsic metabolites. (A) Curcumin analogue EF24, (B) Sodium beta hydroxybutyrate, Polyphenolic phytochemicals Piperine (C) and Ellagic acid (D).

1.10 Serum protein human serum albumin (HSA)

Albumin is a monomeric soluble protein highly abundant in blood serum. Human serum albumin (HSA; Fig. 1.19) carries several endogenous compounds like steroids, thyroid hormones, fatty acids and helps to maintain extracellular fluid balance[115]. Due to its ability to depot various drug molecules, HSA has long been studied and is of interest to the pharmaceutical industry[115]. Moreover, HSA has shown antioxidant property as well as it is a carrier of NO[115]. The primary sequences indicate that there are three homologous domains (I, II and III), each containing two sub-domains (A and B) which are stabilized by 17 disulfide bridges[116]. Heterocyclic and aromatic ligands were found to bind within two hydrophobic pockets in sub-domains IIA and IIIA, namely drug site 1 and drug site 2 (Fig. 1.19). A total of seven fatty acid

binding sites were discovered in subdomains IB, IIIA, IIIB and on the subdomain interfaces[116]. HSA also has a high affinity metal binding site at the N-terminal end[117]. Flexibility of the multiple binding domains enhances the ability of HSA to interact with many organic and inorganic molecules at different physiological conditions. The same drug molecule can also bind to different locations with different affinity in HSA depending on the following competitive and synergistic mechanism[116]. Allosteric conformation change depends on physiological pH, which helps HSA to release the small molecules at diffent locations. Thsese properties make this protein a natural choce for pharmacokinetic study[117].

Therefore, we choose HSA as a carrier protein for our proposed small molecule to its site of delivary. In our study, the binding affinity of small molecules with HAS been carried out in aqueous solution at physiological conditions, using constant protein concentration.

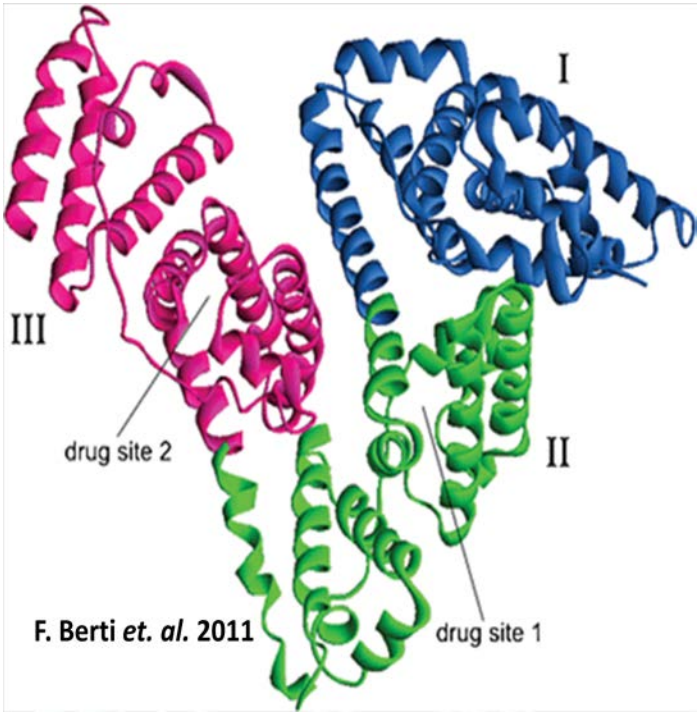

Fig. 1.20. Diagram of human serum albumin (HSA), PDB: 1E7H

1.12 Dissertation hypothesis

We hypothesize that reactive oxygen species/ reactive nitrogen species insult and the associated catalytic dysfunction of protein disulfide isomerase via its chemical modification results in the accumulation of PD and AD-specific aggregates, alpha-synuclein and Aβ, respectively. As a corollary, we posit that select small-molecules are neuroprotective.

We also hypothesize that beta-amyloid (25-35) aggregosome can lead to aggregation of synphillin-1 and α-synuclein, making it cross-reactive.

1.13 Dissertation aim

Specific Aim 1: To investigate neuroprotective effects of the innate metabolite, NaβHB against rotenone-mediated synphilin-1 aggregation in SH-SY5Y cell line.

Specific Aim 2: To determine the efficacy of select polyphenolic phytochemicals against nitrosative stress-induced α-synuclein aggregation and/or aggravated interaction of synphillin-1 and α-synuclein in dopaminergic cells.

Specific Aim 3: To characterize the "prion like propagation" features of aggregated beta-amyloid (25-35) on synphilin-1 and α-synuclein expressed by dopaminergic cells.

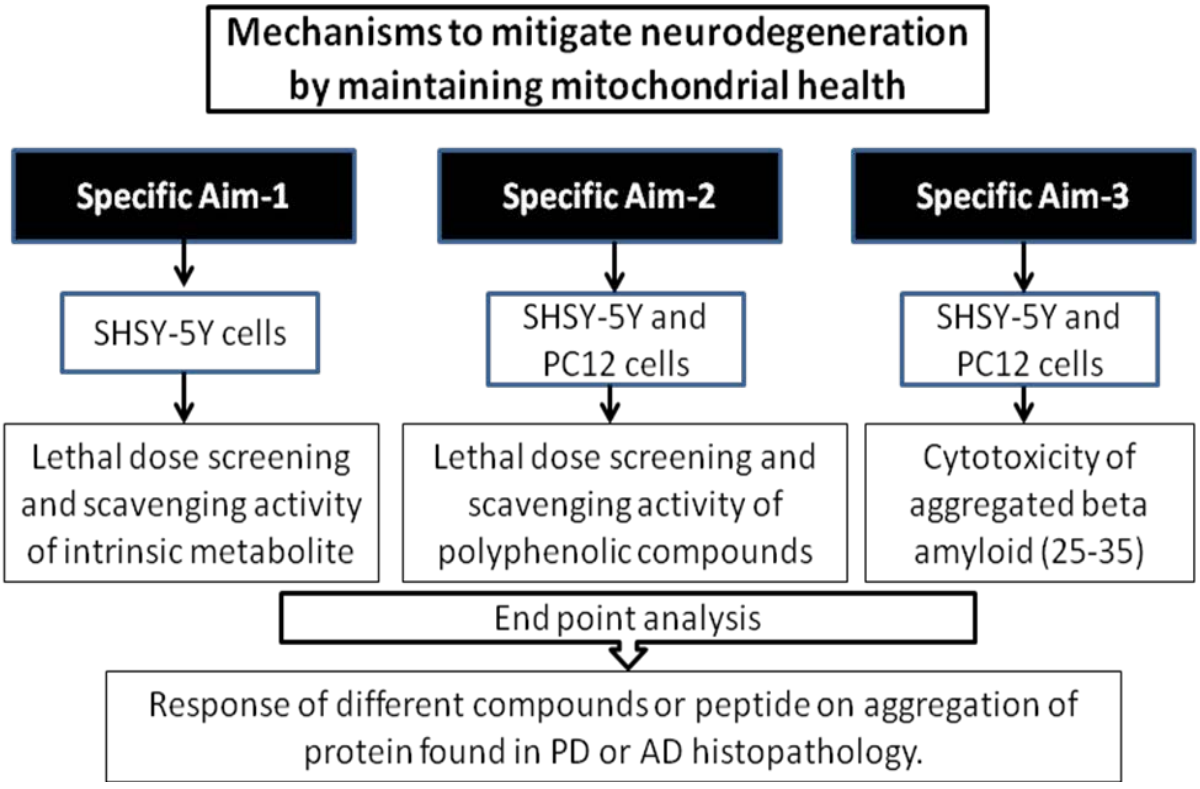

Fig. 1.21. Schematic of experiments followed to test proposed aims.

CHAPTER 2

Nitrosative stress mediated misfolded protein aggregation mitigated by Na-D-b-hydroxybutyrate intervention

2.1 Introduction

Pathologically, Parkinson's disease (PD) is characterized by the progressive loss of dopaminergic neurons in the substantia nigra and the formation of Lewy-body inclusions[1]. Although the molecular mechanisms are not clearly understood, mitochondrial dysfunction is known to be an important factor among other known intra- and extracellular etiological factors[1]. Studies showed that in a particular sporadic form of PD, mitochondrial complex I activities are compromised in the nigro-striatal pathway[2-4]. Rotenone, a plant derived pesticide, induces cell destruction by inhibiting complex I (NADH ubiquinone oxidoreductase) which mimic the biochemical lesions of PD, both in vivo and in vitro[5,6].

The mitochondrial respiratory chain is a key site of reactive oxygen species (ROS) production under physiological conditions which in turn, orchestrates apoptosis[4,7,8]. Rotenone is a model ROS generator via the induced production of NOx. Earlier studies have shown the mechanism of rotenone-induced apoptosis through mitochondrial ROS production[2]. Apoptotic stimuli instigate the release of cytochrome c from the mitochondria into the cytosol, where it triggers autocatalytic processing of procaspase-9. Caspase-3 gets activated along with other effector proteins by caspase-9, resulting in the proteolytic cleavage of substrate nuclear poly (ADP-ribose) polymerase (PARP)[9]. In human PARP, the cleavage occurs between Asp214 and GLY215, which separates the PARP amino-terminal DNA binding domain (24 kDa) from the carboxy-terminal catalytic domain (89 kDa)[5,10]. Cleavage of PARP facilitates cellular disassembly and serves as a marker of cells undergoing apoptosis[11].

A hallmark event characteristic of PD is the accumulation of aggregated proteins to often form Lewy-bodies in the cytosol of human neuronal cells, which results apoptotic cell death of dopaminergic neuronal cells[3]. A common feature observed in the neuronal cells of PD victims in

this sporadic variant was the attachment of nitric oxide (NO) to the redox-active cysteines of protein disulfide isomerase (PDI) to form S-nitroso-PDI because of highlevels of nitrosative stress[3,12]. The formation of S-nitroso-PDI coupled with the pathogenesis of PD making the oxidoreductase a chief target for the prevention of PD in the nitrosative-stress-linked variant of the diseases[12].

Na-D-b-hydroxybutyrate (NabHB; $C_4H_7NaO_3$) is a ketone body produced by hepatocytes and serve as an alternative source of energy in the brain during starvation[13,14]. Neuronal damage induced by glucose deprivation and mitochondrial poisoning is prevented by NabHB[15,16]. Ketone bodies decrease the need for glycolysis[17], bypass the blockade of the pyruvate dehydrogenase multienzyme complex, and reduce the mitochondrial [NAD+]/ [NADH] ratio[18,19].

In this study, we investigated the neuroprotective effect of NabHB against rotenone induced caspase-activated apoptosis by using SH-SY5Y dopaminergic neuroblastoma cells. Our results reveal that NabHB attenuate the apoptotic stimuli by acting against rotenone toxicity. Furthermore, we have monitored the aggrega tion of overexpressed green-fluorescent protein tagged synphilin-1 in SH-SY5Y cells. Our results show that exposure of this cell line to rotenone leads to the aggregation of synphilin-1, as observed by fluorescence microscopy and consistent with previous reports that NO influences Lewy-body formation via PDI modification[12]. Importantly, cells that were pre-incubated with NabHB prior to rotenone insult demonstrated a marked resilience to synphilin-1 aggregation. These results suggest that it may be possible to mitigate nitrosative-stress induced aggregates in cell lines using ketone body-analogs. Our work opens avenues for the design and development of more effective prophylactics against nitrosative stress linked PD.

2.2 Materials and methods

Reagents, cell line and plasmid

Sodium beta hydroxy butyrate (NabHB) and rotenone (RT) were purchased from Sigma–Aldrich (St. Louis, MO). Other reagents were commercially sourced: mouse monoclonal for GAPDH (glyceraldehyde 3-phosphate dehydrogenase) and PARP (Cell Signaling Technology, Danvers, MA); apoptosis/necrosis kit (Beckman Coulter, Miami, FL), horseradish peroxidase (HRP)-conjugated goat anti-mouse (KPL Biomedical); Hoechst 33342 (Invitrogen, Eugene, OR); propidium iodide (PI) (MP Biomedicals, Solon, OH); human neuroblastoma cell line SH-SY5Y (ATCC, Manassas, VA). Cells were transfected with the pEGFP-C2 or synphilin-1/pEGFP-C2 plasmid as previously described[3].

Cell culture and treatment

SH-SY5Y cells were cultured in a 1:1 mixture of DMEM and Ham's F12 medium supplemented with 10% fetal bovine serum, 1% penicillin–streptomycin. Cells were grown at 37 ºC in humidified 5% carbon dioxide atmosphere. SH-SY5Y cells (1 X 10^6 cells/ well) were seeded onto glass coverslips in 6-well plates and incu bated for 12 h. Cell transfections were performed the following day with pEGFP-C2 control (without insert) or pEGFP-C2 carrying the fusion protein GFP-synphilin-1, as recommended by manufacturer using Effectene reagent (Qiagen, Valencia, CA). After transfection, the cells were incubated overnight to allow expression of proteins. Cells were treated with vehicle (DMSO) or with 100 µMNabHB for 6 h followed by exposure to 300 nM of rotenone for 12 h. After incubation, cells were prepared for microscopy as described below.

Differential nuclear staining cytotoxicity assay

Cells were grown for 24 h to allow attachment to multi-well plates. Cells were treated with rotenone or with different concentrations (5–500 µM) of NabHB alone, to determine it's possible cytotoxic effect. As control for non-specific effects, DMSO vehiclecontrol, as contained in the experimental samples, was included at final concentration of 0.2% v/v. Cells were pretreated with100 µMof NabHB for 6 h prior to rotenone exposure. Subsequently, cells were incubated by an extra 24 h and images were captured in live mode[20]. A mixture of PI and Hoechst 33342 at a final concentration of 1 µg/ ml was added to each well 1 h prior to imaging[20]. Images were acquired in a live-cell mode utilizing a BD Pathway 855 Bio imager system (BD Biosciences Rockville, MD). Montages (3 X 3) from nine adjacent image fields were captured per well utilizing a 20 X objective. Captured images and data analysis determining the percentage of death cells from each individual well was performed by using BD AttoVision™ v1.6.2 software (BD Biosciences Rockville, MD). Data were assessed in quintuplicate.

Apoptosis/necrosis assay

SH-SY5Y cells were seeded on 24-well micro plate at density of 20,000 cells/ well and cultured as described. Cells were incubated overnight followed by 6 h pre-incubation in presence of 100 µM NabHB and then added with 300 nM rotenone and incubated for additional 24 h. Cells from each individual well were collected, washed and processed essentially as described previously[21]. Briefly, cells were concurrently stained by resuspending them in a solution containing Annexin V-FITC and PI dissolved in 100 µl of binding buffer (Beckman Coulter, Miami, FL). After incubation for 15 min on ice in the dark, ice-cold binding buffer (400 µl) was added to the cell suspensions, gently homogenized, and immediately analyzed by flow cytometry. The percentage of total apoptotic cells per sample is annotated as the sumof both

early and late stages of apoptosis (Annexin V-FITC positive), bottom right quadrant and top right quadrant, respectively. For each sample, approximately 10,000 individual events were acquired using flow cytometer (Cytomics FC 500; Beckman Coulter,Miami, FL) and data analyzed with CXP software (Beckman Coulter, Miami, FL). Every experimental point, as well as all controls, was assessed in quintuplicate.

Western Blotting

Total cell lysates were prepared by washing the cells with cold Tris-buffered saline, collected by centrifugation (3003g, 5 min at 4 ºC, and extracted by sonication in buffer containing 10 mM Tris–HCl (pH 7.4), 10 mM EDTA, 0.5% (v/v) SDS and protease inhibitors (Sigma). Total protein concentrations were measured using a bicinchonic acid kit (Pierce, Rockford, IL) and BSA as standard. Equal amounts of protein (approximately 10 µg per lane) were separated using SDS–polyacrylamide gel electrophoresis and then transferred to polyvinyldifluoride (PVDF) membranes. Blots were incubated in blocking buffer (5%, w/v, dried skimmed milk in Tris–buffered saline, pH 7.4, and 0.1% Tween 20) followed by incubation with anti-PARP rabbit polyclonal antibody (1:1000) or anti-GAPDH (1:1000 dilution) diluted in blocking buffer for 1 h followed by horseradish peroxidase (HRP)-conjugated goat anti-rabbit in 1% BSA/TBST for 30 min. Chemiluminescence (ECL-plus or SuperSignal West Pico Chemiluminescent Substrate) was used according to the manufacturer's instructions (Amersham or Pierce Biotechnology Inc.). GAPDH was used as housekeeping protein loading control.

Transfection and cell treatment

SH-SY5Y cells (1 X 10^6 cells/well) were seeded onto glass coverslips in 6-well plates and incubated at 37 ºC in 5% CO2 for 12 h. Cell transfections were performed in the following day as recommended by manufacturer using Effectene reagent. Cells were then incubated with

transfection complexes under normal growth condition for expression of pEGFP-C2 control or the fusion protein GFP-synphilin-1 gene. Transiently transfected SH-SY5Y cells were incubated overnight to allow expression of proteins. Cells were treated with DMSO vehicle or with 100 μM NabHB for 6 h followed by exposure to 300 nM of the toxicant rotenone for 12 h. After attachment, cells were prepared for microscopy as described below.

Confocal microscopy and immunocytochemistry

Cells transfected with vector or EGFP-synphilin-1 were washed after treatment, fixed with 4% paraformaldehyde in PBS, stained with DAPI and mounted under ProLong antifade medium (Molecu lar Probes). To stain for synphilin-1, cells were fixed as above, permeabilized with 0.1% (w/v) saponin in PBS, blocked with PBS plus 5% goat serum, 5% FBS and 0.1% TWEEN 20, followed by incubation with primary antibody (overnight at 4 ºC) and secondary rhoda mine-conjugated goat anti-mouse (1:10,000; KPL Biomedical), and DAPI staining. Fluorescence confocal images were captured utilizing LSM 700 confocal microscope and assisted with ZEN 2009 software (Zeiss, New York, NY).

2.3 Results

Differential nuclear staining assay to quantify cytotoxicity

Results from the cells differential nuclear staining assay (DNS) are shown in Fig. 2.1. To define and analyze survival and death of SH-SY5Y, dead cells were detected by using PI (Fig. 2.1B); and, entire, nucleated cells were stained with membrane permeable Hoechst dye (Fig. 2.1A). Colocalization (magenta color) of nuclear fluorescence signals as shown in Fig. 2.1C represents the dead cells. The DNS assay adapted to HTS revealed cytotoxicity of NabHB itself and preventive effect of NabHB against rotenone induced cytotoxicity in SH-SY5Y cell. Fig. 2.1D shows the dose response assay of NabHB in SH-SY5Y cell line. Our data reveals no significant cytotoxicity up to 500 µM NabHB.

The cytotoxicity by rotenone insult was measured in the presence and absence of NabHB. Pre-incubation with 100 µM NabHB lowered the level of 300 nM rotenone cytotoxicity (Fig. 2.1E). Our results illustrated in Fig. 2.1D showed no significant differences between control after DMSO treatment and 100 µM NabHB treatments for 24 h. We found more than 70% toxicity at 300 nM rotenone on SH-SY5Y cells after 24 h of incubation (Fig. 2.1E). It is clear in Fig. 2.1E that pre-treatment with 100 µM NabHB (6 h) followed by rotenone insult for 24 h resulted in reduction of cytotoxicity to a significant level (~25%). Based on these results it is obvious that, NabHB, classified as a ketone body, can prevent the mitochondrial inhibitor rotenone mediated cell death.

Apoptosis/necrosis assay

Fig. 2.2 depicts annexin V-FITC and propidium iodide (PI) flow cytometric analysis to quantitatively estimate the apoptotic/ necrotic profiling of SH-SY5Y cells upon different treatment. Each histogram in Fig. 2.2 is fragmented in four quadrants; left top quadrant –

necrosis, cells permeable to PI that have lost theirmembrane integrity, without Annexin V-FITC signal, one color (red); right top quadrant – late apoptosis, cells with compromised plasma membrane, permeable to PI, but also with Annexin V-FITC signal, two colors (green and red); lower left quadrant – alive unstained cells, without PI or Annexin V-FITC fluorescent signal; lower right quadrant-early apoptosis, cells with only Annexin V-FITC signal, one color (green). Representative histograms of untreated cells (Fig. 2.2A); cells treated with DMSO (Fig. 2.2B) and 100 µM NabHB (Fig. 2.2D), did not show much detrimental effect on the viability of SH-SY5Y cells. Approximately, 2% of cells survive the exposure of 150 µM H_2O_2 (positive control) as shown in Fig. 2.2C. Apoptotic cell death occurred of nearly 70% (early and late apoptosis combined) after 24 h exposure to 300 nM rotenone (RT) in SH-SY5Y cells (Fig. 2.2E). Pretreatment with 100 µM NabHB for 6 h resulted in ~40% and ~10% protection against rotenone (300 nM) induced late and early apoptotic cell death respectively (Fig. 2.2F) and almost preserves the characteristic as of control.

Total percentage of apoptotic cells were expressed as the sum of both early and late stages of apoptosis (light colored bars; Fig. 2.2G). Cells permeable to propidium iodide without Annexin V-FITC signal were considered as necrotic cells (dark colored bars; Fig. 2.2G). Untreated cell (Con.), vehicle control (DMSO) as well as 100 µM NabHB treated cells showing negligible apoptotic and necrotic cell death (Fig. 2.2G) as anticipated from previous data (Fig. 2.1D and E).

Rotenone induced excessive generation of NOx resulted in cell death mostly via apoptotic pathway. Interestingly, rotenone even outcast 150 µM H2O2 induced apoptotic cell death by 10%. Necrotic cell death due to rotenone aggression was very low over control. Our data clearly suggest that rotenone, a known NOx producer, can activate the caspase pathway through

mitochondrial membrane depolarization leading towards apoptotic cell death. Fig. 2.2 also revealed that cells pre-incubated with 100 µM NabHB for 6 h can clearly prevent rotenone induced apoptosis by ~40% in SH-SY5Y.

PARP assay

In Fig. 2.3, lane 1, 2, 3, 4 and 5 (Ln = 1–5) indicates untreated cells, vehicle control (DMSO), cells treated with sodium beta hydroxy butyrate (NabHB; 100 µM), cells pretreated with NabHB (100 µM) for 6 h and exposed to 300 nM of rotenone for another 24 h and cells treated with rotenone (300 nM) alone respectively. Our data show that stress with 300 nM rotenone on cells for 24 h increases cleavage of PARP at a very high level over control (Fig. 2.3). Excess generation of NOx, upon rotenone insult, facilitates cleavage of the PARP carboxy-terminal catalytic domain (89 kDa) from amino-terminal DNA binding domain (24 kDa) (Fig. 2.3, Ln5), which activates the apoptotic pathway. In this experiment we show that 100 µM NabHB can prevent the cleavage of PARP (Fig. 2.3, Ln4), suggesting the generation of low nitrosative stress and thus protecting the SH-SY5Y cells from going through apoptosis.

S-Nitrosylation of PDI mediates synphilin-1 aggregation in model cells of PD

Fig. 2.4 shows the protective effect of NabHB on aggregation of GFP-tagged synphilin-1 by confocal microscopy in transiently transfected SH-SY5Y cells as a function of rotenone insult. The results clearly indicate the aggregation of synphilin-1 when exposed to 300 nM rotenone (Fig. 2.4D). Pre-treatment of cells with 100 µM NabHB prior to 300 nM rotenone exposure shows markedly diminished level of synphilin-1 aggregation (as evidenced through GFP fluorescence; Fig. 2.4E). Fig. 2.4A revealed a relatively homogeneous cytosolic distribution of GFP in cells transfected with pEGFP C2 plasmid alone. In contrast, cells transfected with EGFP- synphilin-1 constructs show a punctuated (or speckled) cytosolic distribution of green

fluorescent signal (Fig. 2.4B). This observation indicates that over expression of synphilin-1 fused to EGFP protein does not display homogenous cytosolic distribution, instead, accu mulating subcellularly in the form of aggresomes. Cells, treated with the vehicle alone (DMSO; Fig. 2.4C) or 100 μM NabHB (Fig. 2.4F) did not differ in the expression of EGFP-synphilin-1 as compared to untreated cells (Fig. 2.4B).

2.4 Discussion

In eukaryotes the mitochondrial respiratory chain (complexes I–V) is the major site of ATP production; additionally, it significantly impacts apoptosis. Inhibition of the mitochondrial respiratory chain by rotenone is linked to ROS production and serves to study the role of the mitochondrial respiratory chain in apoptosis[22]. NOx-stress, an outcome of ROS elevation, results in caspase-9 and caspase-3 activation, PARP cleavage, and DNA fragmentation eventually leading to apoptotic cell death.

The endoplasmic reticulum is a specialized compartment with a redox potential designed to facilitate the (oxidative) formation of disulfide bonds in secretory or membrane-bound proteins[3]. This is an essential process preceding their export from the ER and is catalyzed by protein-disulfide isomerase, the chief ER-resident oxidoreductase chaperone. The catalytic function of PDI, executed through two redox-active cysteine-containing active sites is essential to balance the flux between incoming nascent polypeptides and outgoing biologically viable folded proteins[3]. Compromise or failure in the catalytic efficiency of PDI can reduce the maturation processing of nascent substrates and lead to terminal misfolding, retrotranslocation along the endoplasmic reticulum associated degradation (ERAD) pathway and debris accumulation in the cytosol. This sequence of events is perhaps the rosetta-stone for the onset of apoptotic cell death related neuropathies[3].

Here, we hypothesized that the NabHB can mitigate the incidence of apoptotic cell death propagated by nitrosative stress.

To test our hypothesis, we employed rotenone to initiate nitrosative stress in an SH-SY5Y cell line. We first determined the cytotoxicity of rotenone and prophylactic effect of NabHB against rotenone through differential nuclear staining cytotoxicity assay.

Although we were unable to detect the mechanism of cell death (apoptotic or necrotic) by this assay, out study demonstrated that rotenone induced cytotoxicity was reduced to a significant level in the presence of NabHB.

Next, we determined the mechanism by which rotenone induces nitrosative-stress-related cell death (i.e. via the apoptotic and/or necrotic pathway).We used flow cytometric assay to determine the pathway of rotenone induced cytotoxicity in SH-SY5Y cell line; additionally, we examined the preventive effect of NabHB against rotenone-induced nitrosative-stress-related apoptotic or necrotic cell death. Our data indicate that rotenone causes cytotoxicity in SH-SY5Y cell line primarily through the apoptotic pathway and NabHB mitigates apoptotic cell death at a very significant level by attenuating nitrosative stress.

PARP analysis also confirmed that rotenone-induced nitrosative stress leads to cell death essentially through apoptosis. Excessive generation of NOx by mitochondrial complex-I inhibitor rotenone leads PARP cleavage via caspase activity and that activates apoptotic stimuli in eukaryotic cell. We determined that rotenone induced PARP cleavage is significantly reduced in the presence of NabHB. This reinforces evidence for prophylactic ability of NabHB against apoptotic cell death.

Collectively, our data reveal that rotenone-induced nitrosative stress activates programmed cell death stimuli and leads to apoptotic cell death via caspase-9 and caspase-3 activation. NabHB prophylactic effect against nitrosative-stress-related apoptotic cell death might arise from its inhibitory behavior towards one or more elements within this cascade.

Initially, we examined the cytosolic aggregation of synphilin-1 in the SH-SY5Y cell line under rotenone-induced nitrosative stress as previously demonstrated[12]. GFP-labeled synphilin aggregation was monitored using confocal microscopy. In comparison to control experiments,

incubation of the cell line with rotenone clearly demonstrated cytosolic aggregation of synphilin-1 consistent with previous results suggesting that healthy PDI inhibits aggregation of synphilin-1. In other controls, we examined whether unstressed cells expressing PDI could prevent synphilin-1 Lewy-body-like inclusions in the cytosol after synphilin-1 overexpression. Our data revealed very limited diffused synphilin-1 localization in cytosol (Fig. 2.4B and C). In contrast, rotenone treated cells showed discrete inclusions of synphilin-1 in the cytosol.

These results suggest that rotenone-dependent elevation of nitric oxide attenuated the protective effect of PDI on synphilin-1 inclusions (Fig. 2.4D). Next, cells were preincubated with NabHB prior to rotenone exposure to determine whether NabHB can prevent rotenone induced aggregation formation of misfolded protein. Confocal microscopy data monitoring GFP-tagged synphilin-1 clearly indicate that unlike rotenone-induced nitrosative stressed cells Fig. 2.4D), cells pre-treated with NabHB followed by rotenone treatment showed a drastic decrease in discrete Lewy-like inclusions in cytosol (Fig. 2.4E). These results suggest that NabHB can intracellularly rescue S-nitroso modification of PDI as seen under elevated levels of nitrosative stress and prevent Lewy-neurite formation in our model system.

In conclusion, our data reveals that the innate metabolite NabHB can serve as a potent prophylactic against nitrosative stress induced pathogenesis of PD. It remains to be investigated whether NabHB can intervene in other reactive oxygen species initiated sporadic neuropathies such as Alzheimer’s disease.

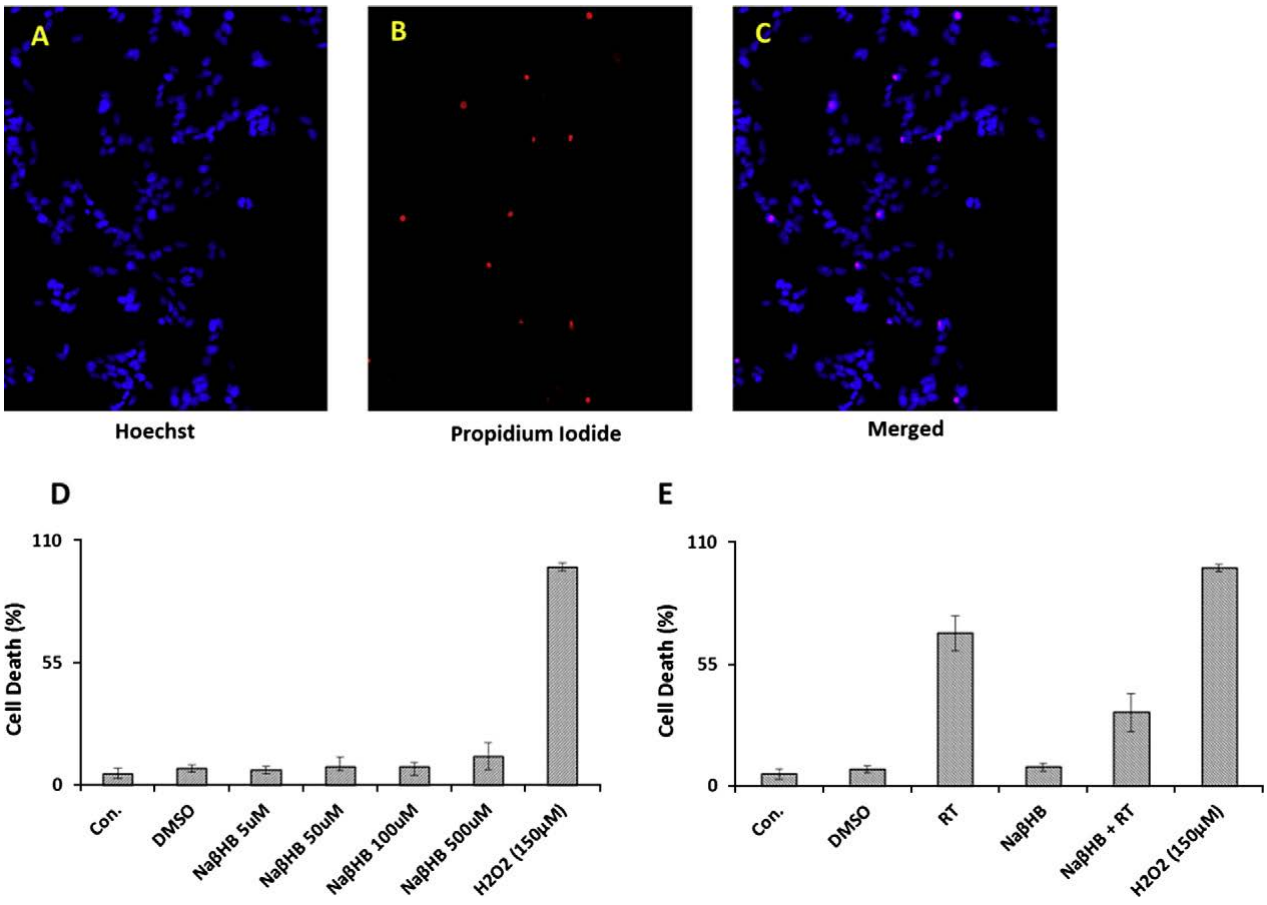

Fig. 2.1. The cytotoxicity and preventive effect of NaβHB was tested utilizing SH-SY5Y cell line, measured by using differential nuclear staining assay (DNS) adapted to high throughput screening (HTS). (A) Hoechst emission signal indicates the total number of nuclei (cells), shown in blue. (B) Propidium iodide emission signal indicates the number of death cell, shown in red. (C) Magenta color is an outcome of co-localization of red (PI) and blue (Hoechst) colors indicating the number of death cells in the image. (D) The cytotoxicity of NaβHB at different concentration after 24 h of treatment and (E) Preventive effect of NaβHB against rotenone toxicity in SH-SY5Y cells. Each bar represents average of triplicate values, and error bars their corresponding standard deviation.

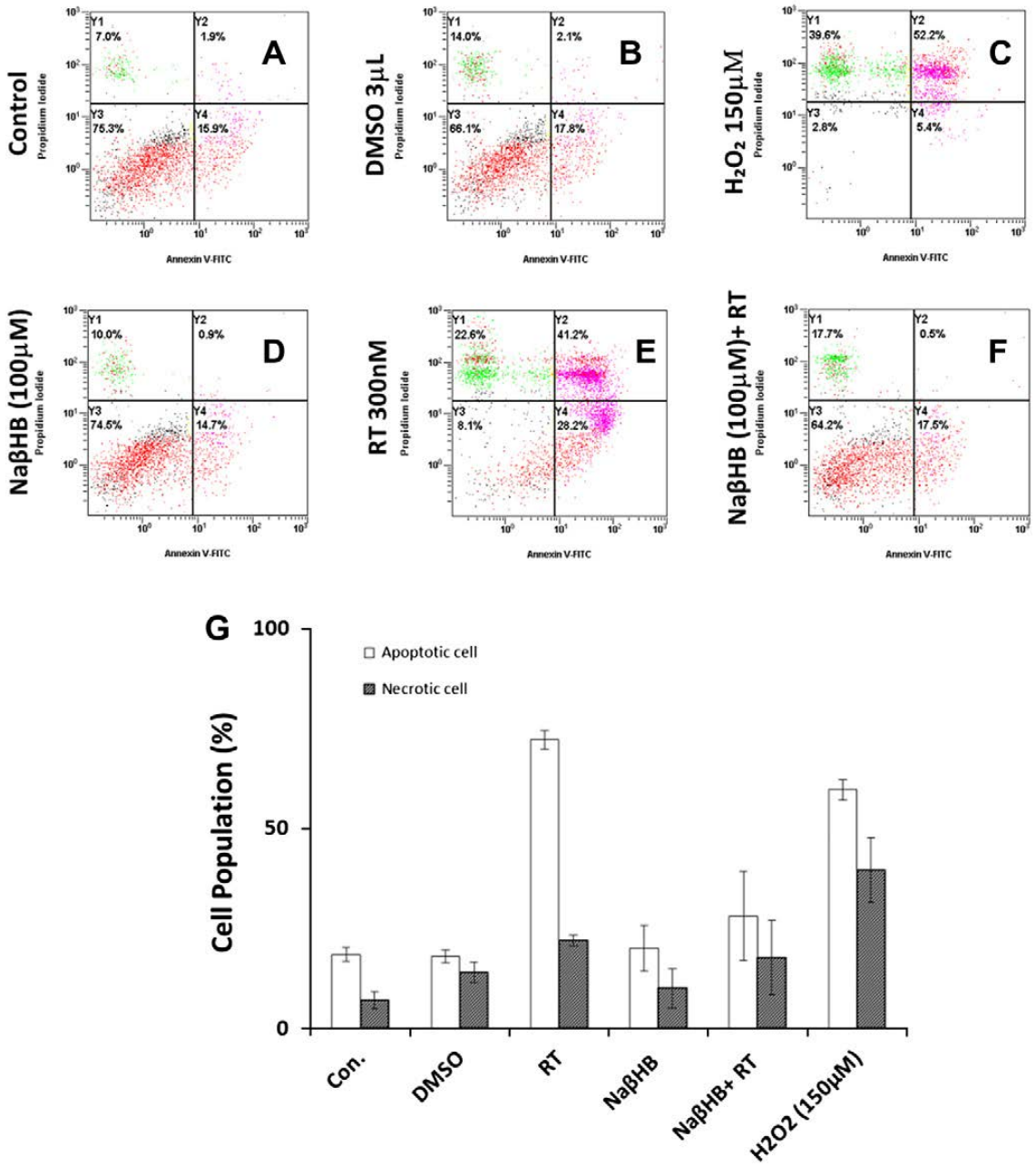

Fig. 2.2. Representative flow cytometric dot plots used to determine the percentages of apoptosis/necrosis effects on SH-SY5Y cells. (A) untreated cells (control), (B) vehicle control (dimethyl sulfoxide; DMSO), (C) positive control (150 µM H_2O_2), (D) cells treated with sodium beta hydroxy butyrate (NabHB; 100 µM), (E) cells treated with rotenone (300 nM), (F) Cells were pretreated with NabHB (100 µM) for 6 h and exposed to 300 nM of rotenone for another 24 h. (G) represent the percentage of apoptotic and necrotic cell population.

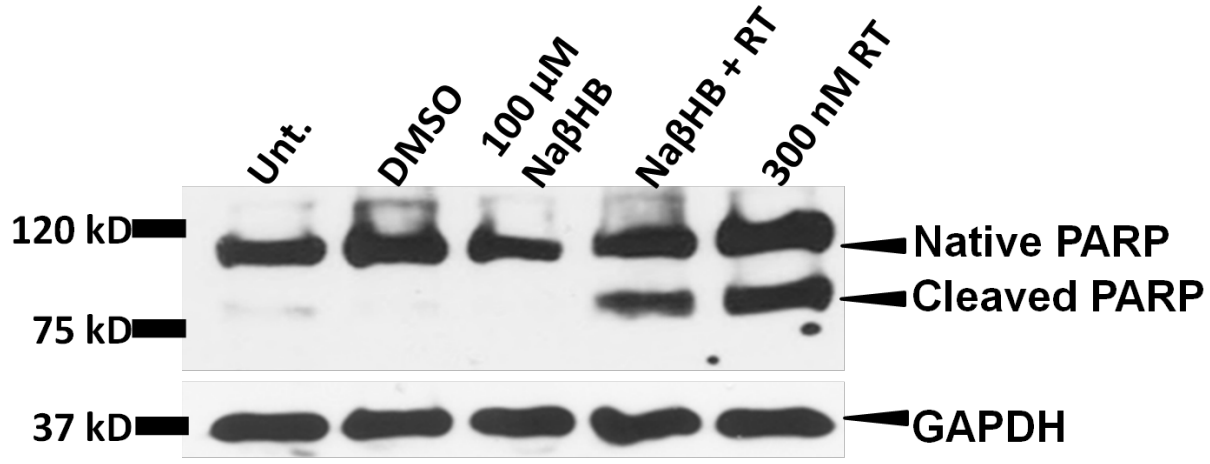

Fig. 2.3. Protective effect of NaβHB (100µM) against rotenone (300nM) induced poly (ADP-ribose) polymerase (PARP) cleavage, marker of apoptosis progression, in SH-SY5Y cells. PARP cleavage was analyzed *via* Western blot analysis.

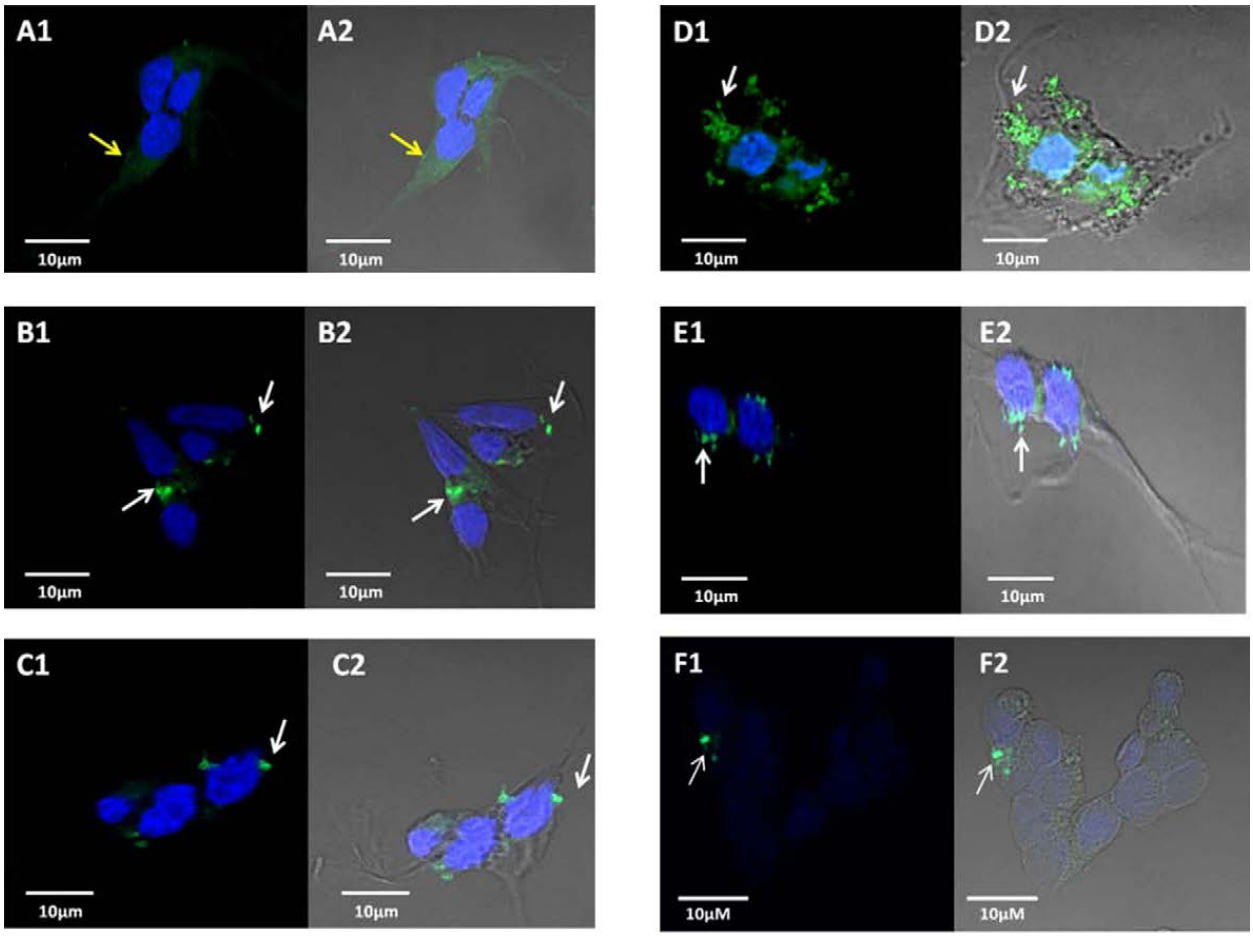

Fig. 2.4. Expression of synphilin-1 in SH-SY5Y cells and rotenone induced aggregation. (A) cells transfected with pEGFP-C2 without synphilin-1 insert; (B) cells untreated; (C) cells treated with DMSO 0.2% v/v; (D) cells exposed to 300 nM rotenone for 12 h; (E) cells pretreated with 100 µM NaβHB for 6 h were exposed to 300 nM rotenone for 12 h; (F) cells exposed to 100 µM NaβHB. All the cells were counterstained with DAPI to delimitate the nucleus (blue color). White arrows indicate the presence of aggregates corresponding to the recombinant fusion protein and yellow arrow represents GFP expression. Second part of each figure represents the differential interference contrast (DIC) picture merged with fluorescence images.

CHAPTER 3

SNO-PDI mediated accumulation of Parkinsonian biomarkers in PC12 cell death: ellagic acid interference

3.1 Introduction

With no cure in sight and care burdens constantly rising and currently estimated at $23 and $216 billion, respectively, Parkinson's and Alzheimer's diseases are emerging as a leading cause of morbidity and mortality in the US[1,2]. Furthermore, recent studies revealed that Hispanics and other minorities are especially prone to neuropathies due to a variety of geo-socio-economic factors including exposure to pesticides in farms and fields and associated reactive oxygen species (ROS) and reactive nitrogen species (RNS) insult[3,4].

The housekeeping chaperone Protein Disulfide Isomerase (PDI) is normally responsible for maturation of proteins and thus regulates traffic flow in the cell[5,6]. However, in post-mortem brains of Parkinson's and Alzheimer's Disease victims, PDI has been found to undergo S-nitrosylation of its catalytic cysteines in response to nitrosative stress[7-11].

In follow-up cell line studies, the chemical modification of PDI promoted the aggregation and accumulation of the minor, but signature, Parkinsonian-specific biomarker synphilin-1 in a nitric oxide (NO)-sensitive manner[9-11]. However, overexpression of wild-type PDI (non-SNO-PDI) attenuated the accumulation of synphilin-1-containing aggregates in the SHSY-5Y cell line[10].

In contrast to these studies involving synphilin-1, a gap exists in studies examining the aggregation of other neurodegeneration-specific biomarkers in response to SNO-PDI formation[12,13]. Specifically, no studies have examined the impact of SNO-PDI formation on the aggregation of α-synuclein, the major Parkinsonian biomarker and principal Lewy body constituent[14-17]. Here, we examined whether SNO-PDI formation provokes α-synuclein aggregation and Lewy-like neurite formation, and thus, causes the nitrosative stress-associated Parkinson's pathogenesis.

Also noteworthy, is the prominent gap in efforts designed to prevent nitrosative damage to PDI. This is despite the fact that over seven years have passed since the discovery of the proven association of this chemical mutation with synphilin-1 aggregation[10]. Lately, the housekeeping chaperone Protein Disulfide Isomerase (PDI) has emerged as a critical neuroprotectant whose catalytic integrity is pivotal to neuronal function[18-21]. Our objective was to test compounds that can prevent SNO-PDI formation and can thus mitigate the accumulation of misfolded protein debris such as Parkinsonian synphilin-1 and perhaps α-synuclein. Importantly, this research may fill the void in molecular-level efforts toward preventing PD, the Lewy Body Variant of Alzheimer's Disease (LBVAD) and other neurodegenerative disorders given that a number of other studies have confirmed that the functional security of cellular housekeeping machinery is pivotal to neuronal health[21-23].

Ellagic acid (EA), 2,3,7,8-tetrahydroxy-chromeno ($C_{14}H_6O_8$), a plant polyphenol present in fruits such as pomegranates, strawberries, raspberries, blackberries, etc. exerts strong antioxidative, anticarcinogenic, and antifibrosis properties[24,25]. Growing interest on natural products as effective prophylactic in many fields, instigated our work on EA as a potential candidate for this study. In addition, we investigated the ability of EA to bind HSA with the objective of improving its systemic distribution. HSA is a prominent carrier protein in the circulatory system[26,27]; thus, having the ability to strongly interact with HSA plays an important role in the transport and delivery of molecules such as EA.

Our results indicate that a rotenone-insult induced increase in ROS and RNS levels in the cell is associated with SNO-PDI formation as well as that SNO-PDI formation triggers the accumulation of the major PD biomarker α-synuclein. Our data also reveal that SNO-PDI formation provokes co-localization and the concomitant formation of α-synuclein:synphilin-1-

containing Lewy body-like aggregates, suggesting that SNO-PDI formation is a key milestone in the pathogenesis of nitrosative stress-induced PD. In addition, we demonstrate that EA intervenes in nitrosative stress-associated endoplasmic reticulum (ER) stress, accumulation of ubiquitinated proteins, apoptosis and the formation of lewy-like aggregates. Furthermore, administration of Ellagic acid to the cell line prior to rotenone insult mitigated SNO-PDI formation and the formation of synphilin-1, α-synuclein, and α-synuclein:synphilin-1-containing Lewy body-like aggregates. Finally, the demonstrated ability of EA to reversibly bind HSA makes it a viable choice to use as a prophylactic in ROS/RNS-induced neuropathies.

2.2 Methods

Reagents, cell line and plasmid

Ellagic acid, Rotenone (RT), 2', 7'-dichlorodihydrofluorescein diacetate (DCFH-DA), Tetranitromethane and 4-amino-5-methylamino- 2",7"-difluorofluorescein diacetate (DAF-FM DA) were purchased for the study (Sigma–Aldrich; E2250, R8875, D6883, T25003 and Life Technologies; D-23842 respectively). Other commercially sourced reagents were: Mouse monoclonal for GAPDH antibody (Glyceraldehyde 3-phosphate dehydrogenase), poly(ADP-ribose) polymerase antibody, Ubiquitin antibody (Cell Signaling Technology; 3683, 46D11, 3933 respectively), protein disulfide isomerase antibody (Abcam; ab2792), HSP70 antibody (SantaCruzBio; sc-66048), Hoechst 33342 (Life Technologies; H1399), propidium iodide (PI) (MP Biomedicals, 195458), annexin V kit (Beckman Coulter; IM3546), horseradish peroxidase (HRP)-conjugated goat anti-mouse and anti-rabbit antibody (KPL Biomedical; 214-1806 and 214-1516); rat pheochromocytoma derived neuronal PC12 cell (ATCC® Number: CRL-1721 ™) from a male origin. Cells were transfected with the pEGFP-C2 or synphilin-1/pEGFP-C2 and pCMV6 or α-synuclein/pCMV6 plasmid (NCBI Reference Sequence: NM_001146054.1) as described[46]. Serum albumin from human ≥ 99% fatty acid free was obtained from Sigma-Aldrich (A9511), DM45 spectrofluorimeter was obtained from Olis on-line instruments systems, INC (Bogart, GA).

Mass spectrometry assay

Ellagic acid stock solution was prepared in acetonitrile then diluted to obtain concentrations ranging from 0.1-80 μM (in acetonitrile). TNM was added from a stock solution (freshly prepared by weight in acetonitrile) to EA at different ratios. The samples were analyzed on a Q-TOF ESI negative mode mass spectrometer.

Cell culture and Transfection

PC12 cells were cultured in Dulbecco's Modified Eagle Medium (DMEM) supplemented with 10% fetal bovine serum, 100 U/ml penicillin and 100 µg/ml streptomycin. Cells were routinely grown at 37°C in humidified 5% carbon dioxide atmosphere on complete DMEM media. Trypsin-EDTA 0.25% (1X) (Life Technologies, 25200-056) was used to detach the cells from the culture surface when needed and once detached, complete DMEM media was added to the cell suspension. Subsequently, the cell suspension was centrifuged at 900 R.P.M. for 5 minutes in order to remove trypsin from incubation media. Cell transfections were performed the following day after plating. Subsequently, cell transfections were performed with pEGFP-C2 control (without insert) or pEGFP-C2 carrying the fusion protein GFP-synphilin-1 and pCMV6 control or pCMV6 inserted with α-synuclein as recommended by manufacturer using Lipofectamine® LTX with Plus reagent (Life technologies; 15338500). Transfected cells were incubated overnight to allow expression of transfection complexes under normal growth condition for expression of pEGFP-C2/pCMV6 (control) or the complex pEGFP-C2 with synphilin1/pCMV6 with α-synuclein gene and both at the same time at a ratio of 1:1. Transiently transfected PC12 cells were incubated overnight to allow expression of proteins.

Differential nuclear staining cytotoxicity assay

Cells were seeded into 96 multi-well plates and incubated for 24 h to allow attachment. Subsequently, cells were treated with different concentrations of RT or EA to determine its possible cytotoxic effects. As control for non-specific effects, DMSO vehicle control, as contained in the experimental samples, was included at final concentration of 0.5% v/v. In addition, in order to measure the ability of RA to intervene and protect against rotenone insult, cells were pre-treated with 10 µM of EA for 6 h prior to rotenone exposure. Subsequently, cells

were incubated for an additional 24 h and images were captured in live mode. A mixture of PI and Hoechst 33342 at a final concentration of 1 μg/ml was added to each well 1 h prior to imaging[46]. Images were acquired in a live-cell mode utilizing a BD Pathway 855 Bioimager system (BD Biosciences Rockville, MD). Montages (3X3) from nine adjacent image fields were captured per well utilizing a 10X objective. Image capture and data analysis determining the percentage of cell death per each individual well was achieved by using BD AttoVision™ v1.6.2 software[46] (BD Biosciences Rockville, MD). Each experimental point was assessed in quintuplicate.

Detection of intracellular ROS and RNS

Intracellular ROS and RNS level was measured using the oxidation-sensitive fluorescent probe DCFH-DA and DAF-FM DA respectively. Cells were seeded (5000/well) on 96-well plate and treated with 10 μM DCFH-DA or 5 μM DAF-FM in 50 μL of DMEM media according to manufacturer's protocol. After treatment, cells were analyzed with a microplate reader fluorometer (Labsystems Fluoroskan Ascent) using excitation at 485 nm and emission at 518 nm. Each data point was assessed in quintuplicate. Images were captured using Carl Zeiss LSM 700 microscope, 20X lens.

Apoptosis/Necrosis assay using Fluorescence-Activated Cell Sorting

Cells were seeded on a 24-well micro plate at density of 20,000 cells/ well and cultured as previously described. Cells were incubated for 6 h in presence of EA and then treated with RT and incubated for additional 24 h. Cells from each individual well were washed, collected and processed essentially as previously described[46]. Briefly, cells were concurrently stained by re-suspending them in a solution containing Annexin V-FITC and PI dissolved in 100 μL of binding buffer. After incubation for 15 min on ice and in the dark, ice-cold binding buffer (400

μL) was added to the cell suspensions. The mixture was gently homogenized and immediately analyzed by flow cytometry. The percentage of total apoptotic cells per sample is annotated as the sum of both early and late stages of apoptosis (Annexin V-FITC positive), bottom right quadrant and top right quadrant, respectively[46]. For each sample, approximately 10,000 individual events were acquired using flow cytometer (Cytomics FC 500; Beckman Coulter) and data analyzed with CXP software (Beckman Coulter). Each data point was assessed in quintuplicate.

Western blot analysis

Total soluble cell lysates were prepared by washing the cells with cold Tris-buffered saline, collected by centrifugation (3003 x*g*, 5 min at 4°C, and extracted by sonication in buffer containing 10 mM Tris–HCl (pH 7.4), 10 mM EDTA, 0.5% (w/v) SDS, protease and phosphatase inhibitors (Thermo Fisher Scientific; 78442). The insoluble cell pellet was boiled for 30 seconds after dissolving in 3X sample buffer (without beta marcaptoethanol) and centrifuged for 1 min before loading to SDS-polyacrylamide gel electrophoresis[46] (SDS-PAGE). We used insoluble protein fraction to detect accumulation of ubiquitinated proteins. On the other hand, after quantification, equal amount of soluble cell lysates (approximately 20 μg per lane) were separated using SDS-PAGE and then transferred to polyvinyldifluoride (PVDF) membranes. Blots were incubated in 5%, w/v, dried skimmed milk/ Tris-buffered saline pH 7.4, and 0.1% Tween 20 (TBST) followed by incubation for 2 h with anti-PARP/ anti-α-synuclein/ anti-PDI/ anti-HSP70/ anti-ubiquitin monoclonal antibodies (1:1000) or anti-GAPDH (Loading control; 1:1000) diluted in 3% BSA/TBST. After washes, blots were exposed to secondary antibodies by incubating 1 h with horseradish peroxidase (HRP)-conjugated goat anti-rabbit in 5% dry skimmed milk/TBST for 30 min. Chemiluminescence (SuperSignal West Pico

Chemiluminescent Substrate; Thermo Fisher Scientific; 34077) was used according to the manufacturer's instructions. Each data point was assessed in triplicate.

Co-immunoprecipitation and Tandem Mass Tag (TMT)-switch assay

Cell lysate was prepared following same procedure as western blot. To prepare positive and negative control, cells were incubated for 30 minutes at room temperature with 200 µM S-nitrosoglutathione or DTT, respectively. Proteins were separated in 10% SDS-PAGE, blotted and visualized with specific antibodies. For detection of S-nitrosylated PDI, 200 µl lysates (1 mg/ml) of PC12 cell homogenates were pre-cleared by the addition of 50 µL protein G agarose[47] (Santa Cruz Biotechnology). Next, 2.5 µg polyclonal anti-S-nitrosocysteine antibody (Abcam; ab50185) or normal rabbit IgG (SantaCruzBio; sc-2027) was added to the supernatant, and the mixture incubated for 1 h at 4°C with agitation. Immuno-complexes were precipitated by the addition of 50 µL protein G agarose, followed by incubation for 1 h at 4°C with agitation, and centrifugation at 5000 R.P.M. for 2 min. The pellets were then washed thrice with 1 mL chilled TBS containing 1% (v/v) tween-20 and 1 mg/ml BSA and once with 0.5 M Tris–HCl. Following the final centrifugation step, the pellet was re-suspended in SDS sample buffer, subjected to western blot analysis, and immunostained for PDI as described previously. We also used Pierce S-Nitrosylation Western Blot Kit (Thermo Fisher Scientific; 90105) to detect S-nitrosylated protein modification. This assay was performed following manufacturer instructions. In short, we used anti-TMT antibody to pull down the cell lysate then detected using anti-PDI antibody. Each data point was assessed in triplicate.

Confocal microscopy and immunocytochemistry

Cells transfected with empty vector or with EGFP-synphilin-1/ α-synuclein insert were washed after treatment, fixed with 4% paraformaldehyde in PBS, stained with DAPI and

mounted under ProLong antifade medium (Molecular Probes). To stain for synphilin-1/ α-synuclein proteins, cells were fixed as above, permeabilized with 0.1% (w/v) saponin in PBS, blocked with PBS plus 5% goat serum, 5% FBS and 0.1% TWEEN 20, followed by incubation with primary antibody (overnight at 4ºC) and secondary rhodamine-conjugated goat anti-mouse[46] (1:10000; KPL Biomedical). Fluorescence confocal images were captured utilizing LSM 700 confocal microscope and assisted with ZEN 2009 software (Zeiss, New York, NY).

Immuno-blot, immuno-fluorescence and inclusion body quantification

To quantify protein expression and fluorescence intensity we used the open source software Image J. Each logical storage manager (LSM) format data were opened in Image J and converted into RGB file (8 bit). In order to quantify the fluorescence of expressed proteins, random fields for each tested condition were obtained at the same magnification (63X oil immersion objective, zoom 1.5X). Then, a region of interest (ROI) with an area of 400 pixels (20X20) was chosen and the average intensity of fluorescence within the ROI was measured in the cytosol of every transfected cell present in the field. Over 200 cells were analyzed for each condition. The values obtained were averaged and were plotted using a bar graph. The results were obtained from more than or equal to three independent experiments. Co-localization of two different fluorescently labeled proteins was determined using ZEN 2009 software[46] (Zeiss; Supplementary Fig. 3). To count the cells with inclusion body we used colocalization finder in Image J software. Randomly selected 5 different fields with more than 200 cells/field were counted in three different sets of experiments to avoid the prejudice (Supplementary Fig. 4).

Protein binding assay

EA from a stock solution of 2.4 mM was aliquotted in a solution of 20 µM serum albumin from human (HSA) (pH 7.5, 20 mM Tris-HCl). Fluorescence emission spectra were

obtained 5 minutes after every titration by scanning the emission from 310 to 340 nm (Ext. 280 nm; DM45 sptecroflurimeter, Olis Instruments, GA). The quenching of fluorescence was fitted to a binding curve[43-45].

Statistical calculation

Every data point was collected independently and in triplicate. To note experimental viability and variability, data were presented as the average with its corresponding standard deviation. Statistical analysis was performed using two-tailed paired Student's *t*-tests to denote the statistical significance of variances between experimental samples and their corresponding controls. To identify if there is a significant difference between two groups, a value of $P < 0.05$ was considered significant. We denote the actual *P*-value in each graph wherever needed.

3.3 Results and discussion

Nitrosative stress-induced chemical mutation of a key housekeeping chaperone, protein disulfide isomerase (PDI), has been convincingly implicated in the pathogenesis of sporadic Parkinson's and Alzheimer's diseases[7-11]. While SNO-PDI formation triggers the aggregation of the minor Parkinsonian biomarker synphilin-1[10], heretofore it remained unknown whether S-nitrosylation-induced loss of catalytic function of PDI provoked the accumulation of the key Parkinsonian protein α-synuclein. Using a variety of biochemical and analytical techniques we investigated the relationship between SNO-PDI formation and the aggregation of α-synuclein and α-synuclein:synphilin-1 containing (Lewy body-like) composites. Furthermore, while previous studies have demonstrated that overexpression of wild-type PDI attenuates the accumulation of synphilin-1[10], it remains an unfeasible mechanism for therapeutic intervention. In contrast, small molecules such as EA may provide therapeutically desirable alternatives for prevention of neurodegeneration. We have assessed the ability of the small molecule polyphenolic phytochemical ellagic acid to protect PDI from becoming S-nitrosylated. We have also analyzed its efficacy in mitigating SNO-PDI associated aggregation of synphilin-1, α-synuclein and synphilin-1:α-synuclein composites (Lewy body-like neurites) and its ability to bind to a carrier protein.

Cytotoxicity of EA and its free radical scavenging potential

Ability of EA as a potential free radical scavenger was determined by mass spectrometric analysis, carried out in a controlled environment (Fig. 3.1A, B). A molecular weight of 301.232 Da in the negative ion mode suggests double deprotonation of EA[28]. In addition, a peak at 602.469 Da was observed which suggests the presence of EA dimers. Nitric oxide reacts with cellular superoxide (O_2^-) to form the peroxynitrite ($ONOO^-$) resulting in ring nitration[29]. We

have employed tetranitromethane (TNM), a model mimic of peroxynitrite, as a NOx donor to examine the ability of EA to scavenge RNS [30-32]. Upon exposure of EA to TNM, a mass increase of ~47 Da was observed which indicates the presence of a NO_2 adduct and two protons on EA. The data indicates that by becoming nitrated in the presence of a NOx radical donor, EA can indirectly impact nitric oxide levels. This is because, even though EA does not react with NO directly, it (partially) consumes total available NO by scavenging the reaction product between NO and superoxide, i.e. peroxynitrite, as evidenced by the reaction product between EA and model peroxynitrite mimic, TNM [30-32].

Cytotoxicity of EA and its protective effect against rotenone (RT) in PC12 cells was determined using highthroughput screening assay. Cells exposed to increasing concentrations of 0.1 µM to 80 µM of EA exhibited a concomitant progressive cytotoxicity from 9% to 24% (Fig. 3.1C). However, up to 20 µM, there is no difference compared to untreated and vehicle controls (as evaluated by the *P*-value). Statistical significance of 80 µM EA treatment against untreated (Unt.) condition is also very low. In contrast, the addition of 5 µM rotenone (RT) induced 60% cell death in the PC12 cell line after 24 h incubation (Fig. 3.1D). The administration of 10 µM EA prior to 1 µM RT exposure resulted in ~20% cell death whereas administration of 1 µM RT resulted in ~55% cell death (Fig. 3.1E). These data imply that EA pre-treatment was able to rescue cell death by ~35% ($P< 0.0001$). Supplementary Figure 1 is a representative image of untreated and 50 µM H_2O_2 (positive control) treated cells. *P*-value was calculated to determine statistical significance of the results between two experimental sample groups. Morphology of cells upon administration of EA prior to RT insult is further evidence of the protective aspects of EA against RT-induced cell death (Fig. 3.1F). Bright field compound microscopy picture provides evidence of cellular morphology when cells were exposed to different conditions. The

pre-treatment with 10 µM EA for 6 h enabled the PC12 cells to retain its morphology (as untreated PC12) even after 1 µM RT insult. Cells exposed to 1 µM rotenone for 24 h showed morphology similar to that observed in the positive control. Hydrogen peroxide (H_2O_2) was used as a positive control for this experiment at a concentration of 50 µM (Fig. 3.1F). All the data collectively indicates that ellagic acid pre-incubation is able to protect PC12 cells against rotenone insult (Fig. 3.1).

Cell-based Reactive Oxygen and Nitrogen Species Scavenging Assays

The effect of EA on the total cellular ROS production was measured using 2', 7'-dichlorodihydrofluorescein diacetate (DCFH-DA) fluorescence assay. The cell-permeable DCFH-DA reagent is reduced by cellular esterase to 2', 7'-dichlorofluorescein (DCF) and is trapped within the intracellular space. Additionally, several ROS agents such as hydrogen peroxide, superoxide anion(O_2^-), hydroxyl radical ($^{\bullet}OH$), as well as other peroxides, can also oxidize DCF, resulting in the origin of the highly fluorescent DCF product[33,34]. Hence, an increment in cellular fluorescence intensity reflects a proportional to a ROS increment. Relative levels of intracellular ROS increased marginally at and above 20 µM EA administration relative to the vehicle (~4%) and untreated controls (~6%; Fig. 3.2A). *P*-value is not significant up to 40 µM EA treatment when compared with untreated control. The corresponding levels of relative ROS production were ~60-80% as a function of RT (Fig. 3.2B). Pre-administration of 10 µM EA to the cell line was able to diminish relative ROS levels significantly from ~ 50% at 1 µM RT alone to ~20% (EA pre-treatment + RT; Fig. 3.2C). The EA dependent diminution in ROS was highly significant in comparison with 1µM RT treatment (P=0.0006). The membrane-permeable 4-amino-5-methylamino-2",7"-difluorofluorescein (DAF-FM) diacetate is transformed by cellular esterases to the fluorescent dye DAF-FM and becomes a direct indicator of intracellular

nitric oxide (NO) production[35]. Our data showed significant increase of DAF-FM fluorescence after 500 nM RT treatment in PC12 cells (P=0.0001; Fig. 3.2D). In contrast, pre-treatment with EA dramatically lowers fluorescence levels indicating its RNS scavenging ability (P=0.0003). Representative confocal microscopy images confirmed the fluorescence intensity of DAF-FM in PC12 cells upon different treatments where panel i-iv stand for dimethyl sulfoxide (DMSO), 10 µM EA, 500 nM RT and 10 µM EA treatment prior to 500 nM RT exposure respectively (Fig. 2E).

Previous work has demonstrated that RT insult primarily results in mitochondrial stress leading to efflux of NOx-based radicals[3,36], thus, the results observed in the cell-dependent *in vitro* analyses are consistent with the cell-independent *in vitro* analysis using the NOx donor model. Our findings suggest that EA is able to mitigate elevated intracellular levels of ROS and RNS (Fig. 3.2). Note that the exact mechanism nevertheless, is not delineated through cellular studies. It is conceivable that NO levels, which constitute a part of the total RNS, may be reduced in the presence of EA, albeit indirectly, through ring nitration of ellagic acid by peroxynitrite (a product of nitric oxide and superoxide).

Inhibition of apoptosis and endoplasmic reticulum (ER) stress through EA intervention

The pathway by which rotenone insult leads to cell death was investigated (Fig. 3.3). The addition of rotenone (500 nM) resulted in early stage apoptosis (Fig. 3.3A, B). However, prior treatment of cells with 10 µM EA resulted in a notably rescue of cells from a rotenone-induced apoptotic cell death. High statistical significance was found when the RT and EA pre-treatment + RT treatment conditions were compared (P=0.0011). Cells treated with DMSO (0.1% v/v), 10 µM EA and untreated cells did not show substantial increase either in necrosis or apoptosis.

H_2O_2 at a concentration of 50 µM was used as a positive control where substantial increase in early and late apoptosis was denoted in the lower right and top right quadrants of the matrix plot.

Considering that cleavage of poly-(ADP-ribose) polymerase (PARP) is a hallmark for apoptotic pathway activation[37,38], we examined the ability of EA to prevent RT induced apoptosis by measuring cleavage of native PARP-1(Fig. 3.3C, D). Cleavage of PARP, therefore activation of apoptosis, occurred when cells were treated with 500 nM RT. This apoptotic biochemical marker was evidenced by a dense band of the cleaved PARP-1 at 89 kD (Fig. 3.3C; third lane from left). In a control, the addition of 10 µM EA induced ~15% cleavage of PARP-1 relative to DMSO treatment (Fig. 3.3D). Densitometric analysis of the protein bands revealed that pre-treatment with EA for 6 h clearly protected PC12 cells from RT insult. About a 35% reduction in PARP-1 cleavage was observed when compared to RT insult alone. These results support the flow cytometric analysis performed to analyze the ability of ellagic acid to protect PC12 cells against apoptosis and necrosis under RT insult.

As a part of their defense mechanism, cells often activate an apoptotic pathway when they fail to circumvent ER stress. The role of RT as an ER-stressor has been documented in previous studies[39]. To evaluate the role of EA in preventing RT mediated ER stress we checked the expression of HSP-70 in PC12 cell (Fig. 3.3E, F). Over-expression of heat shock protein 70 (HSP-70) is an indication of ER-stress[39]. Treatment with 500 nM RT for 24 h showed a significant increase in the expression of HSP-70 (P=0.0014) and pre-treatment with 10 µM EA lowered the expression of HSP-70 to normal levels (P=0.0052; Fig. 3E). A high expression of HSP-70 after RT treatment is an early indication that RT treatment commits the cell to the apoptotic pathway[39]. However, our data indicate that a 10 µM EA pre-treatment was able to

reduce HSP-70 expressed as a result of ER stress. These results suggest a rescue from the apoptotic pathway (Fig. 3.3).

Mitigation of RT-induced S-nitrosylation of PDI and ubiquitination

It has previously been reported that nitrosative stress can compromise the catalytic function of the oxidoreductase chaperone PDI. Specifically, the catalytic cysteines of PDI were found to be S-nitrosylated upon RT insult[7-11]. Such a chemical modification of the housekeeping machinery was found to be RT dependent and most importantly, neurotoxic[18-21].

We examined the role of EA on mitigating levels of RT-induced S-nitroso PDI (SNO-PDI) formation. Immunoglobulin G was used to pre-clean the cell lysate and pulled down using SNO-cysteine BSA or TMT antibody and then detected with anti-PDI antibody in this study (Pre-clean; Fig. 3.4A, C). Dithiothreitol (DTT; negative control) S-nitrosoglutathione (positive control) treated PC12 cells were used to authenticate the experiment (Fig. 3.4A, C). Untreated, DMSO, and 10 µM EA treated cell lysates show no formation of SNO-PDI while total PDI was expressed and identified using an anti-PDI antibody (Fig. 3.4A, B). It is evident that pre-treatment with 10 µM EA for 6 h was successfully capable of mitigating the S-nitrosylation of PDI after 500 nM RT exposure for 24 h (Fig. 3.4A, B). Ratio of SNO-PDI versus total PDI was calculated and plotted in the bar graph to depict true expression level of SNO-PDI upon different treatment conditions (Fig. 3.4B, D). The different RT treatments showed a dose-dependent response when treated with 100 nM and 500 nM RT. The two different RT conditions showed a statistically significant difference (P=0.0053 & 0.0003 respectively) in the formation of SNO-PDI when compared to untreated PC12 cells (Fig. 3.4B). Pre-treatment with EA showed a significant reduction (P=0.0013) in RT induced SNO-PDI formation in PC12 cells (Fig. 3.4B). TMT-switch assay also confirmed the SNO-PDI formation upon RT exposure (P=0.0018) and

mitigation of same when pre-treated with EA (*P*=0.029; Fig. 3.4D). These results suggest that ellagic acid is able to intervene in events leading to SNO-PDI formation within the cell line. We reiterate that the actual mechanism by which EA mitigates SNO-PDI formation is not apparent from the data gathered. It may be an outcome of NO interception via peroxynitrite formation. Nevertheless, these data are consistent with previous cell-based and cell-independent *in vitro* results (Fig. 3.1 and Fig. 3.2) indicating radical scavenging ability by the polyphenol.

Earlier studies confirmed the RT induced ER stress which is marked by over-expression of HSP-70, an ER-resident protein[39]. In this study, we also showed that post-translational modification of the catalytic domain of PDI upon RT treatment for 24 h leads to ER stress and eventually activates the apoptotic pathway (Fig. 3.2, 3.3, 3.4). PDI, an ER resident chaperone, play a major role in proper folding of proteins[40]. Misfolded proteins are tagged by ubiquitin to guide them to proteosomal degradation system as a part of cellular defensive mechanism[41]. Overburden of the proteosomal degradation system results in accumulation of ubiquitinated proteins accompanied by increase in protein aggregation[41]. Using anti-ubiquitin antibody we demonstrated a marked increase of ubiquitinated protein after 24 h RT treatment in insoluble fractions (*P*=0.0129; Fig. 3.4E, F). However, prior treatment with EA dramatically decrease the accumulation of ubiquitinated proteins (*P*=0.0375). Taken together, this data indicates that PDI plays a major role in maintaining ER homeostasis and EA, a polyphenolic phytochemical, can help to prevent ER stress.

Defining the role of EA in synphilin-1 and α-synuclein aggregation

SNO-PDI formation leads to aggregation of the minor Parkinsonian biomarker synphilin-1[10]. Therefore, we examined whether prevention of SNO-PDI formation by ellagic acid intervention can mitigate the aggregation of synphilin-1. Transfected cells displayed high levels

of GFP tagged syphilin-1 expression (Supplementary Fig. 3.2), with tendencies to be located in the cytosolic and sometimes peri-nuclear position under different treatment conditions except the empty pEGFP vector transfected cells (Fig. 3.5A). Panel-i indicates a relatively homogeneous cytosolic distribution of EGFP in cells transfected with pEGFP-C2 plasmid alone. In contrast, cells transfected with pEGFP- synphilin-1 constructs show a punctuated (or speckled) cytosolic distribution of green fluorescent signal (Panel-ii). Cells, treated with the 10 µM EA alone (Panel-iv) did not differ in the expression of EGFP-synphilin-1 as compare to vehicle treatment (DMSO; Panel-iii). When cells were exposed to 500 nM rotenone for 24 h, cytosolic aggregation of synphilin-1 was clearly evident (Panel-v). Pre-treatment of cells with 10 µM EA 6 h prior to 500 nM rotenone exposure resulted in a markedly diminished level of synphilin-1 aggregation (Panel-vi). These findings reveal that cells under rotenone induced nitrosative stress apparently increased the aggregation of EGFP-synphilin-1 fused protein by forming cytosolic inclusion bodies. EA showed to be able to mitigate the aggregation of the fused EGFP-synphilin-1 protein to a statistically significant level (P=0.0310) when PC12 cells were treated with 10 µM EA prior to rotenone insult (Fig. 3.5B).

α-synuclein is a major Parkinsonian biomarker and the primary constituent within Lewy neurites[14-17]. We examined the expression level of α-synuclein upon rotenone toxicity (Fig. 3.5C). Panel-ii shows cytosolic homogeneous distribution of expressed α-synuclein when transiently transfected with pCMV6 plasmid containing α-synuclein genetic sequence. In contrast empty pCMV6 plasmid transfection (Panel-i) showed no expression of α-synuclein relative to panel-ii. Disruption of the homogeneous distribution of expressed α-synuclein protein, an evident of cytosolic aggregation, was clearly seen when transiently α-synuclein transfected cells were exposed to 500 nM rotenone for 24 h (Panel-v). DMSO (0.1% v/v) and 10 µM EA

treatment (Panel-ii and iv respectively) for 24 h showed no deviation in expression level or distribution when compared with the untreated condition (Panel-ii). α-synuclein transfected PC12 cells pre-treated with 10 μM EA for 6 h prior to 24 h rotenone exposure are shown in panel-vi. 10 μM EA treatment markedly reduced (P=0.0161) the aggregated α-synuclein expression (~15% relative to RT treatment) indicating its potency to nullify the nitrosative stress imposed by rotenone exposure (Fig. 3.5D).

EA mitigates the formation of RT-induced α-synuclein:synphilin-1 Lewy body-like inclusions

The Parkinsonian biomarkers α-synuclein and synphilin-1 are found to co-localize in PD patient's brains[14-17]. In order to investigate whether rotenone toxicity implies α-synuclein and synphilin-1 aggregation, PC12 cells were transfected with plasmid constructs carrying tagged fluorescence proteins and monitored via confocal microscopy (Fig. 3.6). Synphilin-1 gene was fused with GFP sequence (green signal) in pEGFP plasmid, whereas α-synuclein gene (red signal as secondary antibody was conjugated with texas red probe) was inserted in pCMV6 plasmid. Co-localization of α-synuclein and synphilin-1 was detected in cells treated with 500 nM RT as evidenced by the presence of the yellow punctuated pattern (Fig. 3.6D). The yellow pattern is the result of the superimposition of the green and red signal. The co-localization of these two biomarkers is an accepted Lewy body[14-17]. The aggregate pattern, as well as co-localization was diminished when transfected PC12 cells were pre-treated with 10 μM EA for 6 h prior to a 500 nM RT treatment for 24 h (Fig. 3.6E). The formation of Lewy body-like aggregates visualized as inclusions was indicated by a white arrow in each figure except figure 3.6A (Cells were transfected with empty pEGFP and empty pCMV6 vector in a 1:1 ratio). A Lewy body-like inclusion is shown as an inset (i) in the right most section of each panel zoom in (3X) (Fig. 6). Around a two fold increase in aggregation of synphilin-1 and α-synuclein (when co-expressed)

(*P*=0.0207 & *P*=0.0049 respectively) is clearly shown upon 500 nM RT exposure relative to the 10 µM EA treatment prior to RT exposure (Fig. 3.6F). Results graphed as bar diagram indicate fluorescent intensity where red bar represents α-synuclein expression (red channel) and green bar represents synphilin-1 expression (green channel; Fig. 3.6F). In the representative bar diagram X-axis depicts different treatment conditions and Y-axis represents fluorescent intensity (Fig. 3.6F). Aggregation of co-expressed synphilin-1 and α-synuclein (*P*=0.0050 & *P*=0.0421 respectively) after rotenone exposure for 24 h in PC12 cell line was convincingly reduced by pre-treatment with 10 µM ellagic acid. Co-localization of these two proteins was confirmed by Zen 2009 software (Supplementary Fig. 3.3). We further counted the cytoplasmic inclusion bodies in PC12 cell co-transfected with synphilin-1 and α-synuclein (Fig. 3.6G; Supplementary Fig. 3.4). The 500 nM RT treatment increased the number of inclusions dramatically relative to the vehicle control (DMSO) treatment (*P*=0.0011; Fig. 3.6G). However, cells treated with 10 µM EA prior to RT exposure, had a significantly lower count of inclusion bodies (*P*=0.0164). This series of experiments indicate that EA possesses protective activity against rotenone toxicity by preventing the aggregation of synphilin-1 and α-synuclein or α-synuclein:synphilin-1 Lewy body-like inclusions in PC12 cells (Fig. 3.6).

EA binding to Human Serum Albumin (HSA)

HSA is a cargo protein for different biologically active small molecules[42]. Reversible binding of a small molecule into the hydrophobic pocket of HSA can provide long shelf life as well as can help the active molecule to release into the gut for absorption[42]. In HSA, the fluorescence intensity due to the tryptophan residue (Trp-214) is proportional to the protein concentration ([P]). At the same time, this fluorescence is proportionally affected by the binding of other molecules ([L]) such as EA, thus, providing a method to determine protein-ligand

complex concentration ([PL]) as well as [P] and [L], ultimately providing a technique to determine binding constants[43-45]. The Langmuir isotherm data indicates that EA reversibly binds to HSA (Fig. 3.7). The K_d value for the binding of EA to HSA was experimentally determined to be $K_d = 1.43 \times 10^{-7}$ M. This reversible binding to HSA suggests that EA has an increased probability of an effective bioavailability in the human body.

3.4 Conclusion

The cytotoxicity of EA and its prophylactic effects against RT–induced nitrosative insult were determined through differential nuclear staining cytotoxicity assay. EA was found to have a low cytotoxic effect on the model PC12 cell line and a protective effect against RT cytotoxicity. Our study demonstrated that RT-induced apoptotic death evidenced by PARP-1 cleavage and flow cytometric analysis was significantly reduced in the presence of EA. EA significantly mitigated the elevated intracellular levels of ROS and RNS induced by rotenone-inhibition of the mitochondrial respiratory chain, an important finding for PD prevention and other neurodegenerative disorders associated with intracellular ROS, RNS and ER stress. *In vitro* data indicate that EA gets nitrated in the presence of NOx donors. These results translate to the cell line where the presence of EA resulted in the mitigation of RNS induced S-nitrosylation of PDI. The mechanism by which SNO-PDI formation is mitigated by EA could be through the consumption of NO generated peroxynitite [30,32]. These data represent an important finding in the methods designed to prevent pathogenesis of sporadic PD. EA intervention was also found to play an important role mitigating the formation of α-synuclein and synphilin-1 aggregates as well as α-synuclein:synphilin-1 Lewy body-like aggregates by maintaining ER homeostasis. In addition, EA was found to have a strong interaction with HSA, which has implications in drug bioavailability.

In conclusion, our results advance the neurodegeneration field by mapping the catalytic failure of cellular housekeeping machinery to PD and also establish a preventative approach against the disease. The reported results can be used for further research in related neuropathies whose onset may be related to the dysfunction of the cellular homeostasis apparatus. It is especially noteworthy that EA has no known side effects and crosses the blood-brain barrier[28].

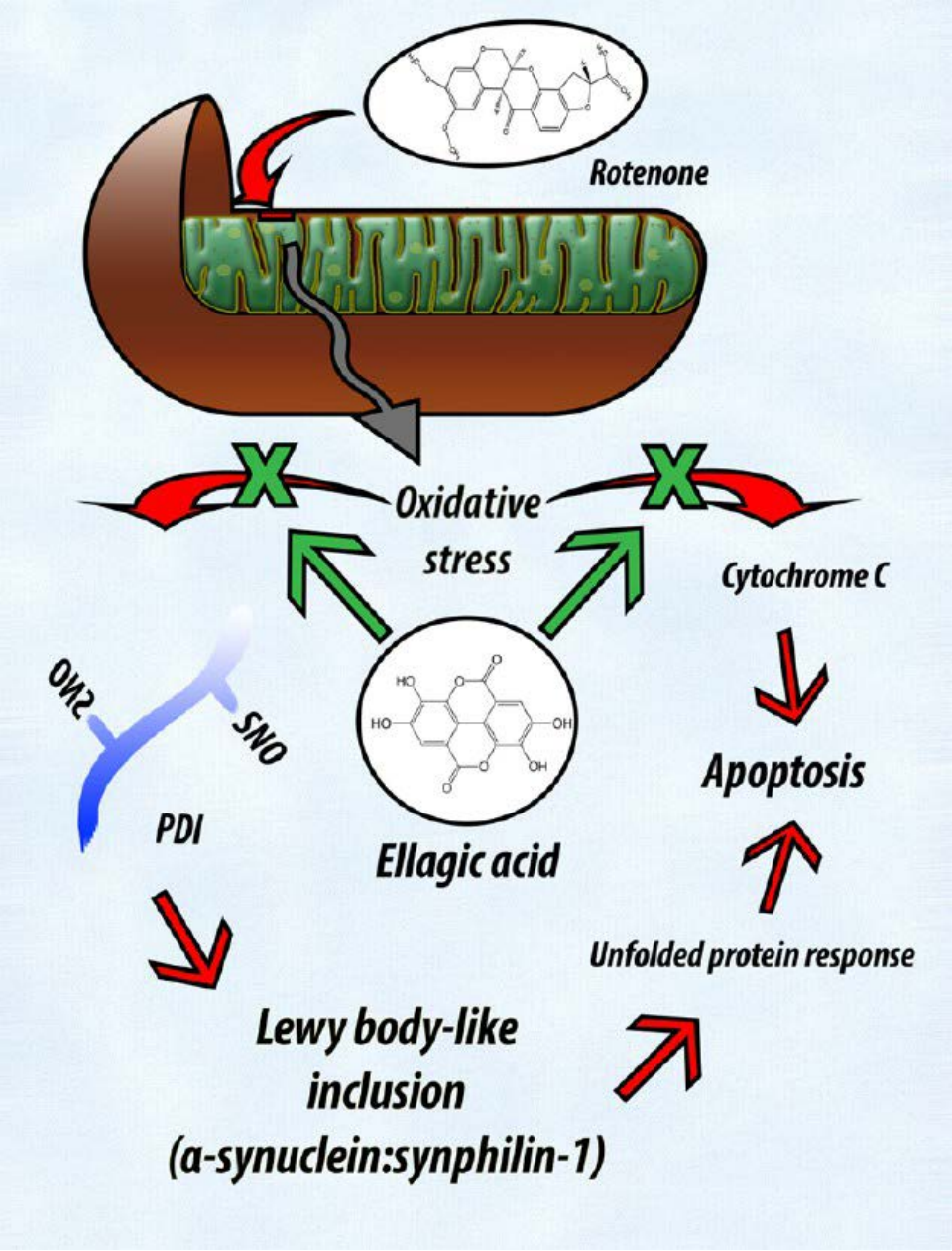

Fig. 3.0. Proposed mechanism of Rotenone-induced S-nytrosilation of PDI results in lewy body-like aggregates.

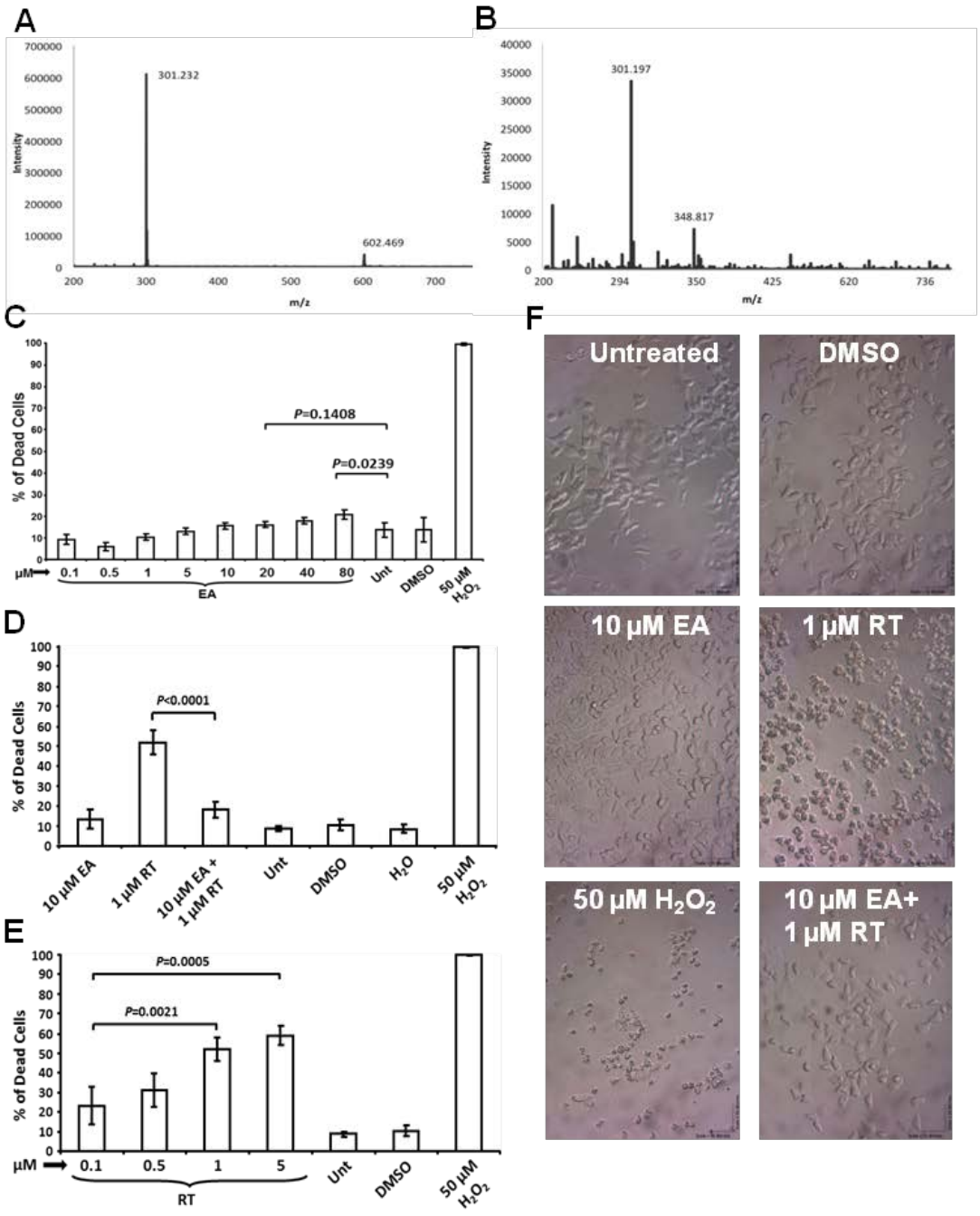

Fig. 3.1. Ellagic acid (EA) scavenging NO radical *in vitro* (A, B). Cytotoxicity and protective ability of ellagic acid on PC12 cell line against rotenone insult (C-F). The cytotoxicity and preventive effect of EA was testified on PC12 cell line, measured by using differential nuclear staining (DNS) assay adapted to high throughput screening (HTS). Cytotoxicity of EA at

different concentration after 24 h of treatment (C). Statistical significance compared with untreated are illustrated as *P*-value. Cytotoxicity of rotenone (RT) at different concentration after 24 h of treatment (D). Preventive effect of EA against RT toxicity in PC12 cells (E). Bright field images of PC12 cells taken by using compound microscope after different treatments, as indicated below of each image (F). White scale bar in each image indicate 50 µm distances. Data were analyzed by using BD AttoVision™ v1.6.2 software. Each experimental point was assessed in quintuplicate.

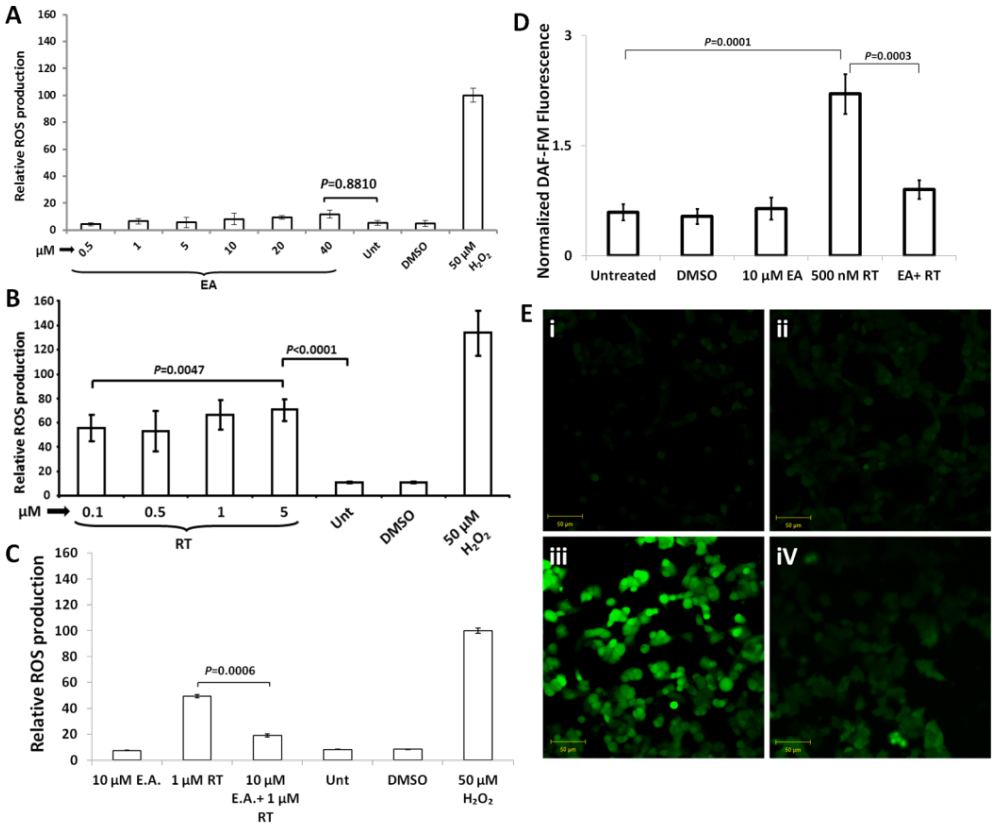

Fig. 3.2. EA treatment attenuates reactive oxygen species (ROS) and reactive nitrogen species (RNS) production in PC12 cell. The ROS levels were measured by DCFH-DA staining assay and analyzed at 24 h after EA treatment (A). The levels of ROS in EA treated cells are presented as fold change compared to the levels in positive control cells. The levels of ROS in RT treated

cells are presented as fold change compared to the levels in positive control cells (B). The ROS quenching activity of EA pretreated PC12 cells followed by 24 h of RT exposure are presented as fold change compared to the levels in positive control cells (C). RT increases RNS production, which is attenuated by EA pre-treatment (D). Representative confocal images confirmed the intracellular RNS production on different treatment (i-DMSO; ii-10µM EA; iii-500 nM RT; iv-EA+RT; E). Statistical significance compared with untreated are illustrated as *P*-value. Each bar represents the average of five replicas and the error bars their standard deviation.

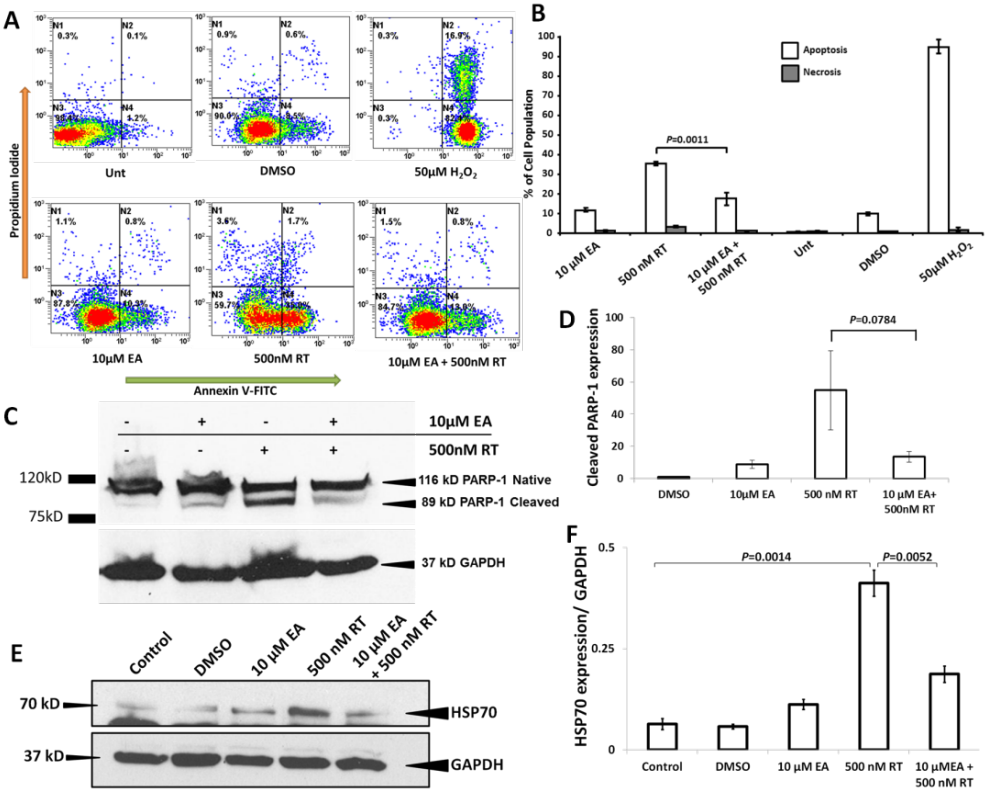

Fig. 3.3. Anti-apoptotic ability of EA through maintaining endoplasmic reticulum (ER) homeostasis. Representative flow cytometric histograms used to measure apoptosis/necrosis distribution: untreated control, vehicle control (DMSO), positive control (50 µM H_2O_2), EA, rotenone and pretreatment with EA and then 24 h rotenone exposure (A). Quantification of apoptotic-necrotic assay under previously mentioned conditions (B). Protective effect of EA (10

μM) against rotenone (500 nM) induced poly (ADP-ribose) polymerase (PARP) cleavage, hallmark of apoptosis progression, in PC12 cells (C). PARP-1 cleavage bands were densitometrically analyzed *via* western blot analysis using Image J software (D). Rotenone (RT) induced over-expression of heat shock protein 70 (HSP70), an ER resident protein, is mitigated by 10μM EA pre-treatment (E). Expression of ER-stress marker protein, HSP70, is quantified under different treatment using Image J (F). Statistical significance between samples is illustrated as *P*-value (n=3).

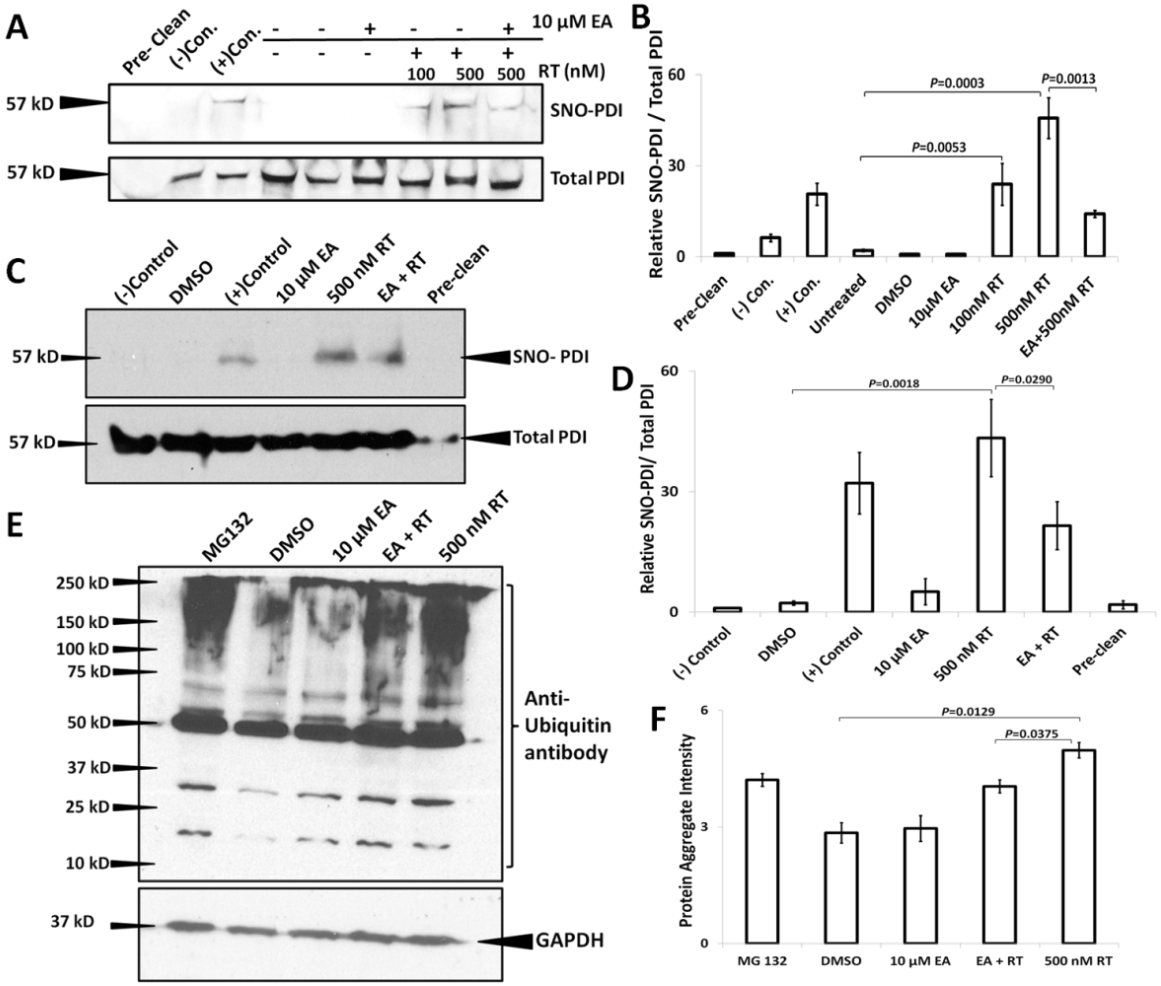

Fig. 3.4. Evaluation of SNO-PDI formation and accumulation of ubiquitinated proteins upon different treatment. Ellagic acid (EA) successfully mitigate the rotenone (RT) induced SNO-PDI

formation (A-D). SNO-PDI signals were detected after pull down the IgG-agarose beads using SNO-CYS BSA antibody then treated with PDI antibody to visualize (A). TMT-switch assay confirm the formation of SNO-PDI after RT treatment and the potential of EA (C). Densitometry analysis of SNO-PDI band (B, D). RT-induced accumulation of ubiquitinated proteins in the insoluble fraction of cell lysate is reduced after 10 µM EA pre-treatment (E, F). All the densitometry analysis were done using Image J software from three independent tests indicated as mean ± S.D. Statistical significance among pairs of samples is annotated as *P*-value (n=3).

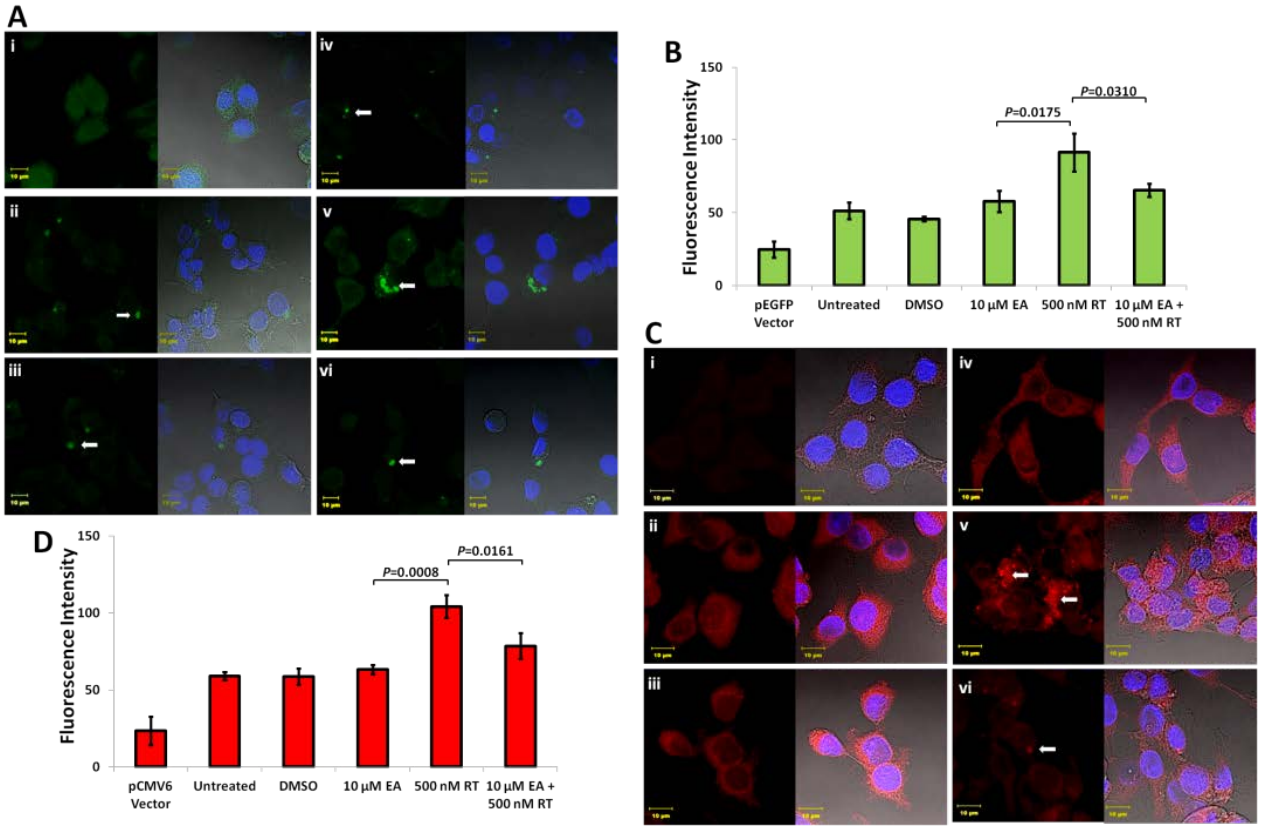

Fig. 3.5. Role of ellagic acid (EA) in GFP-tagged synphilin-1 and α-synuclein aggregation (A-D). Cells transfected with pEGFP-C2 empty vector or pCMV6 empty vector (Panel-i), untreated cells (Panel-ii), cells treated with DMSO 2.5 v/v (Panel-iii), cells treated with 10 µM EA (Panel-iv), cells exposed to rotenone (RT) (500 nM) for 24 h alone (Panel-v) and cells treated with

10μM EA for 6 h before exposed to rotenone (500 nM) for 24 h (Panel-vi) are the different conditions used for this study (A, C). Confocal microscopy images of PC12 cells reveal the presence of cytoplasmic aggregates in cells transfected with pEGFP-tagged synphilin-1 plasmid under different treatment (A). Confocal fluorescence images of PC12 cells revealed the presence of α-synuclein cytoplasmic aggregates under different conditions (C). All the cells were counterstained with DAPI to stain the nucleus (blue color). White arrow indicates expression of synphilin-1/ α-synuclein protein (A, C). Quantification of synphilin-1 (Green channel) or α-synuclein (Red channel) in PC12 cell line upon different treatment using Image J software from n=200 cells indicated as mean ± S.D (B, D). Statistical significance between pairs of samples is illustrated as *P*-value. Each scale bar represents 10μm. Each experiment was assessed in triplicate.

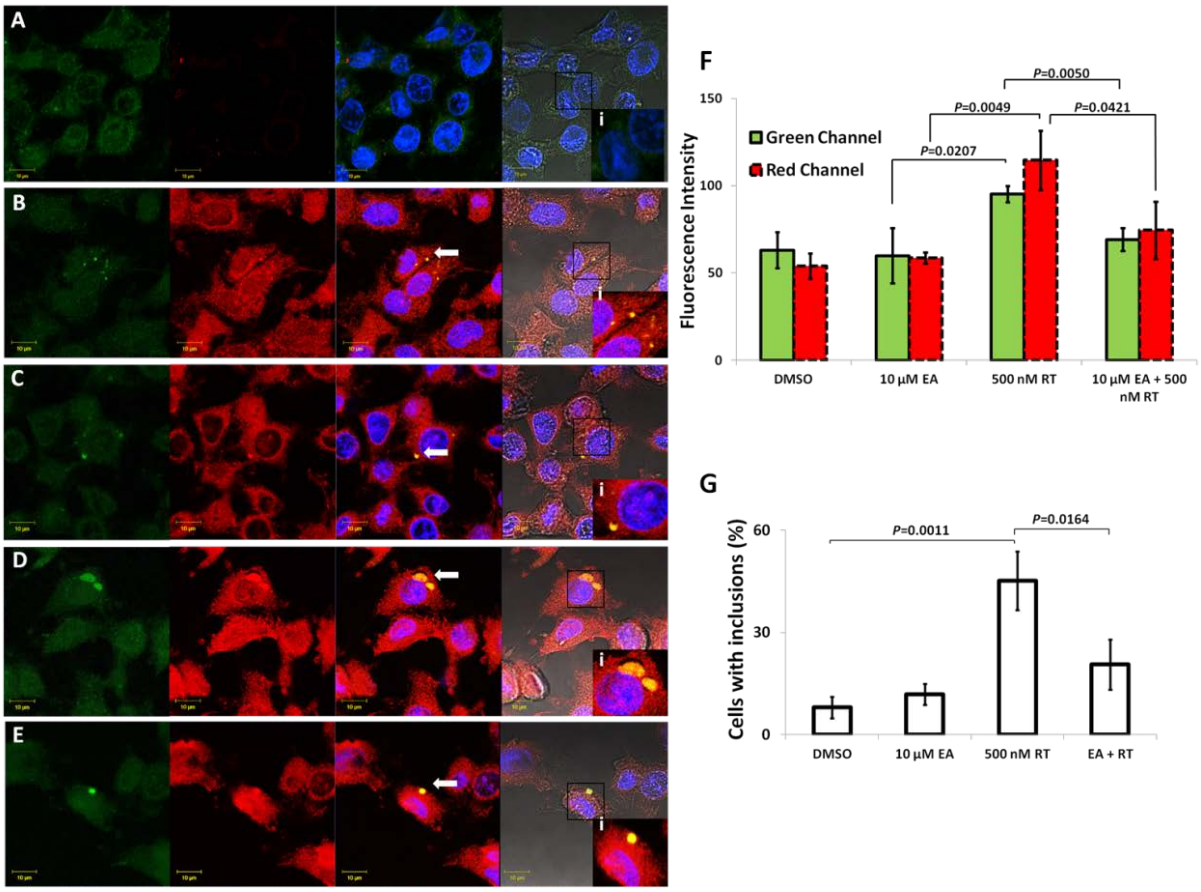

Fig. 3.6. Co-Expression of α-synuclein and synphilin-1 in PC12 cells under rotenone (RT)-induced aggregation and mitigation through ellagic acid (EA) intervention. Cells transfected with pCMV-6 and pEGFP empty vector (A). PC12 cells transfected with α-synuclein and synphilin-1 (2 µg each per condition) and treated with DMSO 0.02% v/v (B). PC12 cells were treated with 10 µM EA for 24 h (C). Cells exposed to 500 nM RT for 24 h (D). Cells pretreated with 10 µM EA for 6 h, then exposed to 500 nM rotenone for 24 h (E). Synphilin-1 was tagged with GFP showing green color and α-synuclein is shown in red color. White arrow indicates co-localization of α-synuclein and synphilin-1 (Yellow color; representative of Lewy body-like inclusion; A-E). Inset-part (i) of each figure at extreme right panel zoomed in the co-localization of α-synuclein and synphilin-1 (1.5X magnification). DAPI was used to stain the nucleus (blue). Quantification of α-synuclein expression (Red channel) and synphilin-1 (Green channel) in PC12 cell line upon

different treatment using Image J software from n=200 cells indicated as mean ± S.D (F). Statistical significance compared with untreated are illustrated as *P*-value. Each scale bar represents 10µm. Each experiment was assessed in triplicate. Total number of cytoplasmic inclusion body significantly elevated after RT treatment although EA pre-treatment decrease the inclusion body count in PC 12 cell (G; Supplementary Fig. 3.4).

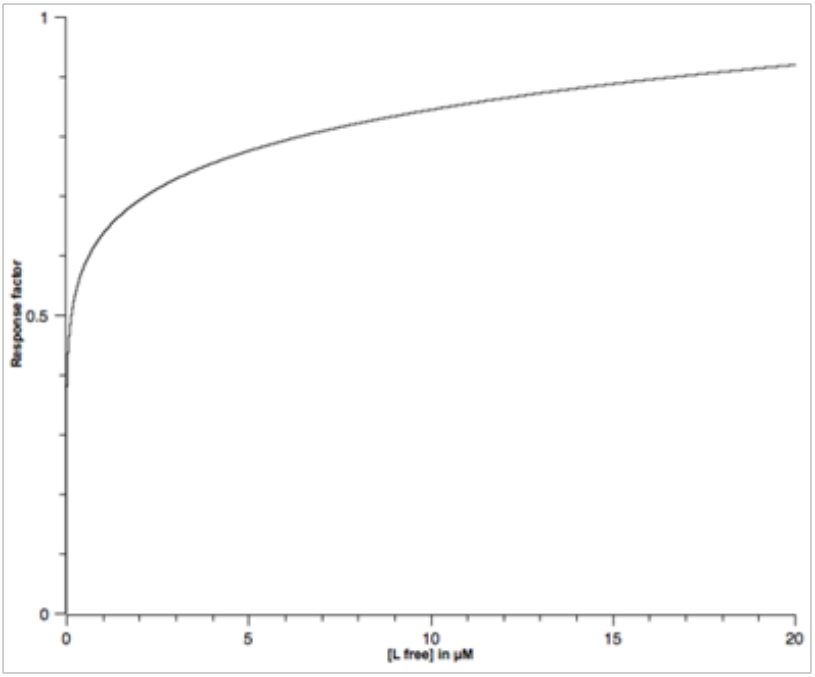

Fig. 3.7. Fluorescence emission profiles for the binding of ellagic acid (0 to 140 µM) to native human serum albumin (20µM). A) Solid line represents a theoretical one-site binding profile. Fluorescence parameters were: λexc = 280 nm and λem = 310 and 340 nm. All solutions were at 200 mM Tris-HCl, 1 mM EDTA, pH 7.5 and were prepared at room temperature 24 ± 1 °C.

3.5 Supportive Information

Live PC12 cell imaging to determine cytotoxicity (Supplementary Fig. 3.1), over-expression of α-synuclein in PC12 cell (Supplementary Fig. 3.2), co-localization quantification of α-synuclein and synphilin-1-GFP (Supplementary Fig. 3.3), quantification of inclusion bodies in PC12 cell (Supplementary Fig. 3.4), Specificity of S-nitrosocysteine antibody (Supplementary Fig. 3.5) and analytical data (Mass spectrometry analysis) of ellagic acid and TNM (Table S1)

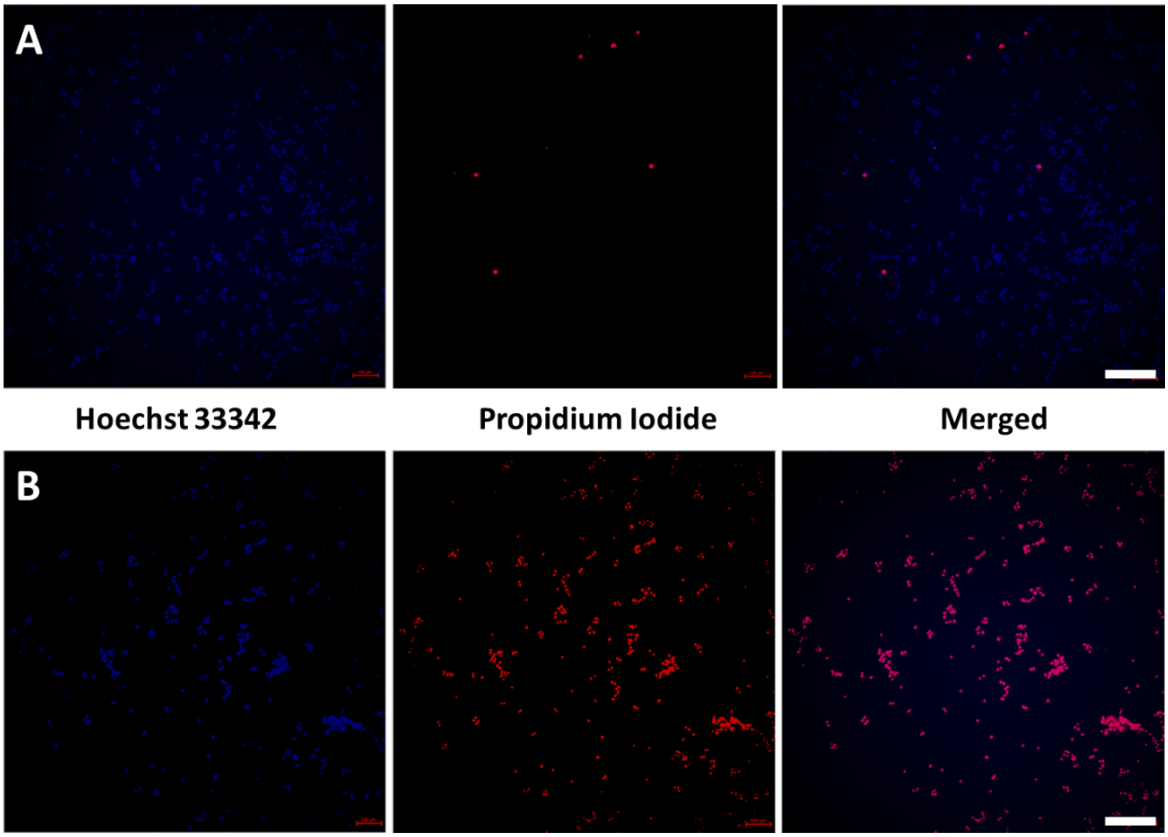

Supplementary Fig. 3.1. Live-cell images utilized to quantify cytotoxicity on PC12 cells. Untreated cells as negative control (A). Cells treated with 50 µM H_2O_2 as positive control (B). Total numbers of cells were labeled with Hoechst, emitting blue signal (left panels); whereas dead cells were labeled with propidium iodide, emitting red signal (middle panels). Merged images (right panels) are depicting cells in blue (live) and cells in magenta color (dead) as an outcome of co-localization of red (PI) and blue (Hoechst) colors. Images were acquired and

analyzed utilizing a BD Pathway 855 Bioimager system, assisted with BD AttoVision v1.6.2 software. The scale bar is equal to 100 µm.

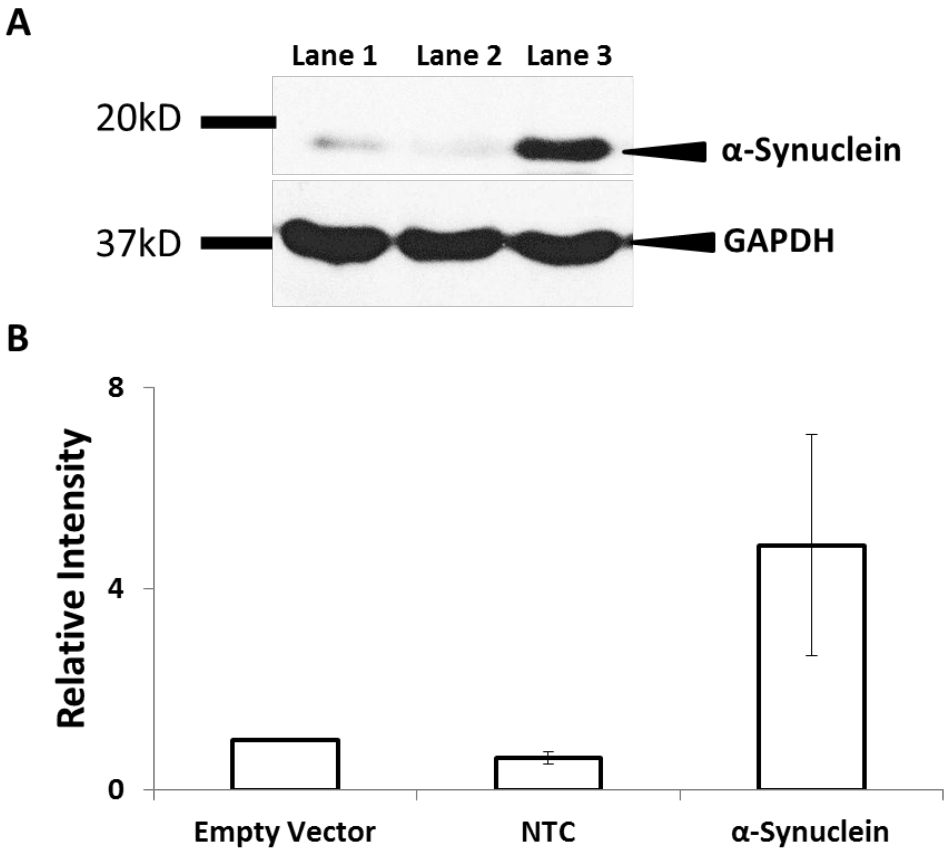

Supplementary Fig. 3.2. Expression of α-Synuclein in transfected PC12 cells (A). Extracts from cells transfected with the empty vector pCMV6 (Lane 1), non-transfected cell (NTC; Lane 2), and transfected with pCMV6-α-synuclein (Lane 3). Quantification of relative intensity of α-synuclein bands using ImageJ software are depicted as average and standard deviation from triplicates (B).

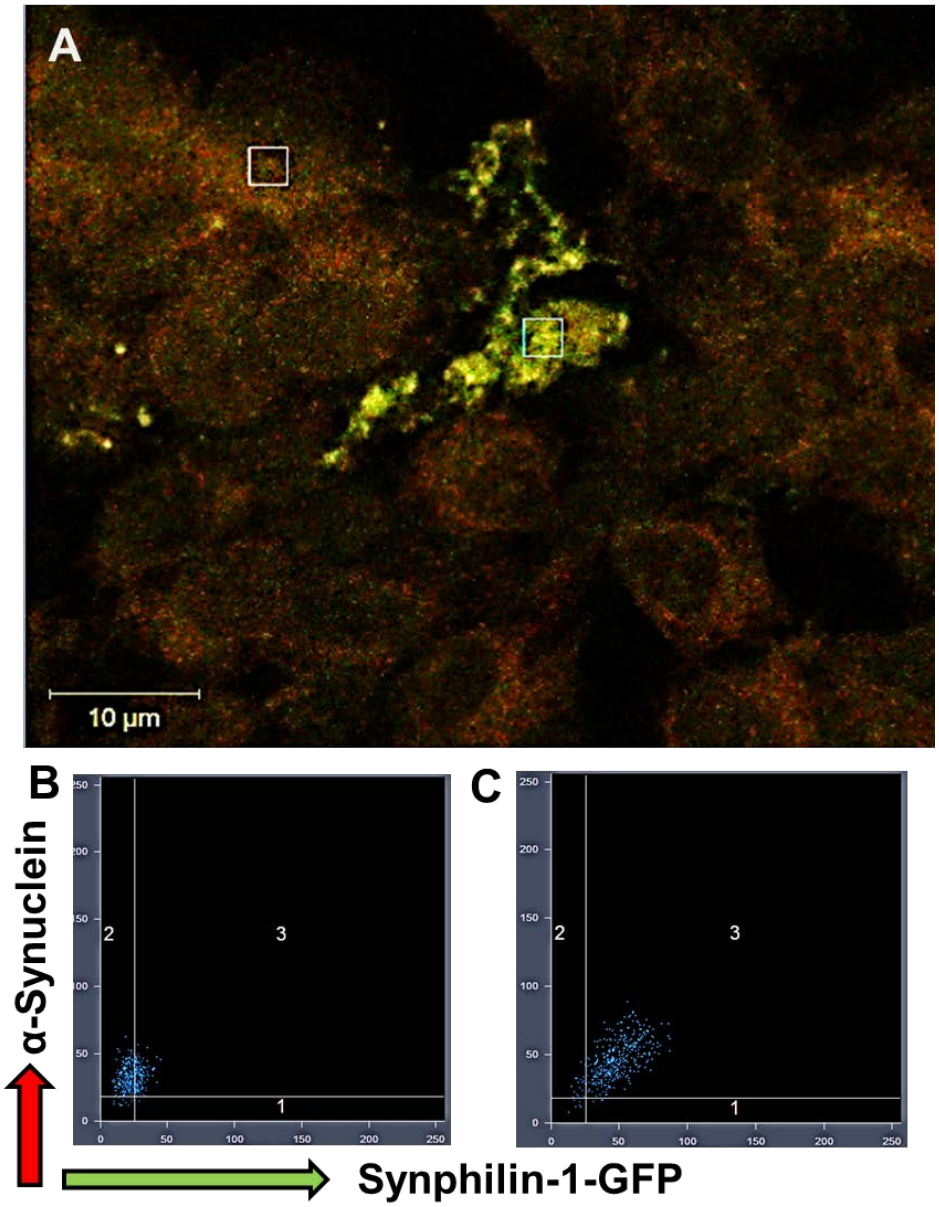

Supplementary Fig. 3.3. Co-localization of synphilin-1-GFP and α-synuclein in PC12 cells. Merged dual-channel image (green and red) from doubly-labelled transfected PC12 cell with two plasmid constructs, carrying a Synphilin-1-GFP or α-Synuclein are shown respectively (A). Note that in the image in panel A, two region of interest (ROI; squares) are included. The numbers at the bottom of each ROI are overlap co-localization coefficient values of the delimitated areas according with Manders.[1] Panels B and C are the co-localization dot plot histograms of the ROIs localized in top left and center in panel A, respectively, where each pixel

is presented as a dot. Pixels with well co-localized signals, appear in the quadrant 3 (top right) of the histograms (B and C), as a scatter diagonal population. Overlap coefficient values range from 0 to 1; a value of 1 represents 100% of co-localization of both fluorescence signals, whereas 0 represent complete absence of co-localization. ZEN 2009 software was utilized to perform the overlap coefficient analysis.

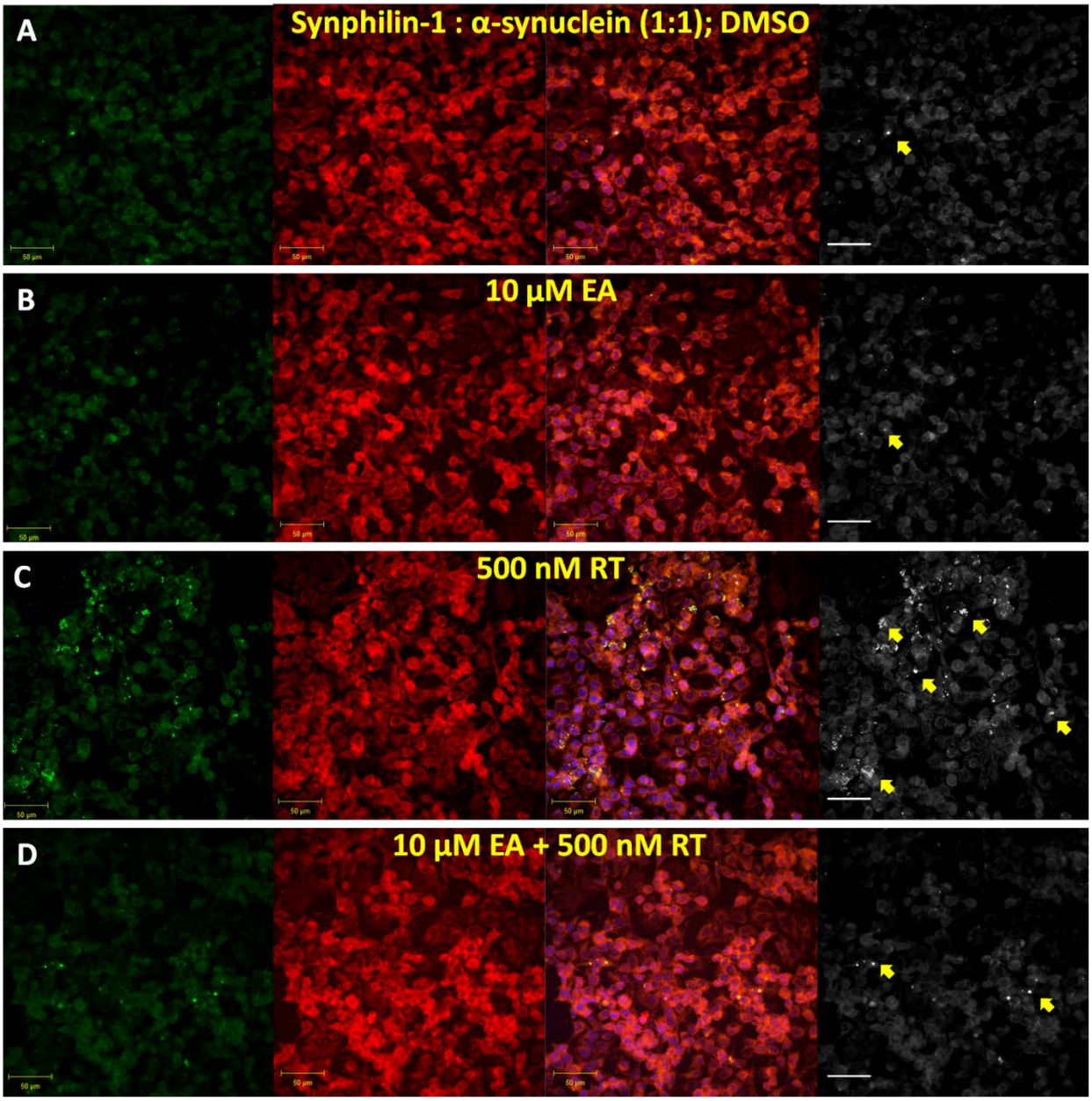

Supplementary Fig. 3.4. Quantification of total co-localized aggregates (mimic of Lewy body) of α-synuclein and synphilin-1 expressed in PC12 cells under different treatment conditions. Transfected PC12 cells were untreated or stressed with different treatments. Cells transfected with α-synuclein and synphilin-1 then treated with DMSO 0.02% v/v (A); cells treated with 10 µM EA (B); cells exposed to 500 nM rotenone for 24 h alone (C); pre-treatment with 10 µM EA

for 6 h and then exposed to rotenone for another 24 h (D). All the cells were counterstained with DAPI to delimitate the nucleus (Blue color). Yellow arrows indicate the presence of aggregates. Synphilin-1 was tagged with GFP showing green color and α-synuclein is shown in red color. Yellow color represents co- localization of α-synuclein and synphilin-1. Extreme right panel of each figure represents the co-localization of α-synuclein and synphilin-1 indicated as white spot using Image J co-localization software (n=200). The scale bar represents 50 µm. Each experiment was repeated in triplicate.

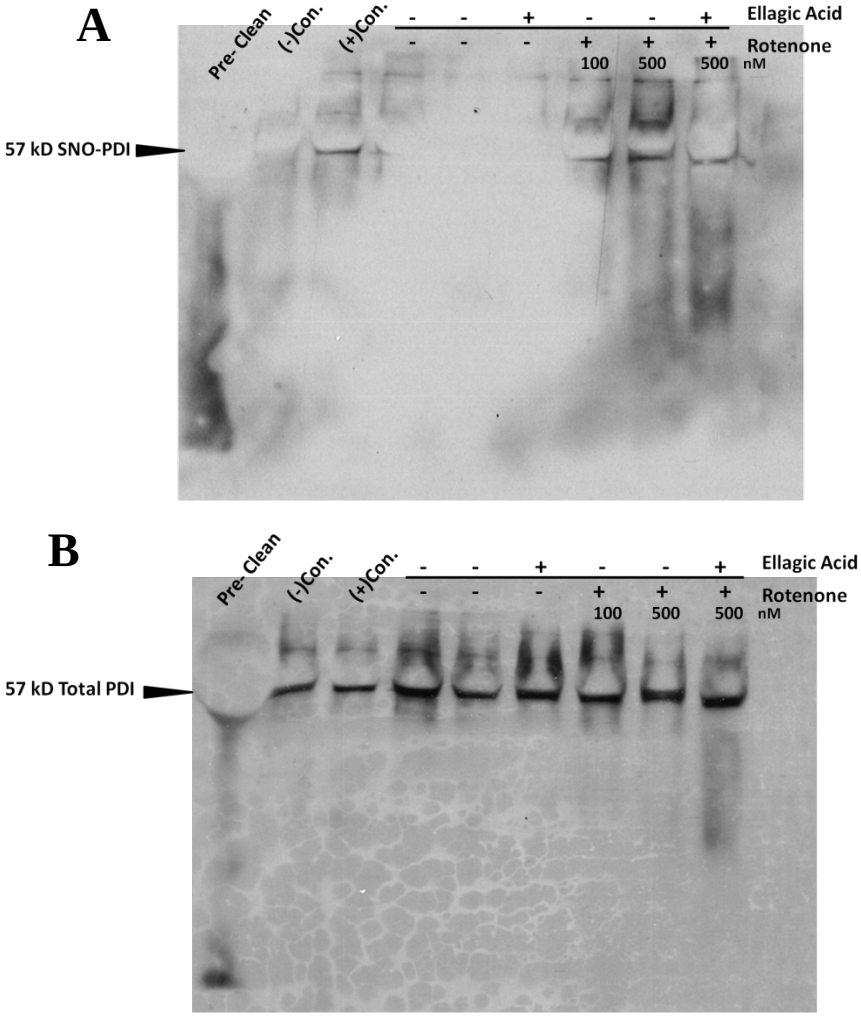

Supplementary Fig. 3.5. Detection of SNO-PDI in rotenone treated PC12 cell line. A) Western blot signals of SNO-PDI in PC12 cell after treatment with or without rotenone and ellagic acid.

To prepare positive and negative control samples, cells were incubated for 30 minutes at room temperature with 200 µM S-nitrosoglutathione or DTT, respectively. SNO-PDI signals were detected using SNO-CYS BSA antibody after pull down the IgG-agarose beads treated whole cell lysate against PDI antibody. Proteins were separated in 12% SDS-PAGE, blotted and visualized with specific antibodies. B) The total PDI bands were detected using specific monoclonal PDI antibody. The experiment was repeated in triplicate.

Supporting Information

Table S1. EA as a NO radical scavenger: *in vitro* study

ESI negative mode		**ESI negative mode after TNM use**	
Mass	Identity	Mass	Identity
301.232	[M - H]	301.197	[M - H]
602.469	[2M – H]	348.817	[M- H + NO_2]

Chapter 4:

Beta amyloid (25-35) induced Lewy body-like inclusions formation mediated by S-nitrosylation of PDI.

4.1 Introduction

Alzheimer's disease, a form of irreversible dementia characterized by slow decline of cognitive function, currently affects around 27 million people worldwide[1]. Now in the United States AD is the sixth leading cause of death, which on an average occurring nine years after diagnosis[1-4]. Transformation from alpha helical to beta sheet dominated structure of different notorious protein is the key event to ignite neurodegenerative diseases. Pathological findings of human AD brain confirm the involvement of extracellular beta-amyloid (Aβ) plaques and hyperphosphorylated intracellular tau tangles[5,6]. Cell surface receptor protein APP is the precursor of Aβ as a result of β-secretase and γ-secretase activity[7]. According to amyloid cascade hypothesis, an increase in the Aβ42/ Aβ40 ratio alter the ionic homeostasis and oxidative stress leading to hyperphosphorylation of tau; tangle formation ultimately causing axonal dysfunction and neuronal cell death [5,8,9]. Interestingly different fragment of Aβ (eg. 1-28; 25-35; 34-42) showcase same bio-physical and toxicological property as the full length version of Aβ (16-18). Aβ (25-35) fragment is more toxic than the other fragments because of its beta-sheet fibrils formation and considered as the active domain of Aβ (1-42)[10-12].

The late onset characteristic of AD, in spite of the presence of the mutation since birth, gave rise to speculation of prion like self-propagating Aβ protein aggregates throughout the brain[13,14]. Several evidences argue that Aβ is a prion[13,15-17]. There are direct confirmation of the presence of Aβ prions, demarcated as Aβ aggresome adept of self-propagation within the brain[16,17]. Though it is not clear what accounts for the different potencies of the brain-derived and synthetic beta-amyloid. Failure of the ubiquitin-proteasome system that normally degrades misfolded proteins leads to the formation of so-called aggresomes, pericentriolar inclusions[18,19]. These proteinaceous aggregates can induce cytosolic assembly of aggregation-prone soluble

proteins through seeding-like mechanism that share similarities with prion propagation[14-16,20]. We hypothesize that peptide fragment inside Aβ (1-42), which is (25-35), will also act like prion. Readily soluble Aβ (25-35) forms aggregate which can be fibriler or oligomeric in nature depending on the pH of the solvent. A beta (25-35) is the smallest peptide segment, which can replicate the same kind of physiochemical and pathological condition as long a beta (1-42) peptide.

Neuro-pathological findings of patients with PD reveal the presence of α-synuclein, an amyloidogenic protein, within Lewy bodies, making it a key biomarker implicated in the pathogenesis of PD[21]. The minor Parkinsonian biomarker, synphilin-1 also found to be coexisted with α-synuclein in the Lewy body [21]. Lewy body pathology is also found in a large number of AD patients, also commonly known as Lewy body variant of Alzheimer's disease (AD-LBV)[22]. Unfortunately, AD-LBV patients showed accelerated cognitive decline as well as early demise rate [22]. Also, the overlapping clinical and pathological features of brain amyloidogenesis in AD and PD patients gave rise to the speculation of mechanistic connection in between AD and PD etiology[21-24]. Previous study suggested that Aβ (1-42) oligomer can influence the folding of amyloidogenic protein via cross-seeding mechanism[15,24]. It has also been reported that the Aβ (1-42) oligomer can induce the formation of oligomeric α-synuclein, but in cell free system[24]. Change in expression and aggregation of α-Synuclein upon Aβ (25-35) incubation will lead us to understand the complexity of AD and alleged relation with PD. As there is little or no clear idea of the mechanism by which Aβ (25-35) exerted its influence on amyloidogenic proteins, we decided to ask why this phenomenon is taking place.

Excess reactive oxygen species (ROS) and reactive nitrogen species (RNS) generation, has been demonstrated with high importance in AD and PD (Parkinson's disease)[19,25,26]. There is

an emerging body of evidence suggesting that Aβ (1-42) could induce apoptotic cell death via ROS stress in a variety of cells[26]. The Aβ (25-35) peptide fragment also follows the same trend in ROS production as of Aβ (1-42)[11]. But the role of Aβ (25-35) in RNS production inside the cell is unclear. It is been well established that nitrosative stress plays an important role in apoptosis[19], therefore, understanding the interface between nitrosative stress generation and apoptosis, is pivotal in neurodegenerative diseases research. Several studies showed that protein-disulfide isomerase (PDI), a key ER-resident chaperone protein, helps in protein folding. PDI get chemically modified by RNS to form S-nitroso-PDI in AD and PD brains[27-29]. Excess amount of RNS production is capable of promoting ER stress by inactivating the catalytic sites of chaperone proteins. Recent study showed not only the modulation of enzymatic activity but redistribution of PDI upon posttranslational modification as well[30]. Reports on the immunoreactivity of PDI with Lewy body (PD pathology) as well as neurofibrilar tangles (AD pathology) give rise to the speculation of direct involvement with AD and PD specific proteins[31-34]. It is interesting to note that amyloidogenic protein, α-synuclein often found at the wrong side of different neurodegenerative disease namely: PD, PD with dementia, Lewy body variant disease and AD-LBV[22-24]. We wanted to investigate the change in PDI expression and its modification, if any, to explain the cause of Aβ (25-35) induced stress in SHSY-5Y cell.

So, we hypothesize that posttranslational modification of PDI as a function of beta-amyloid (25-35) aggregosome, can lead to aggregation of synphillin-1 and α-synuclein when expressed or co-expressed by dopaminergic cells. In addition, Aβ (25-35) peptide fragment could lead to ER stress mediated activation of apoptotic pathway through SNO-PDI formation. We also hypothesized that Aβ (25-35) can influence the interaction of PDI and synuclein protein. To

test our hypotheses, we generated dopaminergic cell line that expresses GFP-tagged synphilin-1 protein and α-synuclein either alone or in combination.

4.2 Experimental Procedure

Genetics

Beta amyloid (25-35) and tagged with Hilyte-488 (Hilyte™ Fluor 488 - Gly - Ser - Asn - Lys - Gly - Ala - Ile - Ile - Gly - Leu - Met - OH) were purchased from AnaSpec Inc (San Jose, CA). Commercially sourced reagents are following: 4-amino-5-methylamino- 2",7"-difluorofluorescein diacetate (DAF-FM diacetate) and Lipofectamine® LTX with Plus reagent (Life technologies); anti-PDI antibody (Abcam); polyclonal anti-S-nitrosocysteine antibody (Abcam); normal rabbit IgG (SantaCruzBio); mouse monoclonal anti- GAPDH (Glyceraldehyde 3-phosphate dehydrogenase) antibody and rabbit monoclonal anti-PARP antibody (Cell Signaling Technology, Danvers, MA); Annexin V-FITC apoptosis kit (Beckman Coulter, Miami, FL), anti-mouse and anti rabbit horseradish peroxidase (HRP)-conjugated (KPL Biomedical); Hoechst 33342 fluorescent stain (Invitrogen, Eugene, OR); Propidium Iodide (PI) (Invitrogen, Eugene, OR); Human neuroblastoma cell line SH-SY5Y (ATCC, Manassas, VA). Cells were transfected with the pEGFP-C2 or synphilin-1/pEGFP-C2 and pCMV6 or α-synuclein/pCMV6 plasmid as previously described [19,25].

Cell culture and transfection

SH-SY5Y cells were cultured in DMEM and Ham's F12 media mixture (1:1) supplemented with 10% fetal bovine serum (Atlanta Biologicals) and 1% penicillin–streptomycin (Sigma). Cells were grown at 37°C in humidified 5% carbon dioxide atmosphere. SH-SY5Y cells (1×10^6 cells/well) were seeded onto suitable plates according to the need of the experiment and incubated for 12 h. Cell transfections were performed, after reaching 60-70%

confluency, with pEGFP-C2 control (without insert) or pEGFP-C2 carrying the fusion protein GFP-synphilin-1, and pCMV6 control or pCMV6 inserted with α-synuclein as per recommendation of manufacture; Lipofectamine® LTX with Plus™ Reagent (Lifetechnologies, NY). After transfection, the cells were incubated overnight to allow expression of proteins.

Detection of intracellular RNS and ROS

DAF-FM is an oxidation-sensitive fluorescent dye where 4-amino-5-methylamino- 2",7"-difluorofluorescein (DAF FM) is the fluorescent part. Then, cells were harvested (5000/well) on 96-well plate, washed with PBS, and analyzed immediately with a micro-plate reader fluorometer (Labsystems Fluoroskan Ascent) using excitation at 485 nm and emission at 518 nm. DCFH-DA is an oxidation-sensitive fluorescent dye where 2', 7'-dichlorofluorescein (DCF) is the fluorescent part. Cells were loaded with the dye by exposing them to 10 µM MDCFH-DA for 20 min at 37^{o}C. The cells were then harvested, washed with PBS, and analyzed immediately with a microplate reader fluorometer (Labsystems Fluoroskan Ascent) using excitation at 485 nm, and emission at 518 nm. Each data point was assessed in quintuplicate[19]. Images were captured using Carl Zeiss LSM 700 microscope, 20X lens.

Dynamic Light Scattering studies

For the dynamic light scattering (DLS) measurements the commercial instrument Zetasizer Nano-S was used (Malvern Instruments Ltd, UK; www.malvern.com). He-Ne laser (633nm) was used as a light source for precise particle sizing in the range of 0.3nm – 10.0 microns (diameter). The aggregation kinetics of Beta amyloid (25-35) was studied by DLS. A solution for the experiment was prepared using double distilled water. The buffer was placed in a cuvette and pre-incubated for 10 min at room temperature. The process of aggregation was begun by the addition of an aliquot of the Beta amyloid (25-35) from the stock solution.

Flow cytometric assay

SH-SY5Y cells were seeded on 24-well micro plate at density of 20,000 cells/ well, and cultured as described. Cells were treated with different concentrations of Amyloid beta (25-35) alone, to determine its possible cytotoxic effect. As control for non-specific effects, distilled water vehicle control, as contained in the experimental samples, was included at final concentration of 0.1% v/v. [19]. Cells from each individual well were collected, washed and processed essentially as described previously[19,25]. Briefly, cells were concurrently stained by re-suspending them in a solution containing Annexin V-FITC, and PI dissolved in 100 µl of binding buffer (Beckman Coulter, Miami, FL). After incubation for 15 min on ice in the dark, ice-cold binding buffer (400 µl) was added to the cell suspensions, gently homogenized, and immediately analyzed by flow cytometry. The percentage of total apoptotic cells per sample is annotated as the sum of both early and late stages of apoptosis (Annexin V-FITC positive), bottom right quadrant and top right quadrant, respectively. For each sample, approximately 10,000 individual events were acquired using flow cytometer (Cytomics FC 500; Beckman Coulter, Miami, FL), and data was analyzed with CXP software (Beckman Coulter, Miami, FL). Every experimental point, as well as all controls, was assessed in quintuplicate.

Biochemistry

Total cell lysates were prepared by washing the cells with cold Tris-buffered saline, collected by centrifugation (3003g, 5 min at 4°C, and extracted by sonication in buffer containing 10 mM Tris–HCl (pH 7.4), 10 mM EDTA, 0.5% (v/v) SDS and protease inhibitors (Sigma). Total protein concentrations were measured using a bicinchonic acid kit (Pierce, Rockford, IL) and BSA as standard. Equal amounts of protein (approximately 10 µg per lane)

were separated using SDS-polyacrylamide gel electrophoresis, and then transferred to polyvinyl difluoride (PVDF) membranes. Blots were incubated in blocking buffer (5%, w/v, dried skimmed milk in Tris-buffered saline, pH 7.4, and 0.1% Tween 20) followed by incubation with anti-PARP/ anti-synphilin-1/ α-synuclein rabbit polyclonal antibody (1:1000), or anti-GAPDH/ anti-actin (1:1000/ 1:2500 dilution) diluted in blocking buffer for 1 h followed by horseradish peroxidase (HRP)-conjugated goat anti-rabbit in 1% BSA/TBST for 30 min. Chemiluminescence (ECL-plus or SuperSignal West Pico Chemiluminescent Substrate) was used according to the manufacturer's instructions (Amersham or Pierce Biotechnology Inc.). GAPDH/actin was used as housekeeping protein loading control.

Confocal microscopy and immunocytochemistry

Cells transfected with vector or EGFP-synphilin-1/ α-synuclein were washed after treatment, fixed with 4% paraformaldehyde in PBS, stained with DAPI and mounted under ProLong antifade medium (Molecular Probes). To stain for synphilin-1/ α-synuclein, cells were: fixed as above, permeabilized with 0.1% (w/v) saponin in PBS, blocked with PBS plus 5% goat serum, 5% FBS and 0.1% TWEEN 20, followed by incubation with primary antibody (overnight at 4ºC) and secondary rhodamine-conjugated goat anti-mouse (1:10000; KPL Biomedical), and DAPI staining. Fluorescence confocal images were captured utilizing LSM 700 confocal microscope and assisted with ZEN 2009 software (Zeiss, New York, NY)[19].

Co-immunoprecipitation

Cell lysate was prepared following the same procedure as western blot[25]. Proteins were separated in 12% SDS-PAGE, blotted and visualized with selected antibodies. 200 µl lysates (1 mg/ml) of SHSY-5Y cell homogenates were pre-cleaned by 50 µL protein G agarose (Santa Cruz Biotechnology) to detect S-nitrosylated PDI, as previously reported[19]. In short, 2.5 µg

polyclonal anti-S-nitrosocysteine antibody (Abcam) was added to the supernatant, and incubated for 1 h at 4°C. After centrigugation, pellet was washed three times with 1 mL chilled TBS containing 1% (v/v) tween-20 and 1 mg/ml BSA and 0.5 M Tris–HCl respectively. Following the final centrifugation step, the pellet was re-suspended in SDS sample buffer, subjected to western blot analysis, and immunostained for PDI as described previously[19]. Chemiluminescence (ECL-plus or SuperSignal West Pico Chemiluminescent Substrate) was used according to the manufacturer's instructions (Amersham or Pierce Biotechnology Inc.). Experiment was assessed in triplicate.

Co-immunoprecipitation, immuno-fluorescence and inclusion body quantification

To quantify protein level detected by western blot, we used the Image J software. In order to quantify the fluorescence of expressed proteins, random fields for each tested condition were obtained at the same magnification (63X oil immersion, zoom 1.5X). Then, a region of interest (ROI) with an area of 400 pixels (20X20) was chosen, and the average intensity of fluorescence within the ROI was measured in the cytosol of every transfected cell present in the field. Over 100 cells were analyzed for each condition. The values obtained were averaged and were plotted using a bar graph. The results were obtained from more than, or equal to three independent experiments. To count the cells with inclusion body, we used colocalization finder in Image J software. Randomly selected 10 different fields (100 cells / field) were counted in three different sets of experiments to avoid the prejudice (Supplementary Fig.4.1).

Statistical calculation

Every data point was collected independently and in triplicate. To note experimental viability and variability, data were presented as the average with its corresponding standard deviation. Statistical analysis was performed using two-tailed paired Student's t-tests to denote

the statistical significance of variances between experimental samples and their corresponding controls. To identify if there is a significant difference between two groups, a value of $P< 0.05$ was considered significant. We denote the actual *P*-value in each graph wherever needed.

4.3 Results and discussion

RNS mediated apoptosis in SH-SY5Y upon Aβ (25-35) insult

Aβ (25-35), an internal fragment of Aβ (1-42), was readily aggregated when it came in contact with distilled water molecule (Fig. 4.1A) because of the hydrophobic property[11,20,26]. Average diameter of the aggregates was measured as 162 nm ± 37.32 using dynamic light scattering under controlled condition. Estimated molecular weight of the aggregates was 9.79 kDa when added to dist. water (1:100), whereas the molecular weight of a single peptide fragment is 1060.3 Da.

SH-SY5Y cell line, designed to mimic the dopaminergic neuronal cell, was used for our whole study. We performed flow cytometry based cytotoxicity analysis of Aβ (25-35) peptide fragment in SH-SY5Y cells using PI dye (Fig 4.1, B and C). Percentage of cell death increased in a dose dependent manner from 1 µM to 50 µM (P=0.0006) (from ~11% at 1 µM to ~42% at 50 µM Aβ (25-35) after 48 h incubation at 37ºC). Quantitative analysis (Fig. 4.1C) suggest that even 5 µM aggregated Aβ (25-35) is significantly toxic, whereas 50 µM is highly toxic to the cell relative to the untreated condition (P=0.0069 & P=0.0003 respectively).

The pathway by which Aβ (25-35) insult leads to cell death was also investigated (Fig. 4.1, D-G). Annexin V-FITC, an apoptotic marker protein, and PI (1:1 mixture) were used in flow cytometry based analysis of apoptosis and necrosis. Cells were treated with different concentrations of Aβ (25-35) (1 µM, 5 µM, 10 µM, 20 µM and 50 µM) for 24 h at proper cell growth conditions. 50 µM H_2O_2 was used as positive control where substantial increase in early and late apoptosis denoted in lower right and top right quadrant of the matrix plot (Fig. 4.1D; top row second histogram from right). Cells treated with distilled H_2O (0.1% v/v), 1 µM Aβ (25-35) and untreated cells did not show substantial increase either in necrosis or apoptosis. However, we

found high statistical significance when compared between 1 μM and 50 μM treatment conditions (*P*=0.0309) in apoptosis segment (Fig. 4.1E). Necrotic cell count after 24 h treatment is not quite high in any conditions, and it is visible only after 48 h exposure to Aβ (25-35). Similar to cytotoxicity data, 5 μM of Aβ (25-35) can significantly induce the apoptotic cell cycle after 24 h relative to untreated condition (*P*=0.026). Representative histograms of cytotoxicity and apoptosis-necrosis are shown in Fig. 4.1, B and D respectively.

We assured the ability of aggregated Aβ (25-35) to induce apoptosis by measuring cleavage of native PARP-1 using immuno-blot technique (Fig. 4.1, F and G). Densitometric analysis (Fig. 4.1G) of the PARP expression revealed that treatment with 1 μM Aβ (25-35) for 24 h clearly can induce apoptotic cycle in SH-SY5Y cells (~25% increase in PARP-1 cleavage compared to untreated; *P*=0.0092). This was confirmed by a dense band of the cleaved PARP-1 at 89kD (Fig. 4.1F; third lane from right). These results also support the flow cytometry analysis performed to detect apoptosis and necrosis in SH-SY5Y cell line. This data supports all the recent work done in this field to confirm the cytotoxicity of small 11 amino acids long peptide fragment of beta amyloid[11,35].

In 96 well plates based fluorometric DAF FM and DCF-DA assay, we confirmed the modulation of RNS and ROS level respectively in SHSY-5Y upon 24 h exposure to different doses of Aβ (25-35) (Fig. 4.1 H-J). In the case of DAF FM based assay, we observed dose dependent increase of RNS level (Fig. 4.1H, I). Confocal microscopy image confirmed the intracellular level of RNS production (Fig. 4H) upon different treatment conditions (panel i, untreated; panel ii, 1μM; panel iii, 10 μM; panel iv, 20 μM Aβ (25-35) treatment respectively). The increase in the intracellular RNS level is highly significant when untreated and 20 μM Aβ (25-35) treatment are compared (*P*=.0573; Fig. 4.1I). Whereas DCF-DA assay data confirmed no

increase in ROS production even at 50 μM Aβ (25-35) treatment for 24 h in SHSY-5Y cell (Fig. 4.1J; *P*=0.3612). It was highly interesting to observe only significant increase in RNS level when compared to ROS level after Aβ (25-35) treatment under same conditions. As the ROS data contradict many findings suggested by different research group[35,36], DCF-DA assay was repeated more than ten times which helped to consolidate the result itself. So, it can be suggested that excess level of RNS formation lead to the activation of apoptotic cycle in SHSY-5Y cell upon Aβ (25-35) treatment.

Role of Aβ (25-35) in Synphilin-1 and α-synuclein aggregation

Failure of the ubiquitin-proteasome system (UPS) that normally degrades misfolded proteins leads to the formation of so-called aggresomes[18,19,37]. Proteinaceous aggregates can induce cytosolic assembly of aggregation-prone soluble proteins through seeding-like mechanism that share similarities with prion propagation[13-16,20,29]. Recent findings indicated the prion-like propagation of Aβ (1-42), demarcated as Aβ aggresome adept of self-propagation within the brain[15,16]. The overlapping clinical and pathological features of brain amyloidogenesis in AD and PD patients gave rise to the speculation of mechanistic connection in between AD and PD etiology[21-24]. The major Parkinsonian biomarker α-synuclein is associated with the synthesis of dopamine neurotransmitter[38]. Synphilin-1 is a minor Parkinsonian biomarker and the primary constituent within Lewy neurites along with α-synuclein[39]. Interestingly, both amyloid beta fragment and α-synuclein are categorized as amyloidogenic proteins where alpha helix dominated functional protein transformed into beta sheet dominated rogue protein[40]. Therefore, we examined whether Aβ can affect the folding of synphilin-1. In figure 4.2, we analyze the cross reaction of Aβ (25-35) in aggregation of synphillin-1, α-synuclein.

Dopaminergic SHSY-5Y cells were transiently transfected or co-transfected (1:1) with synphillin-1 and/ or α-synuclein containing pEGFP C2 and/ or pCMV6 plasmid respectively (Fig. 4.2). Expression pattern of synphilin-1 (Fig. 4.2A.ii) and α-synuclein (Fig. 4.2C.ii) in SHSY-5Y under untreated condition is similar as previously reported by our laboratory[19,25]. In contrast, after Aβ (25-35) treatment the SHSY-5Y cell showed increased cytosolic aggregation (white arrow) of both synphilin-1 (Fig. 4.2A.iv; v; vi) and α-synuclein (Fig. 4.2C.iv; v; vi) proteins. The expression pattern of these two proteins upon vehicle (20 µl H_2O) treatment did not differ from the untreated conditions (Fig. 4.2A.iii; Fig. 4.2C.iii) as expected. The fluorescent intensity of synphilin-1 and α-synuclein under different treatment is plotted in Fig. 4.2B and Fig. 4.2D respectively. In case of fused EGFP-synphilin-1 protein, we did not notice any change in intensity up to 1 µM Aβ (25-35) treatment relative to untreated condition (P=0.1456). However, 10 µM and 20 µM Aβ (25-35) treatment significantly changed (P=0.0075) the intensity level of EGFP-synphilin-1 relative to control (Fig. 4.2B). There is notable difference in intensity of EGFP-synphilin-1 protein upon 1 µM and 10 µM Aβ (25-35) treatment for 24 h (P=0.0466). The effect of Aβ (25-35) on α-synuclein seems like more dramatic. 1 µM Aβ (25-35) treatment for 24 h significantly increased (P=0.0003) the intensity of α-synuclein protein (Fig. 4.2D). Interestingly, at 20 µM Aβ (25-35) treatment the maximum intensity of EGFP-synphilin-1 and α-synuclein proteins are 80 a.u. and 120 a.u. respectively. The difference between the intensity of these two Parkinsonian proteins (~50%) is highly noticeable under the same treatment condition. It is also evident that cellular interaction increased or clumped together dramatically only in case of α-synuclein transfected SHSY-5Y cell after Aβ (25-35) treatment (Fig. 4.2C). It can be interpreted from these data that Aβ (25-35) is more cross-reactive to α-synuclein relative to EGFP-synphilin-1.

Synphilin-1 and α-synuclein are found in Lewy body of PD patient's brains[39,41]. To investigate the effect of Aβ (25-35), we further created the Lewy body like debris by co-transfecting (1:1) synphilin-1 and α-synuclein in SHSY-5Y cell line. pEGFP-synphilin-1 plasmid (green signal) and pCMV6-α-synuclein plasmid (red signal) was used for this study[19]. Co-localization of α-synuclein and synphilin-1 was detected in untreated and vehicle (H_2O) treated cells as evidenced by the presence of the yellow dot pattern (Fig. 4.2E.ii & iii). The yellow color is the combined signal of the green and red channels (third column of each condition; Fig. 4.2F). The co-localization of these two proteins is an accepted Lewy body mimics[39,41]. To determine the co-localization of synphilin-1 and α-synuclein protein (extreme right column of each condition; Fig. 4.2F), the Co-localization Colormap plugin of Image J software was used[42]. The correlation of a pair of pixels is calculated by normalized mean deviation product (nMDP). According to nMDP, values for each pixel ranging from -1 to 1, is visualized on a color scale. Cold colors (towards blue) indicate exclusion of one fluorophore and hot colors (towards red) represent colocalization of both the fluorophore. The white arrow in each panel indicates the localization of Lewy body mimic except Figure 4.2E.i (Empty pEGFP and empty pCMV6 vector transfection in a 1:1 ratio). After 1 μM Aβ (25-35) treatment for 24 h, there was around a two fold increase in aggregation of synphilin-1 and α-synuclein (when co-expressed) (P=0.0112 & P=0.0045 respectively) relative to vehicle treatment (Fig. 4.2F). In the bar diagram X-axis represents treatment conditions and Y-axis depicts fluorescent intensity. This series of experiments indicate that the increase in the aggregation of co-expressed synphilin-1 and α-synuclein is a function of Aβ (25-35) concentration (P=0.0218 & P=0.0083 respectively). SHSY-5Y cells with aggregated Lewy body like debris (white arrow) were also counted using Image J software to interpret the severity of Aβ (25-35) treatment (Supplementary figure 4.2).

The data was plotted as a bar diagram where Y axis indicate the number of cell with aggresome (Fig. 4.2G). It clearly showed the adverse effect of Aβ (25-35) treatment on synphilin-1 and α-synuclein folding (*P*=0.0239; 10 μM Aβ (25-35) treatment relative to untreated condition). There was around 3.0 fold increase in cell containing the toxic aggresome upon 20 μM Aβ (25-35) treatment relative to untreated condition (*P*=0.0005). All these data suggestive of the cross reactive nature of Aβ (25-35) peptide fragment.

We also compared the fluorescent intensity level of synphilin-1 "only" and α-synuclein "only" expression with co-expressed synphilin-1: α-synuclein (1:1) in SHSY-5Y cell under different treatment conditions (Fig. 4.2H). In Fig. 4.2H.i we plotted the fluorescent intensity of green channel (pEGFP-synphilin-1) from Fig. 4.2B and Fig. 4.2F. Whereas only the red channel (α-synuclein) intensity from Fig.4.2D and Fig. 4.2F was plotted in Fig. 4.2H.ii. In both the cases no difference in intensity were found under untreated condition (*P*=0.9101 and *P*=0.3770). A significant increase in fluorescence was recorded in case of green channel of co-expressed synphilin-1: α-synuclein (1:1) (Fig. 4.2H.i; *P*=0.0301) relative to synphilin-1 (when expressed alone) under 24 h 1 μM Aβ (25-35) treatment. The change in fluorescent signal of red channel of co-expressed synphilin-1: α-synuclein (1:1) is not significant relative to α-synuclein (when expressed alone) except 20 μM Aβ (25-35) treatment (*P*=0.0272). There is consistent significant increase of GFP tagged synphilin-1 (when co-expressed along with α-synuclein), protein aggregation relative to GFP tagged synphilin-1 "only" expression, found as a function of Aβ (25-35) concentration (1 μM, 10 μM, 20 μM *vs* untreated; *P*=0.0301, *P*=0.0480 and *P*=0.0058 respectively). It is very clear from this data that there is an effect of α-synuclein on synphilin-1 aggregation under the same treatment conditions when expressed together. It is worthy to mention that coexistence of synphilin-1 and α-synuclein in Lewy body is very common in PD

patient's histopathological sample[41]. We predicted that misfolded α-synuclein synergistically can increase the aggregation of synphilin-1 as they known to interact with each other in diseased condition.

Cytoplasmic Aβ (25-35) influence the interaction of α-synuclein and PDI

From the previous set of data the question arises is how Aβ (25-35) influencing the aggregation of α-synuclein, an amyloidogenic protein. For that purpose Hilyte™ Fluor 488 - Gly - Ser - Asn - Lys - Gly - Ala - Ile - Ile - Gly - Leu - Met – OH (Aβ (25-35) Hilyte-488®) was used to monitor the progression in cell culture medium (DMEM:F12). Our data clearly showed that Aβ (25-35) Hilyte-488® not only going inside the cell it is also interacting with α-synuclein (cell transiently transfected with pCMV6- α-synuclein plasmid) in a time dependent manner (Fig. 4.3A). For this experiment 500 nM Aβ (25-35) Hilyte-488® was used and confocal images were taken at different time (0 h, 0.5 h, 3 h, 6 h, 12 h, 18 h and 24 h) after methanol fixation following previously described immuno-fluorescent protocol. α-synuclein was detected using texas red conjugated secondary antibody after overnight exposure to primary monoclonal α-synuclein antibody. The fourth column of each panel was derived from Colocalization Colormap plug-in of Image J software[42]. Hot color (towards red; nMDP: +1) indicates the colocalization of two fluorophore whereas cold color (towards blue; nMDP: -1) showcase only single fluorophore. The colocalization of Aβ (25-35) Hilyte-488® and synuclein is indicated by white arrow head in third and fourth column of each panel. Intake of Aβ (25-35) Hilyte-488® peptide (green channel) was quantified and plotted in a bar graph (Fig. 4.3B). Data showed statistically significant increase in the uptake of Aβ (25-35) only after 30 min. of exposure (P=0.0011) as well as the interaction with α-synuclein. It is clear from the experiment that the uptake of Aβ (25-35) is only time dependent. It is interesting to note that the increased aggregation of Aβ (25-35) Hilyte-488® was

noticed only in α-synuclein transfected cell but not in non-transfected cell under the same experimental condition (Supplementary fig. 4.2A). To confirm the internalization of Aβ (25-35) Hilyte-488®, but not adhesion, we showed the co-localization of this peptide fragment with mitochondria using Mito Tracker® Red dye (Supplementary fig. 4.2B). Our data comply with the findings of other research groups on larger peptide fragment Aβ (1-42)[43].

Protein di sulfide isomerase, an endoplasmic reticulum (ER) resident chaperone protein, guide in proper folding of di sulfide mediated proteins[32-34,39]. Malfunction of PDI also implicated in different disorder, especially neurodegenerative diseases [19,25,39]. The site of predilection for PDI is the organelle endoplasmic reticulum[32-34]. α-synuclein is reported to be found in cell membrane, cytoplasm as well as mitochondria[21,24,32,38]. Several studies reported the interaction of PDI and α-synuclein both *in vitro* and *in vivo* and protective nature of PDI against α-synuclein fibril formation[32]. PDI is also found to be a part of the neurofibrillary tangles of AD patients and Lewy body of PD patients[41]. Hereby we decided to look into the plausible interaction of Aβ (25-35) Hilyte-488® and PDI (Fig. 4.3C). Alexa Fluor® 555 conjugated with secondary antibody was used after monoclonal PDI primary antibody treatment to detect the PDI. 1 μM Aβ (25-35) Hilyte-488® treated SHSY-5Y cell was methanol fixed and images were taken using LSM 700 microscope. The colocalized pixel scatter plot (inset in the fourth column) and nMDP color image (fourth column) strongly suggest the colocalization of PDI and Aβ (25-35) Hilyte-488® (marked by white arrow head). Our previous two data (Fig. 4.3A & C) leads to the speculation that interaction can be possible between PDI, α-synuclein and Aβ (25-35). To test the hypothesis we treated the α-synuclein transfected SHSY-5Y cell with different doses of Aβ (25-35) ranging from 1μM to 20 μM for 24 h under controlled conditions (37ºC and 5% CO_2). To our surprise there was no colocalization of PDI and α-synuclein protein found in case of non-transfected cell

under 10 μM Aβ (25-35) treatment and untreated but α-synuclein transfected cell (Fig. 4.3D). Interestingly the scatter plot and nMDP color map strongly suggest the perinuclear colocalization of PDI (green channel; Alexa Fluor 488 conjugated secondary antibody) and α-synuclein (red channel; Texas Red conjugated secondary antibody) when treated with 1μM Aβ (25-35) for 24 h. When increased the concentration of Aβ (25-35) to 10 μM we found perinuclear as well as cytoplasmic colocalization (white arrow head) of these two distinctly located proteins. Our immunoprecipitation assay consolidates the same finding (Fig. 4.3E & F; see method section). The bar diagram was plotted using Image J software where Y axis represent the α-synuclein / PDI ratio signal (Fig. 4.3F). Significant increase (P=0.0001) in α-synuclein signal found under 1 μM Aβ (25-35) treatment when compared with the untreated condition. There was also dose dependent increase in α-synuclein signal recorded (P=0.0071; 1 μM *vs* 10 μM). Recent finding suggests the activity and subcellular redistribution of PDI is strongly correlated with the ER stress as well as its s-nitrosylation status[31]. So, Aβ (25-35) mediated α-synuclein and synphilin-1 aggregation might cause the ER stress which in turn forced the redistribution PDI. Cytoplasmic PDI then become available for the interaction with α-synuclein.

Consequences of Aβ (25-35) induced S-nitrosylation of PDI

Our previous data (Fig. 4.1H & I) showed excessive increased level of RNS upon Aβ (25-35) treatment. Previous study indicates a strong relation between excess cytoplasmic RNS and post-translational modification of PDI[19]. Reactive NO• radical can readily oxidize the labile thiol (-SH) group of cysteine amino acid of PDI[39]. Many group including us also suggested the influence of S-nitrosylated PDI on misfolding of major and minor Parkinsonian protein[33,39]. SNO-PDI is also implicated on the ER-stress mediated activation of apoptotic pathway[19,33]. To investigate the role of excess cytosolic RNS on the chaperone PDI, we performed the

immunoprecipitation assay (Fig. 4.4A & B). Equal amount of cell lysate after different treatment was pulled down using anti-PDI and then immunoblotted with SNO-Cys-BSA antibody and anti-PDI antibody[19]. The protein signal was quantified using Image J software and plotted as bar diagram (Fig. 4.4B). We found significant increase in SNO-Cys-BSA signal around 57 kD molecular weight, indicative of SNO-PDI, when treated with 1 μM Aβ (25-35) compared to untreated condition (P=0.0174). We also confirmed dose dependent (1 μM *vs.* 10 μM Aβ (25-35) treatment; P=0.0229) increase in SNO-PDI level. We further checked heat shock protein (HSP) 70 level and PDI as an indicator of ER stress (Figure 4.4C). There was substantial increase in the expression level of both HSP 70 and PDI after 24 h Aβ (25-35) treatment (1 μM, 10 μM, 20 μM and 50 μM). Data suggests major increase (P=0.0028; 1 μM *vs*. untreated) in HSP 70 level (white box; Fig. 4.4D) whereas the same trend noticed in PDI expression level (grey box; Fig. 4.4D) only after 10 μM Aβ (25-35) exposure (P=0.0304; relative to untreated condition). Progressive decrease in dopamine level is a major concern in PD patients[38]. Tyrosine hydroxylase (TH) enzyme plays a major role dopamine synthesis from the amino acid tyrosine[38]. So we decided to check the TH level in dopaminergic SHSY-5Y cell line after Aβ (25-35) treatment (Fig. 4.4C; second row). To our surprise dose dependent increase in TH level was recorded, which does not comply with the normal notion of dopamine chemistry in PD patients. It might be possible that the problem lies in dopamine secretion but not the production[44]. Significant increase in TH expression (black box) was graphed in bar diagram (P=0.0075; 1 μM *vs.* untreated; Fig.4.4D). GAPDH was used as a loading control.

Misfolded non-functional proteins are tagged by ubiquitin to guide them for proteosomal degradation for maintaining of cellular homeostasis[18]. The upper limit of this ubiquitin proteasome system (UPS) is very critical between cell survival and controlled death[18,20].

Whenever the ubiquitinated protein aggregates reach beyond the level of tolerance (failure of UPS system) the cell activates cascades of event leading to apoptosis[18-20,29,35]. In light of the previous discussed results, I decided to check the aggregated cytosolic protein load under different Aβ (25-35) treatment (Fig. 4.4E & F). We separated the insoluble protein fraction and ran in 12% SDS-PAGE gel. Gradual increase in the signal of ubiquitinated protein aggregates was graphed in the bar diagram as a function of Aβ (25-35) concentration (Fig. 4.4E). Nearly two folds increase in accumulated ubiquitinated protein was found after 20 μM Aβ (25-35) treatment when compared against the untreated condition (P=0.0222). These set of analysis strongly suggest a strong correlation between the posttranslational modification of PDI, ER stress, accumulation of ubiquitinated proteins and cell death.

4.4 Conclusion

In this study we have investigated the effect of 11 mer peptide fragment, amyloid beta (25-35) which considered as the functional domain of amyloid beta (1-42)[9-11]. A beta was found to have a high toxicity on the neuronal and neuroblastoma cell line[16]. We showed that Amyloid beta (25-35) aggregates have the potential to activate the apoptotic pathway in SH-SY5Y cell as evidenced by PARP-1 cleavage and Annexin V-FITC, both used as apoptotic marker. Our data indicate the excessive cytosolic RNS production as a function of Aβ (25-35) treatment leading to S-nitrosylation of protein disulfide isomerase. This set of work also suggests that Aβ (25-35) aggregates not only cross the cell membrane but also can initiate aggregation of GFP tagged synphilin-1 as well as α-synuclein whether expressed separately or combined in SH-SY5Y cell line. Time lapse study clearly showed strong interaction of probed Aβ (25-35) with α-synuclein and PDI. Here for the first time we reported the interaction of PDI and α-synuclein as a function of Aβ (25-35) treatment. It can be suggested that ER stress and posttranslational modification of PDI make it cytosolic to interact with α-synuclein and Aβ (25-35).

In conclusion, our results advance the understanding of the intricacy of neurodegeneration field by mapping putative mechanism behind the failure of cellular housekeeping machinery but also a plausible explanation of overlapping histopathological findings in neurodegenerative diseases. The reported results can further research in related neuropathies whose onset may be related to the dysfunction of the cellular homeostasis apparatus. The current report can be used for developing preventative approach against the disease.

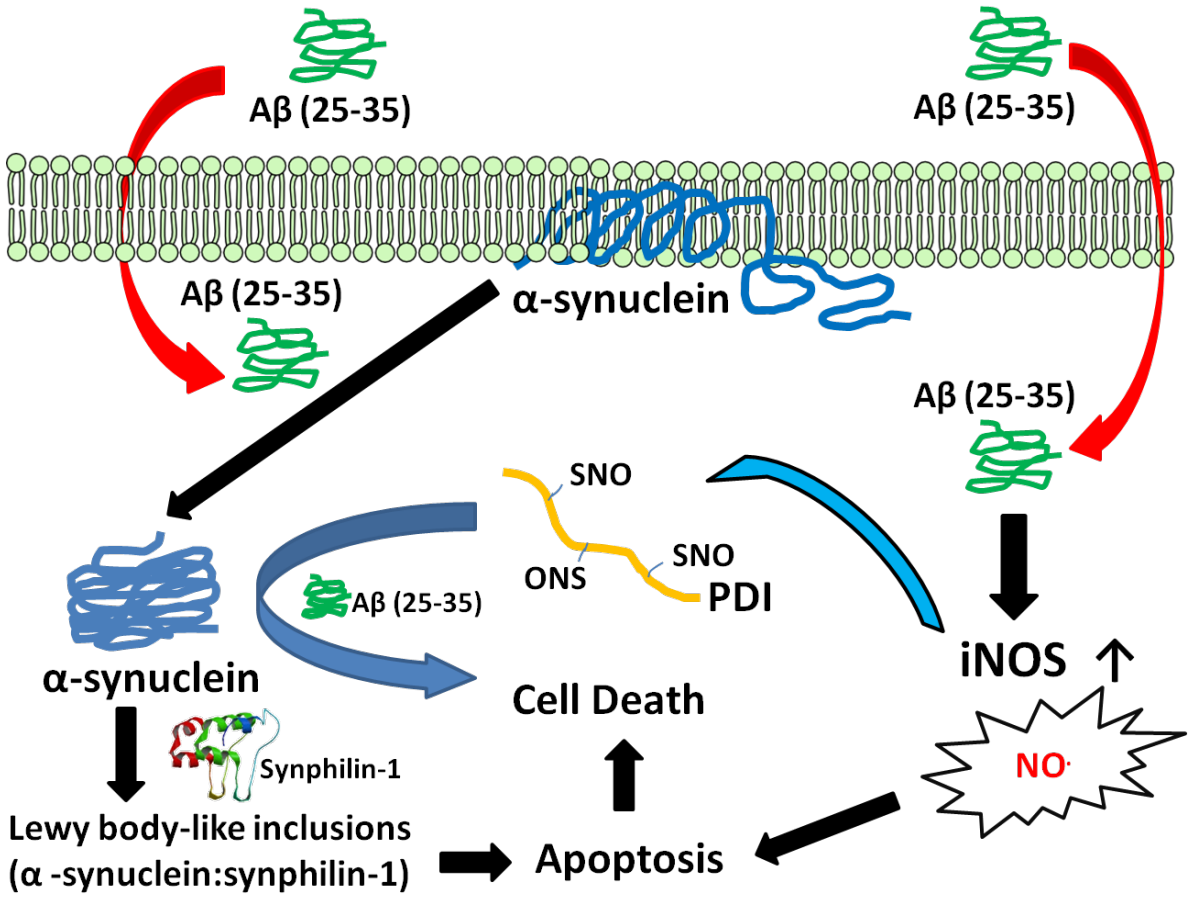

Fig. 4.0. Proposed mechanism of Aβ (25-35) induced formation of Lewy body inclusion which resulted in Er stress mediated cell death.

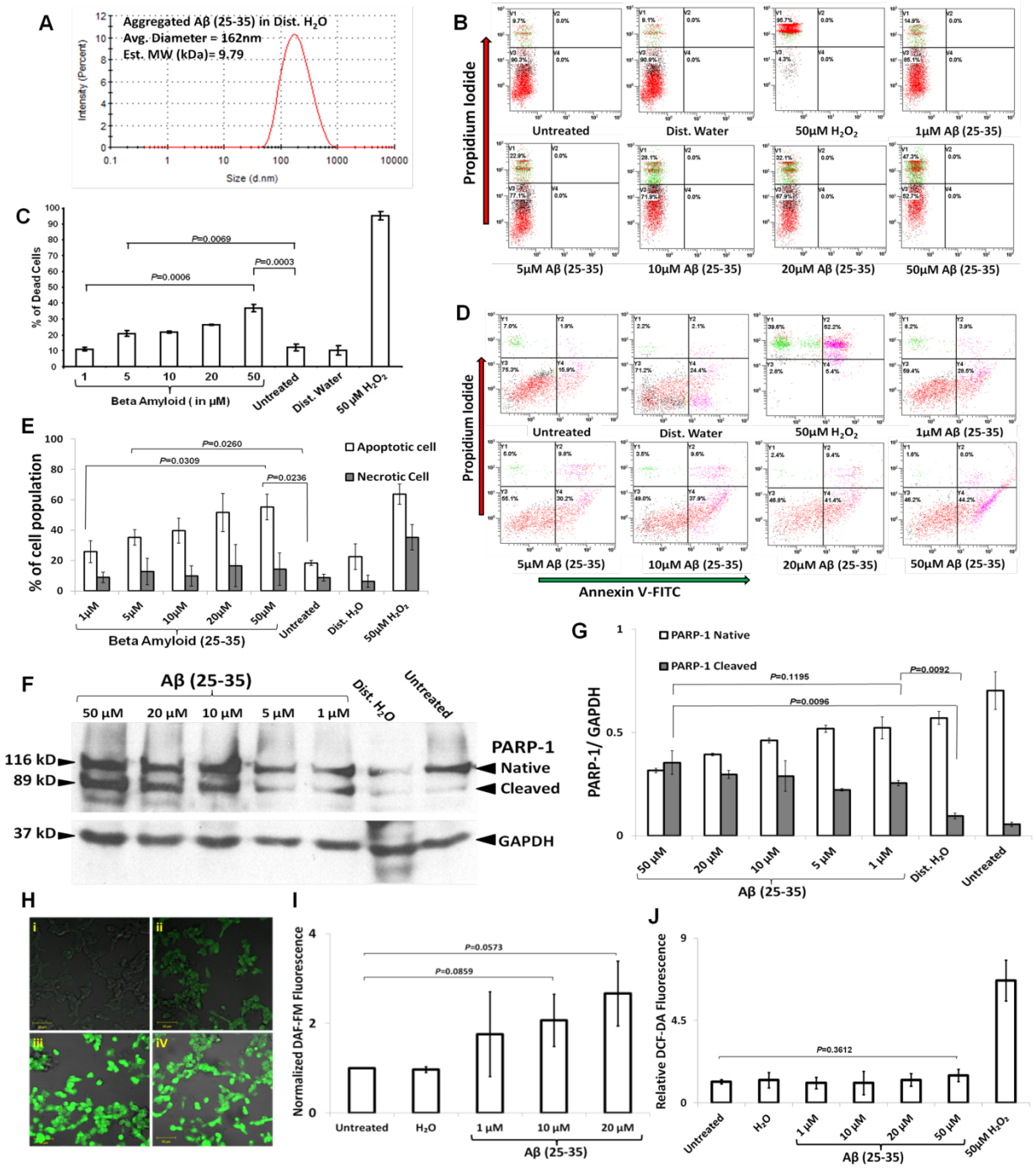

Figure 4.1. RNS dependent activation of apoptotic pathway upon Aβ (25-35) treatment. Fig. (A) Dynamic Light Scattering of Aβ (25-35) showing aggregation. Panel (B) showing the cytotoxic effect upon different concentrations of beta-amyloid (25-35) treatment (48 hrs) on SH-SY5Y cells, staining them with PI and further quantitated using the flow cytometry shown in histogram

Fig. (C). (D) Detection of cellular apoptosis/ necrosis in SH-SY5Y cells induced by beta-amyloid (25-35) treatment. Cells were treated with beta-amyloid for 24 hrs duration followed by staining with annexin-V FITC (apoptotic marker) and PI (necrotic marker) mixture for 15 minutes on ice in the dark. Afterwards the percentage (Fig. 4.1A) of apoptotic and necrotic cell population was quantitated using a flow cytometer. The histogram is shown in panel (E). (F) Effect of Aβ (25-35) induced poly (ADP-ribose) polymerase (PARP) cleavage, hallmark of apoptosis progression, in SH-SY5Y cells. (G) PARP-1 cleavage bands were densitometrically analyzed *via* Western blot analysis using Image J software. DAF-FM fluorescence image was taken using LSM700 confocal microscope to detect intracellular RNS (H) and was quantified (I) by Fluoroskan software in 96 well format after 24 h Aβ (25-35) treatment. Reactive oxygen species (ROS) level was detected using DCF-DA dye after 24 h exposure to Aβ (25-35) in SHSY-5Y cell line (J). Each experimental point was assessed in triplicate or more. Statistical significance comparing two groups are illustrated as *P* value.

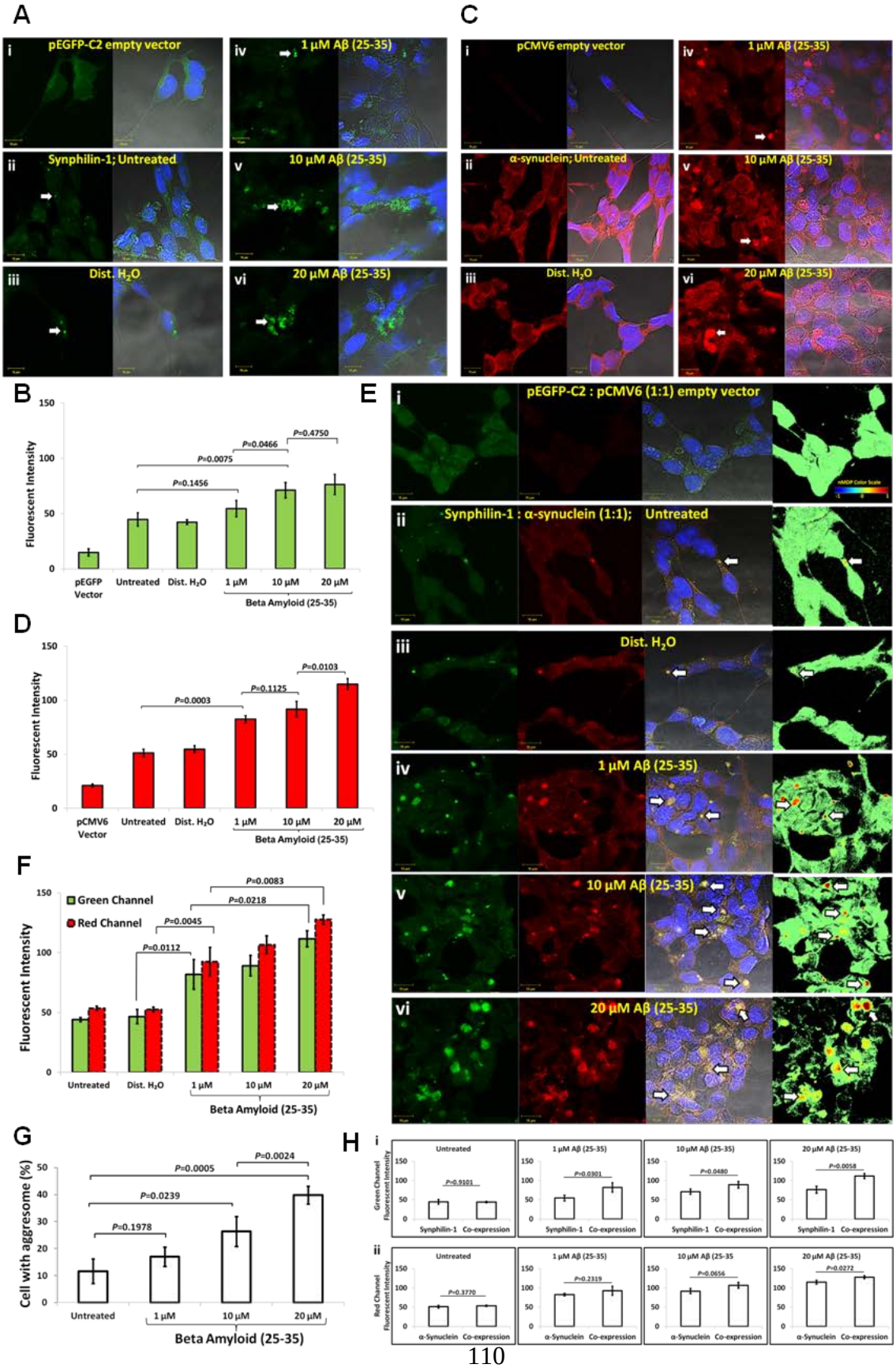
A
i pEGFP-C2 empty vector
iv 1 μM Aβ (25-35)
ii Synphilin-1; Untreated
v 10 μM Aβ (25-35)
iii Dist. H2O
vi 20 μM Aβ (25-35)
C
i pCMV6 empty vector
iv 1 μM Aβ (25-35)
ii α-synuclein; Untreated
v 10 μM Aβ (25-35)
iii Dist. H2O
vi 20 μM Aβ (25-35)
B
Fluorescent Intensity
P=0.4750
P=0.0466
P=0.0075
P=0.1456
pEGFP Vector
Untreated
Dist. H2O
1 μM
10 μM
20 μM
Beta Amyloid (25-35)
D
Fluorescent Intensity
P=0.0103
P=0.1125
P=0.0003
pCMV6 Vector
Untreated
Dist. H2O
1 μM
10 μM
20 μM
Beta Amyloid (25-35)
E
i pEGFP-C2 : pCMV6 (1:1) empty vector
ii Synphilin-1 : α-synuclein (1:1); Untreated
iii Dist. H2O
iv 1 μM Aβ (25-35)
v 10 μM Aβ (25-35)
vi 20 μM Aβ (25-35)
F
Green Channel
Red Channel
Fluorescent Intensity
P=0.0083
P=0.0218
P=0.0045
P=0.0112
Untreated
Dist. H2O
1 μM
10 μM
20 μM
Beta Amyloid (25-35)
G
Cell with aggresome (%)
P=0.0005
P=0.0024
P=0.0239
P=0.1978
Untreated
1 μM
10 μM
20 μM
Beta Amyloid (25-35)
H
i
Green Channel Fluorescent Intensity
Untreated
P=0.9101
1 μM Aβ (25-35)
P=0.0301
10 μM Aβ (25-35)
P=0.0480
20 μM Aβ (25-35)
P=0.0058
Synphilin-1
Co-expression
ii
Red Channel Fluorescent Intensity
Untreated
P=0.3770
1 μM Aβ (25-35)
P=0.2319
10 μM Aβ (25-35)
P=0.0656
20 μM Aβ (25-35)
P=0.0272
α-Synuclein
Co-expression

Figure 4.2. Aβ (25-35) induced Lewy body-like inclusions formation in SH-SY5Y cells. Transfected SHSY5Y cells were untreated or stressed with Aβ (25-35) for 24 h. Panel (A) confocal fluorescence images of SH-SY5Y cells reveal the presence of cytoplasmic aggregates in cells transfected with EGFP or EGFP-tagged synphilin-1 plasmid. Panel (C) fluorescence images of SH-SY5Y cells revealed the presence of α-synuclein cytoplasmic aggregates under different conditions. (E) Cells transfected with α-synuclein: synphilin-1 (1:1) and then treated under different conditions. Figure 4.2 (A; C; E) (i) cells transfected with pEGFP-C2 empty vector and / or pCMV6 empty vector; (ii) cells untreated but transfected with Synphilin-1 and / or α-synuclein; (iii) treated with distilled water; (iv, v, vi) Cells treated with different concentration of Aβ (25-35) for 24h alone; All the cells were counterstained with DAPI to stain the nucleus (blue color). White arrows indicate the presence of aggregates. Synphilin-1 was tagged with GFP showing green color and α-synuclein is shown in red color. Yellow color represents co-localization of α-synuclein and synphilin-1 (white arrow). Colocalization Colormap plug-in of Image J software used to find the colocalization as indicated by nMDP color scale ranging from (-)1 to (+)1. Each scale bar represents 10 µm. Panel (B; D) Quantification of synphilin-1 (Green Channel) and α-synuclein expression (Red Channel) in SHSY-5Y cell line upon different treatment. (F) Quantification of total co-localized aggregates (mimic of Lewy body) in α-synuclein and synphilin-1 co-transfected SHSY-5Y cell treated with different conditions. (G) Total number of SH-SY5Y cells showing Lewy body-like aggregation upon Aβ (25-35) exposure (n= 200; Supplementary Figure 1). (H) Comparative quantitative study of individual expression and co-expression of Synphilin-1 (i) and α-synuclein (ii) upon treatment at different Aβ (25-35) concentrations. Statistical significance compared with untreated are illustrated as P value (n= 100). All the quantitative analysis was done using Image J software from n=100 cells

indicated as mean ± S.D. Y-axis represents the fluorescence intensity and X-axis represents 24 h. treatment conditions. Region of Interest (ROI) was 400 pixels (20x20). S.S illustrated as *P* value.

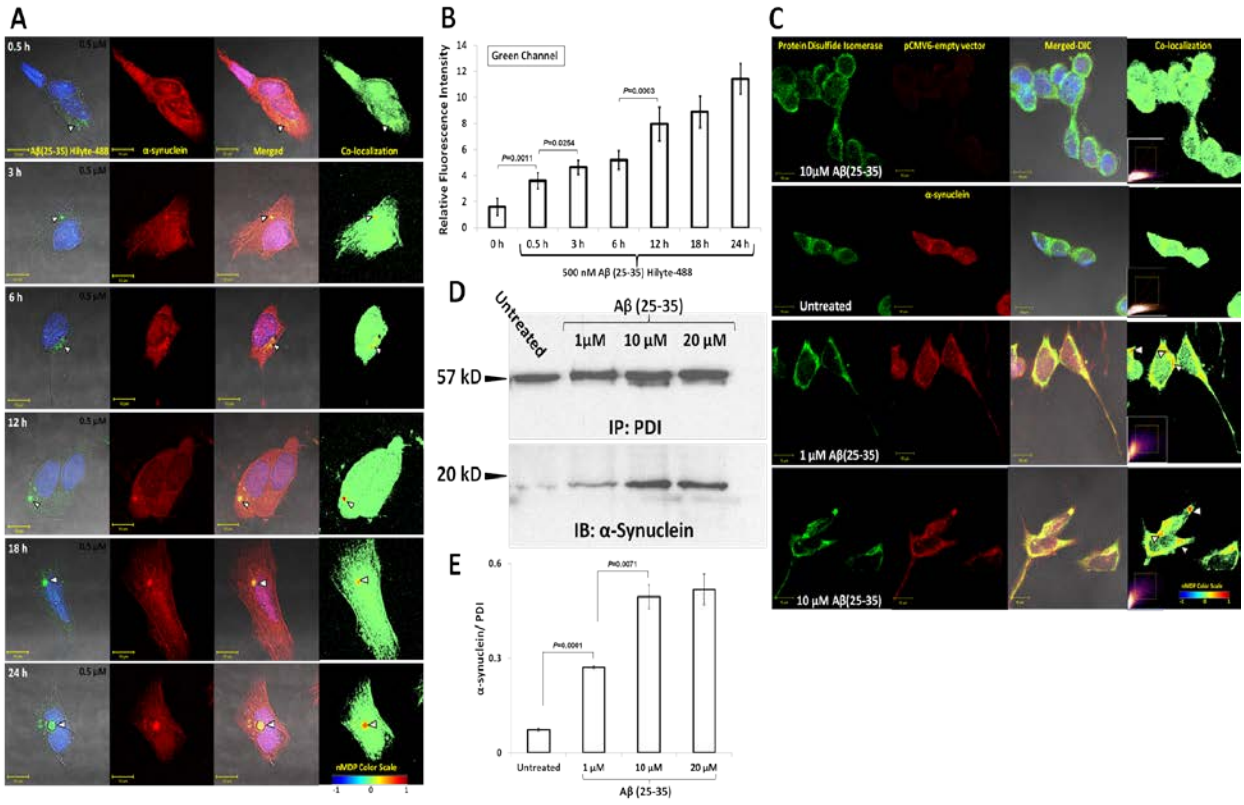

Fig. 4.3. Spatiotemporal dependence of Aβ (25-35) induced PDI and α-synuclein interaction. Time dependent interaction of Aβ (25-35) Hilyte-488® (Green channel) with α-synuclein (Red channel) showed perinuclear localization of both proteins after 24 h in SHSY-5Y cell line (A). Fluorescent intensity of green channel quantified to assess the uptake the Aβ (25-

35) Hilyte-488® by SHSY-5Y as a function of time (B). Colocalization (Yellow in third column and red in fourth column; white arrow head) of PDI (Green) with α-synuclein (Red) upon Aβ (25-35) treatment was imaged using fluorescent microscopy (C). Equal amount of cell lysate after 24 h Aβ (25-35) treatment were ran in 12% SDS-PAGE gel after immunoprecipitated by PDI then blotted proteins detected using α-synuclein primary antibody (D) and quantified by Image J software (E). Each fourth column of image (Red indicates colocalization) as well as inset of scatter plot was processed by Image J software (A; C). Colocalization Colormap plug-in of Image J software used to find the colocalization as indicated by nMDP color scale ranging from (-)1 to (+)1. Each scale bar represents 10 μm. Statistical significance annotated as *P* value (n=3).

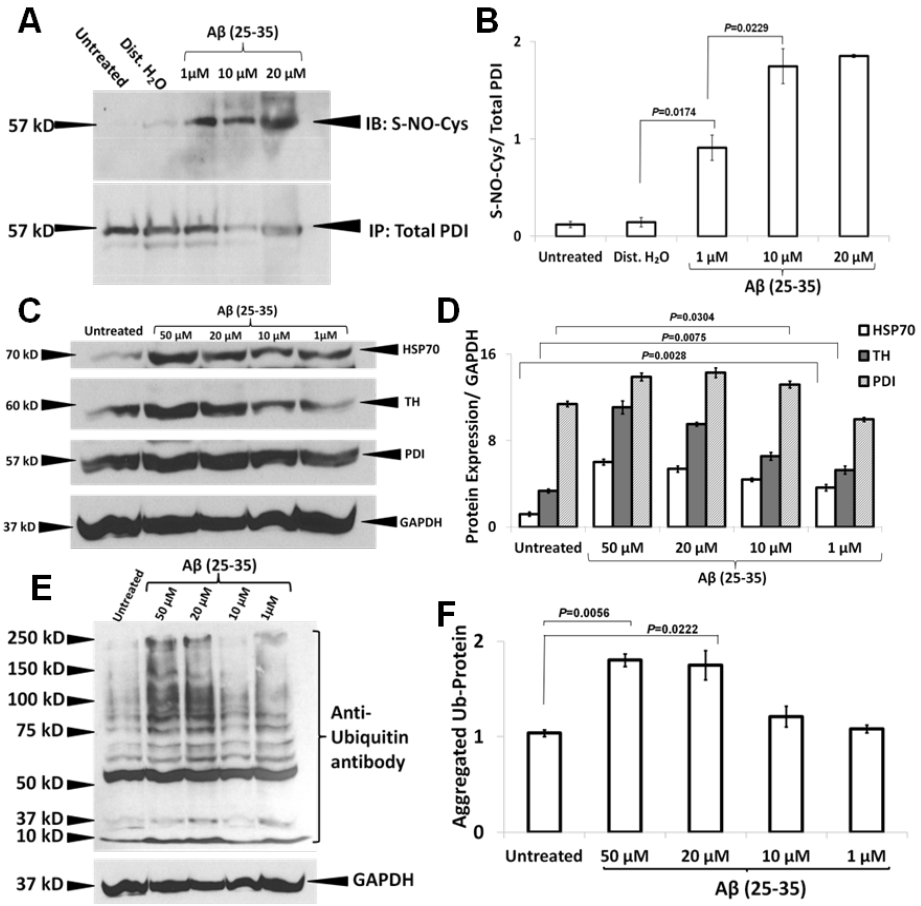

Fig. 4.4. Cellular impact on Aβ (25-35) treatment. S-nitrosylation of PDI in Aβ (25-35) treated SHSY-5Y cell line detected by immunoprecipitation (A) and quantified (B). Aβ (25-35) induced over-expression of heat shock protein 70 (HSP70), an ER-stress marker protein (C). Level of tyrosine hydroxylase (TH), PDI and GAPDH expression detected using respective antibodies (C) and quantified (D). Aβ (25-35) induced accumulation of ubiquitinated proteins in the insoluble fraction of cell lysate detected using ubiquitin primary antibody (E) and quantified (F). Equal amount of protein (10 µg/ well) was loaded for each condition. GAPDH was used as a loading control. Western Blots signals were densitometrically quantified using Image J software from three independent tests indicated as mean ±S.D. Statistical significance among pairs of samples is annotated as *P* value (n=3).

Supplementary Figure

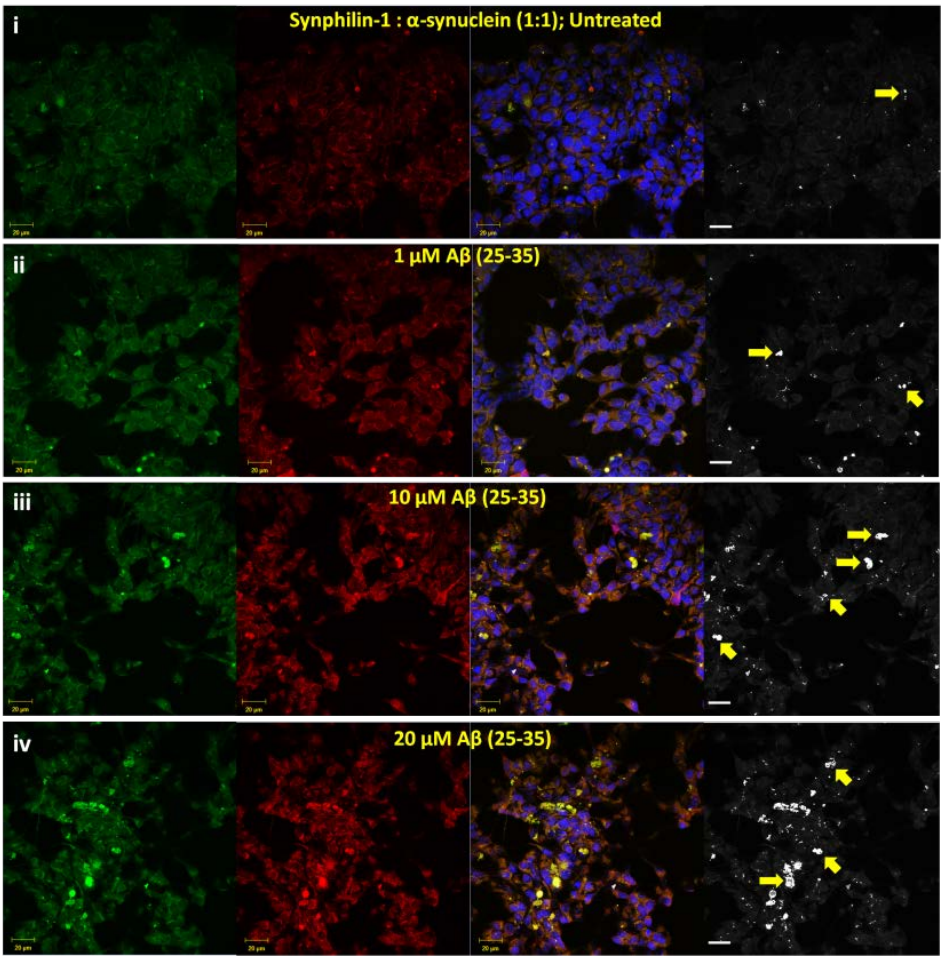

Supplementary Figure 4.1. Co-localized aggregates (mimic of Lewy body) of α-synuclein and synphilin-1 (1:1) expressed in SHSY-5Y cells under Aβ (25-35) treatment. Transfected SHSY-5Y cells were untreated or stressed with different treatments. Cells transfected with α-synuclein and synphilin-1 without any treatment (i); cells treated with 1 µM, 10 µM, 20 µM Aβ (25-35) respectively for 24 h (ii, iii, iv). All the cells were counterstained with DAPI to delimitate the nucleus (Blue color).. Synphilin-1 was tagged with GFP showing green color and α-synuclein is shown in red color. Yellow color represents co- localization of α-synuclein and synphilin-1. Extreme right panel of each figure represents the co-localization of α-synuclein and synphilin-1 (white spot) whereas yellow arrows indicate the presence of aggregates determined using Image

J co-localization software (n=200). The scale bar represents 50 µm. Each experiment was repeated in triplicate

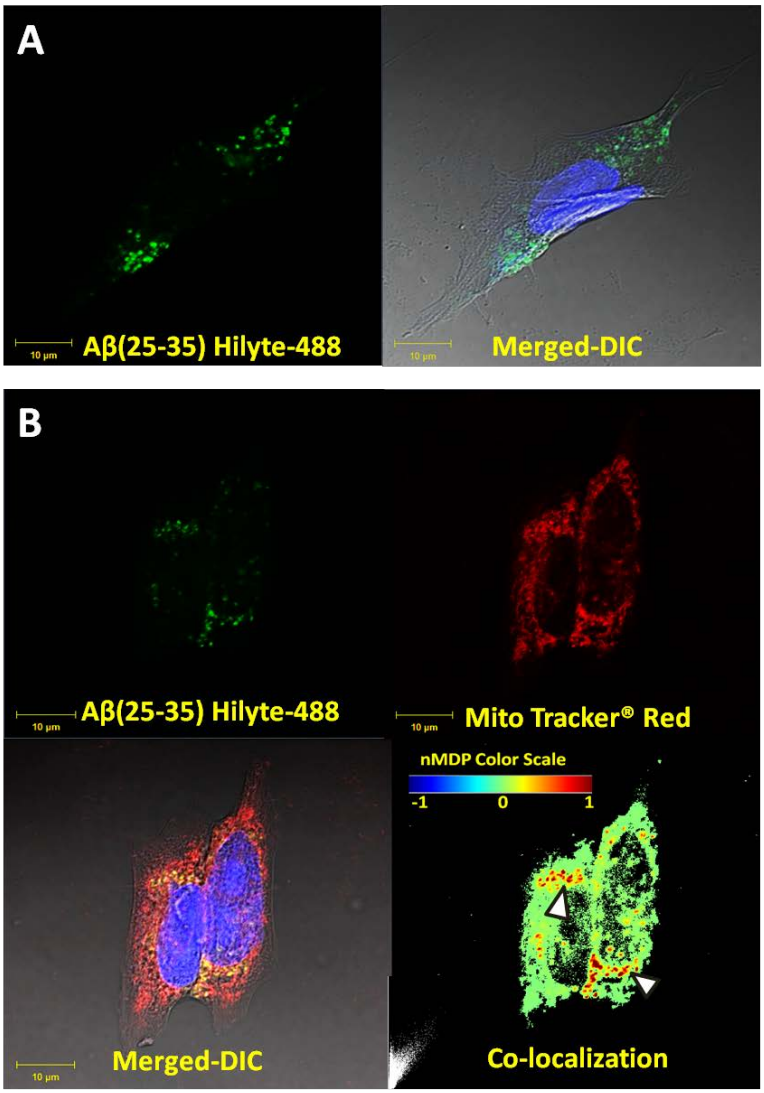

Supplementary Figure 4.2. Internalization of Aβ (25-35) Hilyte-488® after 24 h treatment in SHSY-5Y cell. SHSY-5Y cell harvested in DMEM: F12 medium under proper condition after 500 nM Aβ (25-35) Hilyte-488® (green channel) treatment (A). To prove that Aβ (25-35) Hilyte-488® is going inside the cell (not adhesion with plasma membrane), we stain the mitochondria using Mito Tracker® Red (B). Colocalization with mitochondria confirmed the internalization of Aβ (25-35). Second column bottom image (Red indicates colocalization; white

arrow head) as well as inset of scatter plot was processed by Image J software (B). Colocalization Colormap plug-in of Image J software used to find the colocalization as indicated by nMDP color scale ranging from (-)1 to (+)1. Each scale bar represents 10 µm.

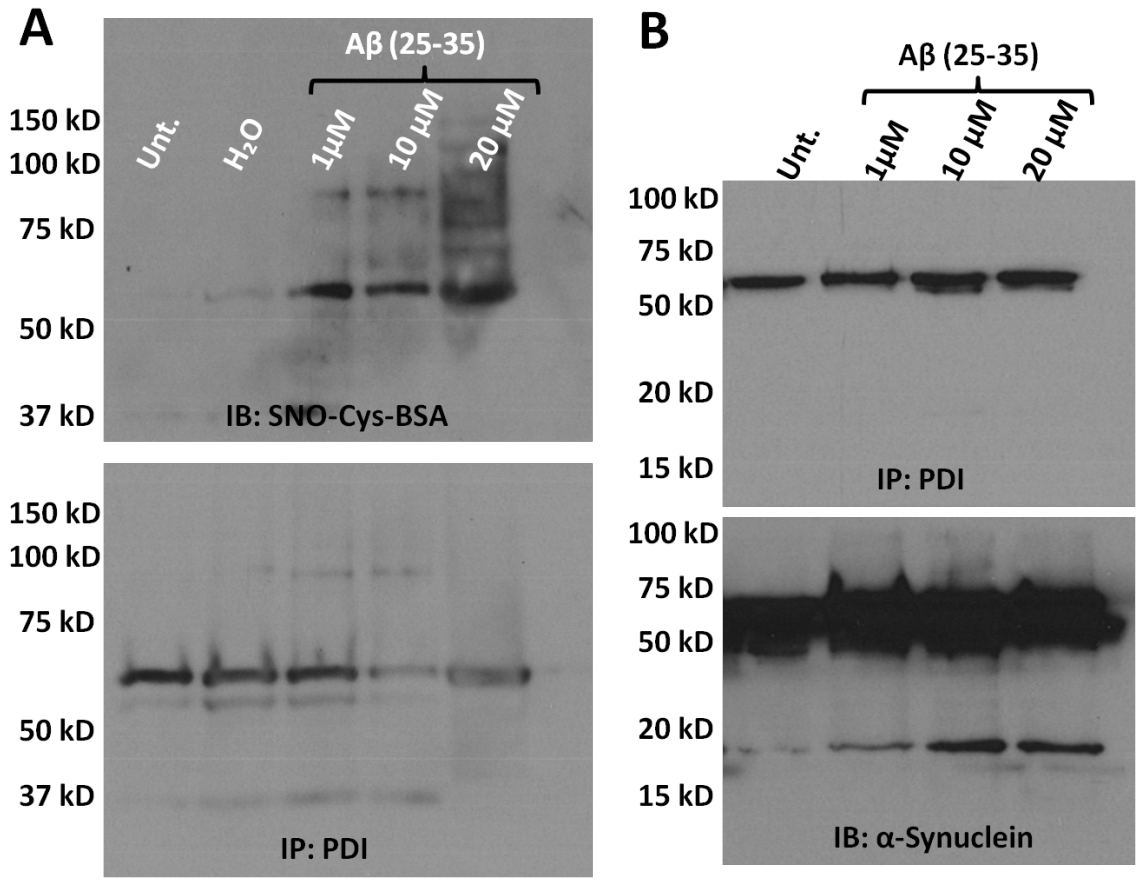

Supplementary Figure 4.3. Supportive gel for Figure 4.4A (A) and supportive information for Figure 4.3E (B).

Chapter 5:

Overall discussion and concluding remarks

5.1 Overall discussion and concluding remarks

The overall studies in this dissertation have been done using dopaminergic neuroblastoma cell line SHSY-5Y and PC12. First we created a toxin induced Parkinsonian cell model to mimic the environmental stress conditions on neuronal cell. Rotenone and MPTP were used as ER stressor, the known toxic compounds found to be evidence for Parkinsonian symtoms when exposed to human[1]. Looking for the lead compounds against free radical stress, we tested the neuroprotective effect of Na-D-β-hydroxybutyrate (NaβHB), ellagic acid (EA), piperine and EF24 against rotenone toxicity by using SH-SY5Y or PC12 cells. Pretreatment of cells with NaβHB and EA provided significant protection relative to EF24 and piperine to SHSY5Y cells. NaβHB and EA also found to attenuate the rotenone-induced activation of native PARP-1 protein. The dietary small molecule EA can also scavenge the rotenone induced reactive oxygen and recative nitrogen species thus inhibits posttranslational modification of PDI. We concluded that the healthy PDI hinder the Lewy body like inclusion formation as well as apoptotic cell death. Major and minor constituents of Lewy body are α-synuclein and synphilin-1 respectively. We have created cytoplasmic Lewy body mimic inside dopaminergic cell by co-transfecting α-synuclein and synphilin-1 (1:1). Our data suggest that rotenone can increase these Lewy body-like inclusions significantly due to excessive production of reactive oxygen and nitrogen species. Pretreatment of EA (6 h prior to rotenone treatment) is protective against rotenone induced increased production of Lewy body inclusions. It is clear from our findings that maintaining healthy PDI would be the key to find the cure of neurodegenerative disese. Studied small molecules NaβHB and EA can be a good scaffold to build on agaist reactive species mediated neuronal cell death.

Overlapping pathological and clinical symtoms of many neurodegenerative diseases has always baffeled the scientist community to find the exact etiology[2-4]. It is belived that a common mechanism lies behind all these neurodegenerative disorders[3,4]. Designing of a pharmacophore can be achieved if we can understand the molecular mechanism of behind aggregation of proteins associated with neurodegenerative diseases i.e. PD, AD, LBV, AD-LBV etc. We have decided to address the question using simple Parkinsonian cell model where we selectively expressed or co-expressed synuclein and synphilin-1 protein. We found the 11-mer functional domain of amyloid beta (1-42), Aβ (25-35), can induce aggregation of amyloidogenic proteins. Aβ (25-35) mediated s-nitrosylation of PDI lead to cellular toxicity by hampering the ER homeostasis as well as aggravated the Lewy body like inclusion formation in dopaminergic SHSY-5Y cell line.

Our study suggests that the posttranlational modification of PDI due to excessive free radicals is one of the major concerns for neuronal cell death. Whereas dietary small molecules have the potential to deter the reactive species therefore can be used as therapeutic scaffold against neurodegenerative diseases.

5.2 Future direction

Chronic exposure of environmental toxins (rotenone, MPTP etc.) can lead to neuronal cell death through elevated free radical stress. Failure of mitochondrial electron transfer chain to produce ATP can lead to endoplasmic stress as well as the ATP dependent activation of UPS[1]. Our study indicates that utilization of ketone body can surpass the consequences of mitochondrial complex I inhibitors. Ketogenic diets are often encouraged by physician to correct cellular metabolism anomalies, loose extra fat, increasd brain activity also believed to detarr the possibilities of AD and PD[1]. A long term study of ketone bodies on toxic induced Parkinsonian *in vivo* model would be very fruitful to understand the mechanism in detail.

Ellagic acid, a polyphenolic fruit derived small molecule, is found to be effective against both ROS and RNS from our study. It also can protect the PDI from nitrosative insult thus can alleviate the ER stress and protein aggregation induced cell death. As this small molecule can cross the blood brain barrier, it will be very interesting to investigate the effect of EA in toxin induced PD *in vivo* model. As we nonstop looking at various other small molecules we found ferristatin analogues as well as monocurcumin to be very promising against ROS and RNS from our initial screening. We also created a stable α-synuclein-SHSY-5Y cell line for further studies.

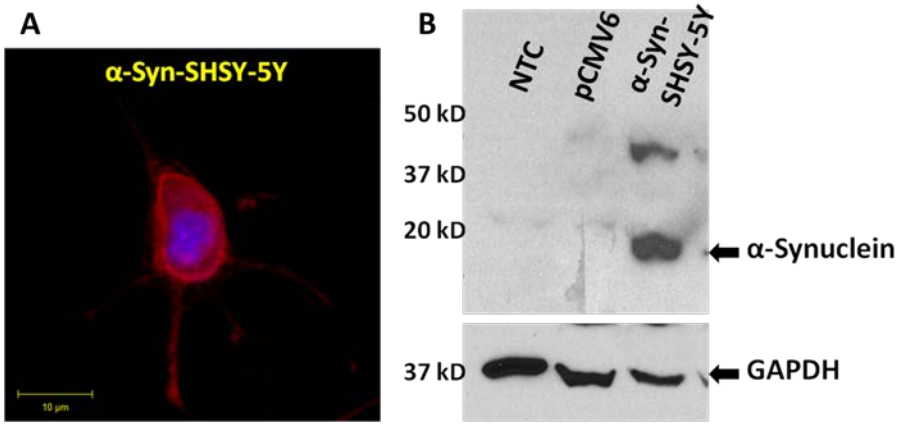

Fig. 5.1. Stable α-synuclein-SHSY-5Y (α-syn-SHSY-5Y) created after G418 (900 µg/ml) selection. Typical α-synuclein expression is shown using specific primary α-synuclein antibody (A). Texas red conjugated seconady anibody (red channel) used to detect the expression by confocal microscope Zen LSM 700. Again primary α-synuclein antibody was used to qualify α-synuclein by Immunoblot technique (B). C terminal MYC/DDK tagged α-synuclein inserted in pCMV6 vector was used. The 19 kDa and 38 kDa molecular weight is suggestive of monomer and dimer of α-synuclein protein expressed in SHSY-5Y cell.

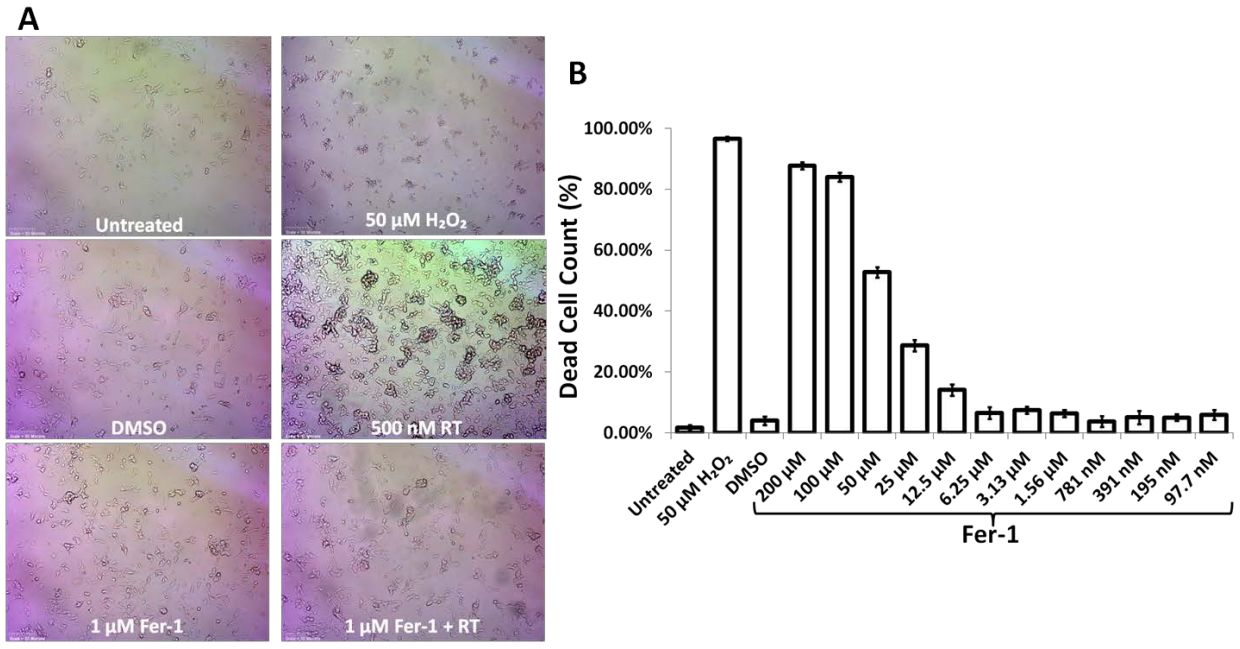

Fig. 5.2. Cytotoxicity of Fer-1 on SHSY-5Y. Bright field image of SHSY-5Y upon different treatment condition for 24 h (A). Propidium Iodide and Hoechst based high throughput screening assay for cytotoxicity study of fer-1 compound at different concentration (B).

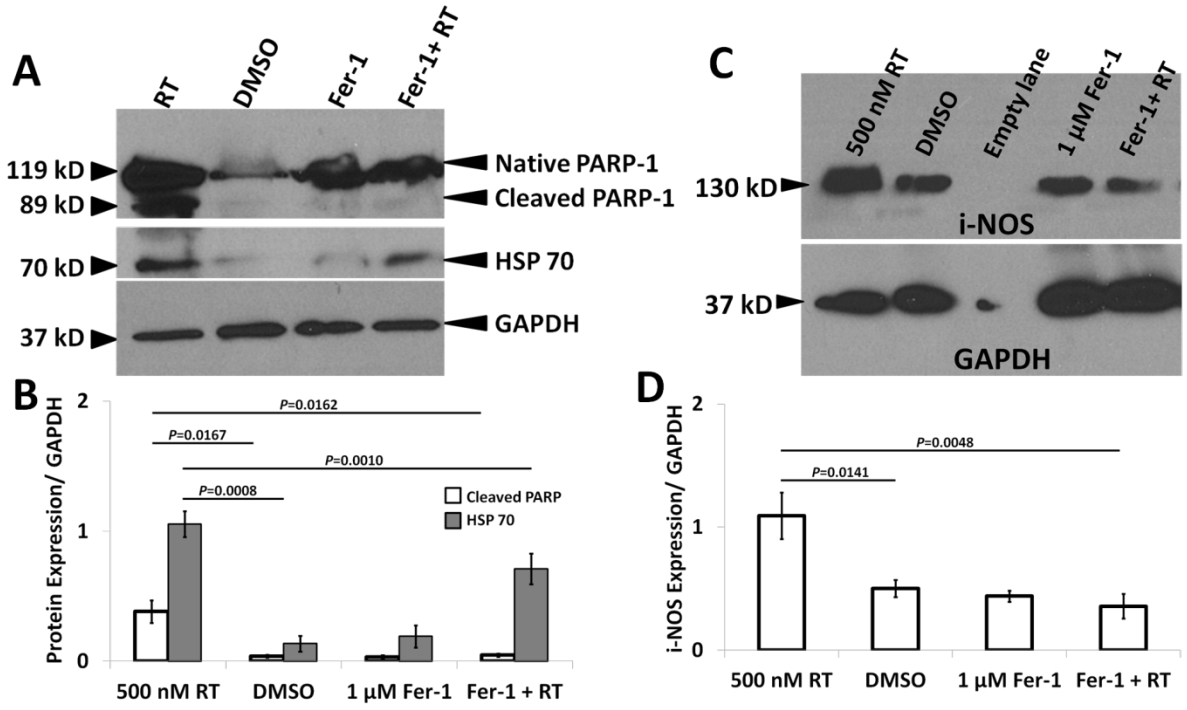

Fig. 5.3. Anti-apoptotic ability of Fer-1 through maintaining endoplasmic reticulum (ER) and i-NOS homeostasis. Immunoblot technique was used to detect the apoptotic activation: vehicle control (DMSO), Fer-1, rotenone and pretreatment with Fer-1 and then 24 h rotenone exposure (A). Rotenone (RT) induced over expression of heat shock protein 70 (HSP70) is mitigated by 1 µM Fer-1 pre-treatment (A). Expression of ER-stress marker protein, HSP70, is quantified under different treatment using Image J (B). RT induced over expression of i-NOS is inhibited by 1 µM Fer-1 pre-treatment (C). Quantification of i-NOS expressions, after GAPDH normalization, using Image J (D). Statistical significance between samples is illustrated as *P*-value (n=3).

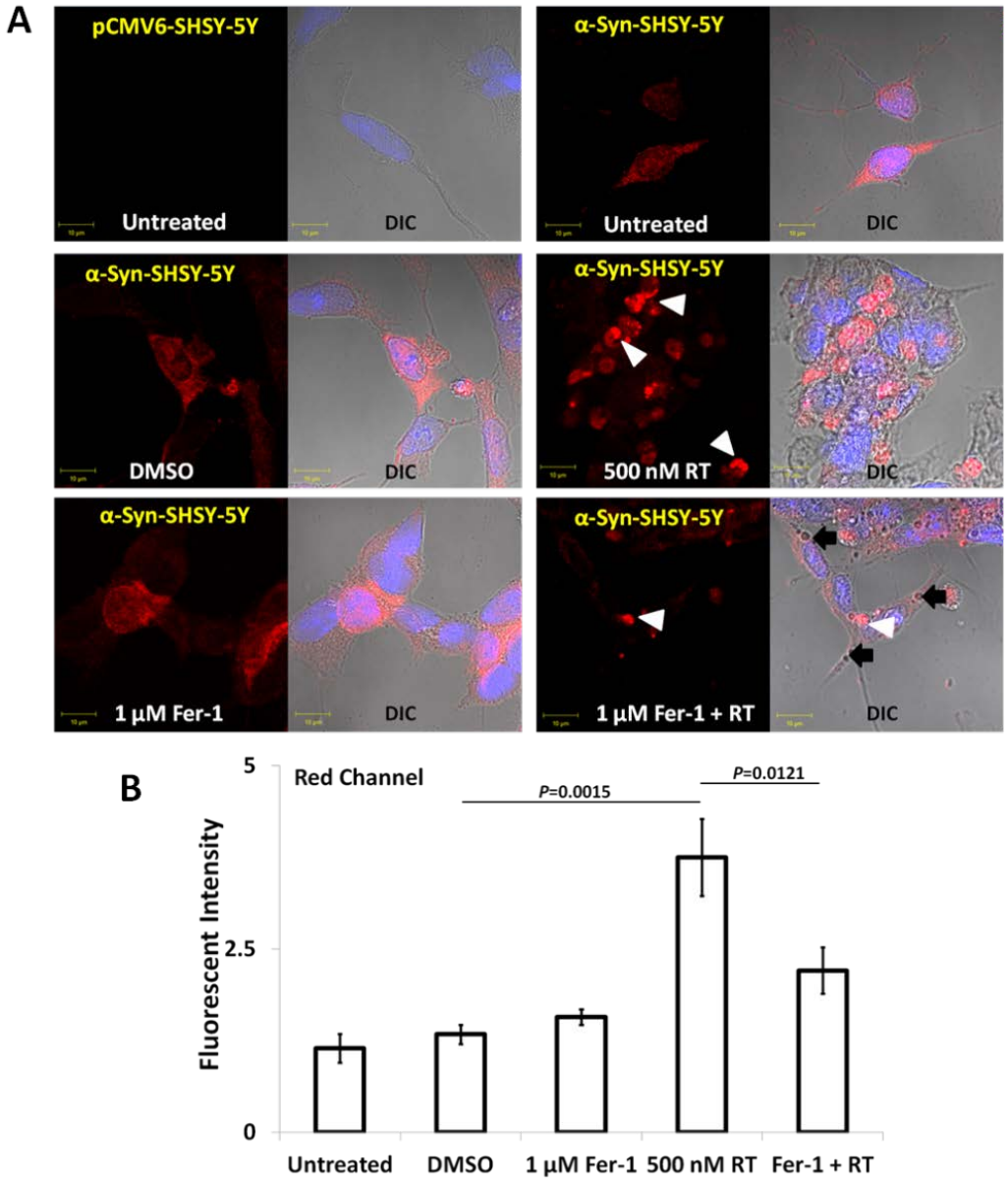

Figure 5.4. Role of Fer-1 in α-synuclein aggregation in α-syn-SHSY-5Y cell. Cells transfected with pCMV6 empty vector, untreated α-syn-SHSY-5Y cells, treated with DMSO 0.02% v/v, treated with 1 µM Fer-1, cells exposed to rotenone (RT) (500 nM) for 24 h alone and cells treated with 1 µM Fer-1 for 4 h prior exposed to rotenone (500 nM) for 24 h are the different conditions used for this study (A, B). Confocal fluorescence images of SHSY-5Y cells after 100% methanol fixation revealed the presence of α-synuclein cytoplasmic aggregates under

different conditions (A). All the cells were counterstained with DAPI to stain the nucleus (blue color). White arrow head indicates aggregation of α-synuclein protein. Black arrow is representative of vesicle shown in DIC image. Quantification of α-synuclein (Red channel) in SHSY-5Y cell line upon different treatment using Image J software from n=200 cells indicated as mean ± S.D (B). Statistical significance between pairs of samples is illustrated as *P*-value. Each scale bar represents 10µm. Each experiment was assessed in triplicate.

Our study on cross reaction of Aβ (25-35) ensures the importance of PDI in neuronal cell. As a future direction we are looking at dirrerent small molecules like myrecetin, monocurcumin along with EF24, 31 curcumin analogues, ellagic acid to intervene the β sheet stacking of amyloid beta fragment. Monocurcumin compound came out as the most promising candidate from our primary screening. It also can be promising in drug designing if we can replicate our findings in AD-LBV rat model.

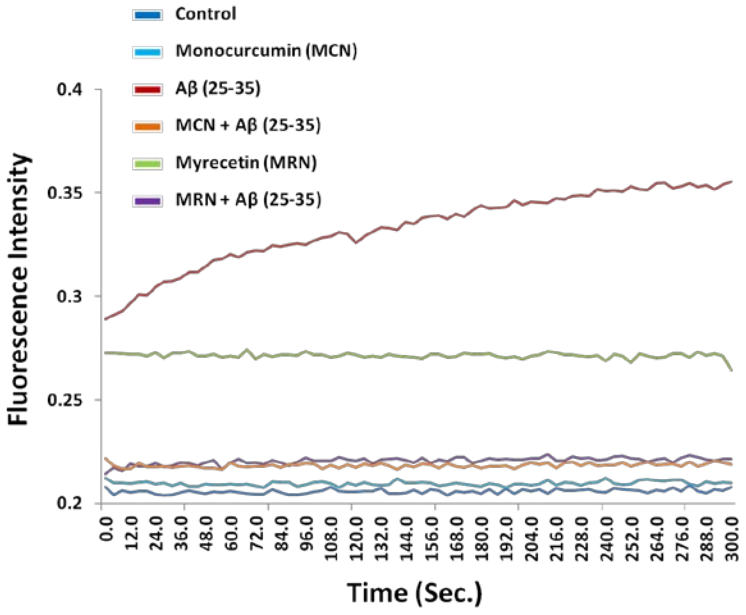

Fig. 5.5. Thioflavin T (ThT) fluorophore based spectroflurometric assay showed different fluroscence profile of treated or untreated Aβ (25-35). X-axis represents time in seconds and Y-axis depicts the fluorescent intensity.

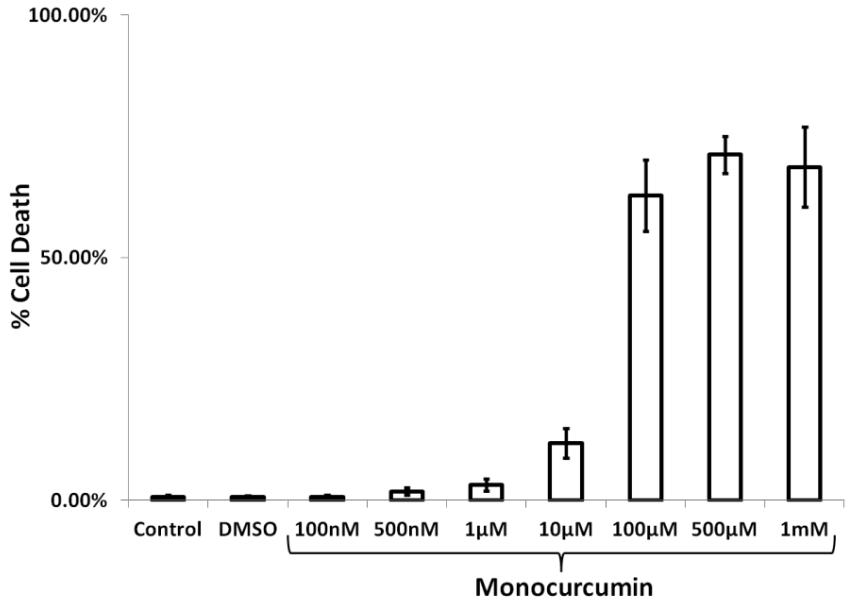

Fig. 5.6. Cytoxicity of monocurumin on SHSY-5Y cell. Different concentration of monocurcumin was used as treatment for 24 h on SHSY-5Y cell. Highthroughput screening was employed using propidium iodide a necrotic cell marker where as Hoechst used as total cell count.

Reference

Chapter 1

1. Federal Interagency Forum on Aging Related Statistics: Older Americans 2012: Key Indicators of Well-Being. http://www.agingstats.gov/Main_Site/Data/2012_Documents/docs/EntireChartbook.pdf.
2. Plassman, B. L. *et al.* Prevalence of dementia in the United States: the aging, demographics, and memory study. Neuroepidemiology 29, 125–32 (2007).
3. Hebert, L. E., Scherr, P. A., Bienias, J. L., Bennett, D. A. & Evans, D. A. Alzheimer Disease in the US Population. 60, 1–4 (2003).
4. Alzheimer's Association. Early-Onset Dementia: A National Challenge, A Future Crisis. Washington, D.C.: Alzheimer's Association, 2006.
5. Thomas, B. & Beal, M. F. Parkinson's disease. Human molecular genetics 16 Spec No, R183–94 (2007).
6. Davis, K. L. & Samuels, S. C. in Pharmacological Management of Neurological and Psychiatric Disorders (eds Enna, S. J. & Coyle, J. T.) 267–316 (McGraw-Hill, New York, 1998).
7. Dipiro J, Talbert RL, Yee GC, Matzke GR, Wells BG. Alzheimer's disease. In: Jennifer Dea, ed. Pharmacotherapy: A Pathophysiology Approach. New York, NY: McGraw-Hill; 2005.
8. Raffi MS, Aisen PS. Recent development in Alzheimer's disease therapeutics. BMC Med. 7(7), 1741 (2009).

9. Minati L, Edginton T, Bruzzone MG, Giaccone G. Current concepts in Alzheimer's disease: a multidisciplinary review. Am J Alzheimers Dis Other Demen. 24(2), 95-121 (2009).
10. McNabney MK, Samus QM, Lyketsos CG, et al. The spectrum of medical illness and medication use among residents of assisted living facilities in central Maryland. J Am Med Dir Assoc. 9(8), 558-564 (2008).
11. Ferrer I, Gomez-Isla T, Puig B, et al. Current advances on different kinases involved in tau phosphorylation, and implication in Alzheirmer's disease and tauopathies. Curr Alzheimer Res. 2(1), 3-18 (2005).
12. Chun W, Johnson GV. The role of tau phosphorylation and cleavage in neuronal cell death. Front Biosci. 12, 733-756 (2007).
13. Zhang L, Song L, Terracina G, et al. Biochemical characterization of the gamma-secretase activity that produces beta-amyloid peptides. Biochemistry. 40, 5049-5055 (2001).
14. Yin YI, Bassit B, Zhu L, et al. {gamma}-Secretase Substrate Concentration Modulates the Abeta42/Abeta40 Ratio: Implications For Alzheimer Disease. J Biol Chem. 282, 23639-23644 (2007).
15. Rovelet-Lecrux, A. et al. APP locus duplication causes autosomal dominant early-onset Alzheimer disease with cerebral amyloid angiopathy. Nature Genet. 38, 24–26 (2006).
16. Corder, E. H. et al. Gene dose of apolipoprotein E type 4 allele and the risk of Alzheimer's disease in late onset families. Science. 261, 921–923 (1993).
17. Michael A van Es & Leonard H van den Berg. Alzheimer's disease beyond APOE. Nature Genetics 41, 1047-1048 (2009).

18. Stockley JH, O'Neill C. The proteins BACE1 and BACE2 and beta-secretase activity in normal and Alzheimer's disease brain. Biochem Soc Trans. 35, 574-576 (2007).
19. Nathalie P, Jean-Noe¨ l O. Processing of amyloid precursor protein and amyloid peptide neurotoxicity. Curr Alzheimer Res. 5, 92-99 (2008).
20. El-Agnaf OM, Mahil DS, Patel BP, Austen BM. Oligomerization and toxicity of beta-amyloid-42 implicated in Alzheimer's disease. Biochem Biophys Res Commun. 273, 1003-1007 (2000).
21. Brion JP. The role of neurofibrillary tangles in Alzheimer disease. Acta Neurol Belg. 98, 165-174 (1998).
22. Sorrentino G, Bonavita V. Neurodegeneration and Alzheimer's disease: the lesson from tauopathies. Neurol Sci. 28, 63-71 (2007).
23. Grundke-Iqbal, I. *et al.* Abnormal phosphorylation of the microtubule-associated protein τ (tau) in Alzheimer cytoskeletal pathology. Proc. Natl Acad. Sci. USA 83, 4913–4917 (1986).
24. Kosik, K. S., Joachim, C. L. & Selkoe, D. J. Microtubule-associated protein τ (tau) is a major antigenic component of paired helical filaments in Alzheimer disease. Proc. Natl Acad. Sci. USA 83, 4044–4048 (1986).
25. Nukina, N. & Ihara, Y. One of the antigenic determinants of paired helical filaments is related to τ protein. J. Biochem. 99, 1541–1544 (1986).
26. Haass, C. & Selkoe, D. J. Soluble protein oligomers in neurodegeneration: lessons from the Alzheimer's amyloid beta-peptide. Nature reviews. Molecular cell biology 8, 101–12 (2007).

27. Reitz, C. Alzheimer's disease and the amyloid cascade hypothesis: a critical review. International journal of Alzheimer's disease 2012, 369808 (2012).

28. Forno, L.S. Neuropathology of Parkinson's disease. J. Neuropathol. Exp. Neurol., 55, 259–272 (1996).

29. Nussbaum, R.L. & Polymeropoulos, M.H. Genetics of Parkinson's disease. Hum. Mol. Genet. 6, 1687–1691 (1997).

30. Polymeropoulos, M.H. *et al*. Mutation in the α-synuclein gene identified in families with Parkinson's disease. Science 276, 2045–2047 (1997).

31. Kruger, R. et al. Ala30Pro mutation in the gene encoding α-synuclein in Parkinson's disease. Nature Genet. 18, 106–108 (1998).

32. Spillantini, M.G. et al. α-synuclein in Lewy bodies. Nature 388, 839–840 (1997).

33. Spillantini, M.G. et al. α-synuclein in filamentous inclusions of Lewy bodies from Parkinson's disease and dementia with Lewy bodies. Proc. Natl Acad. Sci. USA 95, 6469–6473 (1998).

34. Ribeiro, C. S., Carneiro, K., Ross, C. A., Menezes, J. R.&Engelender, S. J. Biol. Chem. 277, 23927–23933 (2002).

35. Kawamata, H., McLean, P. J., Sharma, N.&Hyman, B. T. J. Neurochem. 77, 929–934 (2001).

36. Neystat, M., Rzhetskaya, M., Kholodilov, N. & Burke, R. E. Neurosci. Lett. 325, 119–123 (2002).

37. Marx, F. P., Holzmann, C., Strauss, K. M., Li, L., Eberhardt, O., Gerhardt, E., Cookson, M. R., Hernandez, D., Farrer, M. J., Kachergus, J., *et al*. Hum. Mol. Genet. 12, 1223–1231 (2003).

38. Abeliovich A, Schmitz Y, Farinas I, Choi-Lundberg D, Ho WH, Castillo PE, Shinsky N, Verdugo JM, Armanini M, Ryan A, Hynes M, Phillips H, Sulzer D, Rosenthal A. Mice lacking alpha-synuclein display functional deficits in the nigrostriatal dopamine system. Neuron 25, 239–252 (2000).

39. Thomas, B. & Beal, M. F. Parkinson's disease. Human molecular genetics 16 Spec No, R183–94 (2007).

40. Polymeropoulos, M.H., Lavedan, C., Leroy, E., Ide, S.E., Dehejia, A., Dutra, A., Pike, B., Root, H., Rubenstein, J., Boyer, R. *et al*. Mutation in the alpha-synuclein gene identified in families with Parkinson's disease. Science 276, 2045–2047 (1997).

41. Kruger, R., Kuhn, W., Muller, T., Woitalla, D., Graeber, M., Kosel, S., Przuntek, H., Epplen, J.T., Schols, L. and Riess, O. Ala30Pro mutation in the gene encoding alpha-synuclein in Parkinson's disease. Nat. Genet. 18, 106–108 (1998).

42. Zarranz, J.J., Alegre, J., Gomez-Esteban, J.C., Lezcano, E., Ros, R., Ampuero, I., Vidal, L., Hoenicka, J., Rodriguez, O., Atares, B. et al. The new mutation, E46K, of alpha-synuclein causes Parkinson and Lewy body dementia. Ann. Neurol. 55, 164–173 (2004).

43. Periquet, M., Fulga, T., Myllykangas, L., Schlossmacher, M.G. and Feany, M.B. Aggregated alpha-synuclein mediates dopaminergic neurotoxicity in vivo. J. Neurosci. 27, 3338–3346 (2007).

44. Cooper, A.A., Gitler, A.D., Cashikar, A., Haynes, C.M., Hill, K.J., Bhullar, B., Liu, K., Xu, K., Strathearn, K.E., Liu, F. et al. Alpha-synuclein blocks ER-Golgi traffic and Rab1 rescues neuron loss in Parkinson's models. Science 313, 324–328 (2006).

45. Abeliovich, A., Schmitz, Y., Farinas, I., Choi-Lundberg, D., Ho, W. H., Castillo, P. E., Shinsky, N., Verdugo, J. M., Armanini, M., Ryan, A., Hynes, M., Phillips, H., Sulzer,

D., and Rosenthal, A. Mice Lacking α-Synuclein Display Functional Deficits in the Nigrostriatal Dopamine System. Neuron 25, 239–252 (2000).

46. Perez, R. G., Waymire, J. C., Lin, E., Liu, J. J., Guo, F., and Zigmond, M. J. J. A role for α-synuclein in the regulation of dopamine biosynthesis. Neurosci. 22, 3090–3099 (2002).
47. Sung, J.Y., Lee, H.J., Jeong, E.I., Oh, Y., Park, J., Kang, K.S. and Chung, K.C. alpha-Synuclein overexpression reduces gap junctional intercellular communication in dopaminergic neuroblastoma cells. Neurosci. Lett. 416, 289–293 (2007).
48. Ribeiro, C. S., Carneiro, K., Ross, C. A., Menezes, J. R., and Engelender, S. Synphilin-1 is developmentally localized to synaptic terminals, and its association with synaptic vesicles is modulated by alpha-synuclein. J. Biol. Chem. 277, 23927–23933 (2002).
49. Engelender, S., Kaminsky, Z., Guo, X., Sharp, A. H., Amaravi, R. K., Kleiderlein, J. J., Margolis, R. L., Troncoso, J. C., Lanahan, A. A., Worley, P. F., Dawson, V. L., Dawson, T. M., and Ross, C. A. Synphilin-1 associates with alpha-synuclein and promotes the formation of cytosolic inclusions. Nat. Genet. 22, 110–114 (1999).
50. Wakabayashi, K., Engelender, S., Yoshimoto, M., Tsuji, S., Ross, C. A., and Takahashi, H. Synphilin-1 is present in Lewy bodies in Parkinson's disease. Ann. Neurol. 47, 521–523 (2000).
51. Engelender, S., Kaminsky, Z., Guo, X., Sharp, A. H., Amaravi, R. K., Kleiderlein, J. J., Margolis, R. L., Troncoso, J. C., Lanahan, A. A., Worley, P. F., et al. α-Synuclein phosphorylation enhances eosinophilic cytoplasmic inclusion formation in SH-SY5Y cells. Nat. Genet. 22, 110–114 (1999).

52. Kawamata, H., McLean, P. J., Sharma, N.&Hyman, B. T. Parkin ubiquitinates the alpha-synuclein-interacting protein, synphilin-1: implications for Lewy-body formation in Parkinson disease. J. Neurochem. 77, 929–934 (2001).

53. Neystat, M., Rzhetskaya, M., Kholodilov, N. & Burke, R. E. Analysis of synphilin-1 and synuclein interactions by yeast two-hybrid β-galactosidase liquid assay. Neurosci. Lett. 325, 119–123 (2002).

54. Marx, F. P., Holzmann, C., Strauss, K. M., Li, L., Eberhardt, O., Gerhardt, E., Cookson, M. R., Hernandez, D., Farrer, M. J., Kachergus, J., *et al*. Identification and functional characterization of a novel R621C mutation in the synphilin-1 gene in Parkinson's disease. Hum. Mol. Genet. 12, 1223–1231 (2003).

55. Chung, K.K.K. et al. Parkin ubiquitinates the α- synuclein-interacting protein synphilin-1: Implications for Lewy body formation in Parkinson disease. Nature Med. 7, 1144–1150 (2001).

56. Ito, T., Niwa, J. I., Hishikawa, N., Ishigaki, S., Doyu, M., and Sobue, G. Dorfin localizes to Lewy bodies and ubiquitylates synphilin-1. J. Biol. Chem. 278(31):29106-14 (2003).

57. Ranjan P., Shrivastava P., Singh M. S., Sodhi A., Heintz H. N. Baculovirus P35 inhibits NO-induced apoptosis in activated macrophages by inhibiting cytochrome c release. J. of Cell Sci. 117, 3031-3039(2004).

58. Nakamura, T.; Lipton, S.A. Molecular mechanisms of nitrosative stress-mediated protein misfolding in neurodegenerative diseases. Cell. Mol. Life Sci. 64 (2007) 1609 – 1620

59. Chauvin, C., De Oliveira, F., Ronot, X., Mousseau, M., Leverve, X., Fontaine, E. Rotenone inhibits the mitochondrial permeability transition-induced cell death in U937 and KB cells. J. Biol. Chem. 276, 41394–41398 (2001).

60. Higuchi, M., Proske, R. J., Yeh, E. T. Altered mitochondrial function and overgeneration of reactive oxygen species precede the induction of apoptosis by 1-O-octadecyl-2-methyl-*rac*-glycero-3-phosphocholine in p53-defective hepatocytes. Oncogene 17**,** 2515–2524 (1998).

61. Shimizu, S., Eguchi, Y., Kamiike, W., Waguri, S., Uchiyama, Y., Matsuda, H., Tsujimoto, Y. Bcl-2 prevents apoptotic mitochondrial dysfunction by regulating proton flux. Oncogene 12, 2045–2050 (1996).

62. Sherer, T. B., Betarbet, R., Stout, A. K., Lund, S., Baptista, M., Panov, A. V., Cookson, M. R., Greenamyre, J. T. An in vitro model of Parkinson's disease: linking mitochondrial impairment to altered α-synuclein metabolism and oxidative damage. J. Neurosci. 22, 7006–7015 (2002).

63. Heussler, V. T., Fernandez, P. C., Botteron, C., and Dobbelaere, D. A. N-acetylcysteine blocks apoptosis induced by N-alpha-tosyl-L-phenylalanine chloromethyl ketone in transformed T-cells. Cell Death Differ. 6**,** 342–350 (1999).

64. Kelso, G. F., Porteous, C. M., Coulter, C. V., Hughes, G., Porteous, W. K., Ledgerwood, E. C., Smith, R. A., Murphy, M. P. Selective targeting of a redox-active ubiquinone to mitochondria within cells: antioxidant and antiapoptotic properties. J. Biol. Chem. 276, 4588–4596 (2001).

65. Koren, R., Hadari-Naor, I., Zuck, E., Rotem, C., Liberman, U. A., Ravid, A. Vitamin D is a prooxidant in breast cancer cells. Cancer Res. 61**,** 1439–1444 (2001).

66. Chrestensen, C. A., Starke, D. W., Mieyal, J. J. Acute cadmium exposure inactivates thioltransferase (Glutaredoxin), inhibits intracellular reduction of protein-glutathionyl-mixed disulfides, and initiates apoptosis. J. Biol. Chem. 275, 26556–26565 (2000).
67. Kroemer, G., Dallaporta, B., Resche-Rigon, M. The mitochondrial death/life regulator in apoptosis and necrosis. Annu. Rev. Physiol. 60**,** 619–642 (1998).
68. Martinou, J. C. Apoptosis. Key to the mitochondrial gate. Nature 399, 411–412 (1999).
69. Tan, S., Sagara, Y., Liu, Y., Maher, P., Schubert, D. The regulation of reactive oxygen species production during programmed cell death. J. Cell Biol. 141, 1423–1432 (1998).
70. *Fesik,* SW Insights into programmed cell death through structural biology. Cell, 103(2), 273-82 (*2000).*
71. Tewari, M., Quan, L.T., O'Rourke, K., Desnoyers, S., Zeng, Z., Beidler, D.R., Poirier, G.G., Salvesen, G.S., and Dixit, V.M. Yama/CPP-32b, a mammalian homolog of CED-3, is a CrmA-inhibitable protease that cleaves the death substrate poly(ADP-ribose) polymerase. Cell 81, 801–809 (1995).
72. Yoshida, H. ER stress and diseases. FEBS J. 274 (2007) 630-658.
73. Wilkinson, B. and Gilbert, H.F. Protein Disulfide Isomerase. Biochim. Biophys. Acta 1699 (2004) 35-44.
74. Edman, J.C.; Ellis, L.; Blacher, R.W.; Roth, R.A.; Rutter, W.J. Sequence of protein disulfide isomerase and implications of its relationship to thioredoxin. Nature 317 (1985) 267-278.
75. Appenzeller-Herzog, C.B.; Ellgard, L. The human PDI family: versatility packed into a single fold. Biochim. Biophys. Acta 1783 (2008) 535-548.

76. Hatahet, F.; Ruddock, F.W. Substrate recognition by the protein disulfide isomerases. FEBS J. 274 (2007) 5223-5234.

77. Wickner RB. [URE3] as an altered URE2 protein: Evidence for a prion analog in Saccharomyces cerevisiae. Science 264, 566–569 (1994).

78. Coustou V, Deleu C, Saupe S, Begueret J. The protein product of the het-s heterokaryon incompatibility gene of the fungus Podospora anserina behaves as a prion analog. Proc Natl Acad Sci USA. 94, 9773–9778 (1997).

79. Si K, Choi YB, White-Grindley E, Majumdar A, Kandel ER. Aplysia CPEB can form prion-like multimers in sensory neurons that contribute to long-term facilitation. Cell 140, 421–435 (2010).

80. Hou F, *et al.* MAVS forms functional prion-like aggregates to activate and propagate antiviral innate immune response. Cell 146, 448–461 (2011).

81. Aguzzi A, Polymenidou M. Mammalian prion biology: one century of evolving concepts. Cell 116, 313-27 (2004).

82. Prusiner SB. Prions. Proc Natl Acad Sci USA. 95, 13363-83 (1998).

83. Weissmann C. The state of the prion. Nat Rev Microbiol. 2, 861-71 (2004).

84. Colby DW, Prusiner SB. Prions. Cold Spring Harb Perspect Biol. 3, a006833 (2011).

85. Braak H, Braak E. Neuropathological stageing of Alzheimer-related changes. Acta Neuropathol. 82, 239–259 (1991).

86. J. Stöhr *et al*. Purified and synthetic Alzheimer's amyloid beta(Aβ) prions. Proceedings of the National Academy of Sciences. doi: 10.1073/pnas.1206555109.

87. Kopito RR. Aggresomes, inclusion bodies and protein aggregation. Trends Cell Biol. 10, 524-30 (2000).

88. Iwata A, Christianson JC, Bucci M, Ellerby LM, Nukina N, Forno LS, Kopito RR. Increased susceptibility of cytoplasmic over nuclear polyglutamine aggregates to autophagic degradation. Proc Natl Acad Sci USA. 102, 13135-40 (2005).
89. Lundmark K, Westermark GT, Nystrom S, Murphy CL, Solomon A, Westermark P. Transmissibility of systemic amyloidosis by a prion-like mechanism. Proc Natl Acad Sci USA. 99, 6979-84 (2002).
90. Kane MD, Lipinski WJ, Callahan MJ, Bian F, Durham RA, Schwarz RD, *et al*. Evidence for seeding of beta-amyloid by intracerebral infusion of Alzheimer brain extracts in beta-amyloid precursor protein-transgenic mice. J Neurosci. 20, 3606- 11 (2000).
91. Meyer-Luehmann M, Coomaraswamy J, Bolmont T, Kaeser S, Schaefer C, Kilger E, *et al.* Exogenous induction of cerebral beta-amyloidogenesis is governed by agent and host. Science 313, 1781-4 (2006).
92. Cheng AL, Hsu CH, Lin JK, Hsu MM, Ho YF, Shen TS, Ko JY, Lin JT, Lin BR, Ming-Shiang W, Yu HS, Jee SH, Chen GS, Chen TM, Chen CA, Lai MK, Pu YS, Pan MH, Wang YJ, Tsai CC, Hsieh CY. Phase I clinical trial of curcumin, a chemopreventive agent, in patients with high-risk or pre-malignant lesions. Anticancer Res. 21, 2895-900 (2001).
93. Adams BK, Cai J, Armstrong J, Herold M, Lu YJ, Sun A, Snyder JP, Liotta DC, Jones DP, Shoji M. EF24, a novel synthetic curcumin analog, induces apoptosis in cancer cells via a redox-dependent mechanism. Anticancer Drugs. 16, 263-75 (2005).
94. M. Guzman, C. Blazquez, Is there an astrocyte-neuron ketone body shuttle? Trends Endocrinol. Metab. 12, 169–173 (2001).

95. O.E. Owen, Brain metabolism during fasting. J. Clin. Invest. 46, 1589–1595 (1967).

96. Y. Izumi, K. Ishii, H. Katsuki, A.M. Benz, C.F. Zorumski, β-Hydroxybutyrate fuels synaptic function during development. Histological and physiological evidence in rat hippocampal slices, J. Clin. Invest. 101, 1121–1132 (1998).

97. Y. Kashiwaya, D-beta-hydroxybutyrate protects neurons in models of Alzheimer's and Parkinson's disease, Proc. Natl. Acad. Sci. U. S. A. 97, 5440–5444 (2000).

98. K. Sato, Y. Kashiwaya, C.A. Keon, N. Tsuchiya, M.T. King, G.K. Radda, B. Chance, K. Clarke, R.L. Veech, Insulin, ketone bodies, and mitochondrial energy transduction, FASEB J. 9, 651–658 (1995).

99. Y. Kashiwaya, M.T. King, R.L. Veech, Substrate signaling by insulin: a ketone bodies ratio mimics insulin action in heart, Am. J. Cardiol. 80, 50A–64A (1997).

100. D.H. Williamson, P. Lund, H.A. Krebs, The redox state of free nicotinamide- adenine dinucleotide in the cytoplasm and mitochondria of rat liver, Biochem. J. 103, 514–527 (1967).

101. Singh, YN. Kava an overview. J. Ethanopharmacol. 37, 18–45 (1992).

102. Song Li, Che Wang, Minwei Wang, Wei Li, Kinzo Matsumoto, Yiyuan Tang. Antidepressant like effects of piperine in chronic mild stress treated mice and its possible mechanisms. Life Sciences 80, 1373–1381 (2007).

103. Vijayakumar RS, Surya D, Nalini N. Antioxidant efficacy of black pepper (Piper nigrum L.) and piperine in rats with high fat diet induced oxidative stress. Redox Rep. 9(2), 105-110 (2004).

104. Choi BM, Kim SM, Park TK, Li G, Hong SJ, Park R, Chung HT, Kim BR. Piperine protects cisplatin-induced apoptosis via heme oxygenase-1 induction in auditory cells. J Nutr Biochem. 18(9), 615-622 (2007).
105. Badmaev, V. V. *et al*. Piperine derived from black pepper increases the plasma levels of coenzyme Q10 following oral supplementation, J. Nutr. Biochem., 11, 109–113 (2000).
106. Lambert, J. D. *et al*. Piperine enhances the bioavailability of the tea polyphenol (-)-epigallocatechin-3-gallate in mice, J. Nutr. 134, 1948–1952 (2004).
107. Velpandian, T. *et al*. Piperine in food: interference in the pharmacokinetics of phenytoin, Eur. J. Drug Metab. Pharmacokinet. 26, 241–247 (2001).
108. Shoba, G. *et al*. Influence of piperine on the pharmacokinetics of Curcumin in animals and human volunteers, Planta Med. 64, 353–356 (1998).
109. Mukhtar H, Das M, Khan WA, Wang ZY, Bik DP, Bickers DR. Exceptional activity of tannic acid among naturally occurring plant phenols in protecting against 7,12-dimethylbenz(a)anthracene-, benzo(a)pyrene-, 3-methylcholanthrene-, and N-methyl-N-nitrosourea-induced skin tumorigenesis in mice. Cancer Res. 48, 2361-2365 (1988).
110. Thresiamma KC, Kuttan R. Inhibition of liver fibrosis by ellagic acid. Indian J Physiol Pharmacol. 40, 363-366 (1996).
111. Osawa T, Ide A, Su JD, Namiki M. Inhibition of lipid peroxidation by ellagic acid. J. Agric. Food Chem. 35, 808-812 (1987).
112. Stoner GD, Gupta A. Etiology and chemoprevention of esophageal squamous cell carcinoma. Carcinogenesis. 22, 1737-1746 (2001).

113. Feldman KS, Saharabudhe K, Smith RS, Scheuchenzuber WJ. Immune-stimulation by Plant polyphenols: Relationship between tumor necrosis factor- production and tannin structure. Bioorganic Med. Chem. Lett. 9(7), 985-990 (1999).
114. Ruibal BIJ, Marta-Dubed EM, Martínez FL, Noa RE, Vargas GLM, Santana RJL. Inhibition of HIV replication by tannin extracts from Pinus Caribaea Morelet. Rev. Cubana Farm. 37(2), 2-9 (2003).
115. Kratochwil, N.A.; Huber, W.; Muller, F.; Kansy, M.; Gerber, P.R. Chemogenomics in drug discovery: a medicinal chemistry perspective. Biochem. Pharmacol. 64, 1355–1374 (2002).
116. Mandeville, J.S.; Froehlich, E.; Tajmir-Riahi, H.A. Study of curcumin and genistein interactions with human serum albumin. J. of Pharmaceutical and Biomed. Anal. 49 468–474 (2009).
117. Carter, D.C.; Ho, J.X. Structure of serum albumin. Adv. Protein Chem. 45 153–203 (1994).

Chapter 2

1. K. Imamura, T. Takeshima, Y. Kashiwaya, K. Nakaso, K. Nakashima, D-b hydroxybutyrate protects dopaminergic SH-SY5Y cells in a rotenone model of Parkinson's disease, J. Neurosci. Res. 84 (2006) 1376–1384.
2. S. Tan, Y. Sagara, Y. Liu, P. Maher, D. Schubert, The regulation of reactive oxygen species production during programmed cell death, J. Cell Biol. 141 421 (1998) 1423–1432.

3. R. Pal, M. Miranda, M. Narayan, Nitrosative stress-induced Parkinsonian Lewy- like aggregates prevented through polyphenolic phytochemical analog intervention, BBRC (2010) 324–329. 425
4. M.S. Satoh, T. Lindahl, Role of poly(ADP-ribose) formation in DNA repair, Nature (1992) 356–358. 427
5. Y.A. Lazebnik, Cleavage of poly(ADP-ribose) polymerase by a proteinase with properties like ICE, Nature 371 (1994) 346–347.
6. G.M. Cohen, Caspases: the executioners of apoptosis, Biochem. J. 326 (1997) 1– 43016.
7. G. Kroemer, B. Dallaporta, M. Resche-Rigon, The mitochondrial death/life regulator in apoptosis and necrosis, Annu. Rev. Physiol. 60 (1998) 619–642.
8. J.C. Martinou, Apoptosis. Key to the mitochondrial gate, Nature 399 (1999) 411–412.
9. S.W. Fesik, Insights into programmed cell death through structural biology, Cell 103 (2000) 273–282.
10. D.W. Nicholson, Identification and inhibition of the ICE/CED-3 protease necessary for mammalian apoptosis, Nature 376 (1995) 37–43.
11. F.J. Oliver, Importance of poly (ADP-ribose) polymerase and its cleavage in apoptosis. Lesson from an uncleavable mutant, J. Biol. Chem. 273 (1998) 33533–33539.
12. T. Uehara, T. Nakamura, D. Yao, Z.Q. Shi, Z. Gu, Y. Ma, E. Masliah, Y. Nomura, S.A. Lipton, S-Nitrosylated protein-disulphide isomerase links protein misfolding to neurodegeneration, Nature 441 (2006) 513–517.
13. M. Guzman, C. Blazquez, Is there an astrocyte-neuron ketone body shuttle?, Trends Endocrinol Metab. 12 (2001) 169–173.
14. O.E. Owen, Brain metabolism during fasting, J. Clin. Invest. 46 (1967) 1589– 448 1595.

15. Y. Izumi, K. Ishii, H. Katsuki, A.M. Benz, C.F. Zorumski, B-hydroxybutyrate fuels synaptic function during development. Histological and physiological evidence in rat hippocampal slices, J. Clin. Invest. 101 (1998) 1121–1132.
16. Y. Kashiwaya, D-beta-hydroxybutyrate protects neurons in models of Alzheimer's and Parkinson's disease, Proc. Nat. Acad. Sci. USA 97 (2000) 5440–5444.
17. K. Sato, Y. Kashiwaya, C.A. Keon, N. Tsuchiya, M.T. King, G.K. Radda, B. Chance, K. Clarke, R.L. Veech, Insulin, ketone bodies, and mitochondrial energy transduction, FASEB J. 9 (1995) 651–658.
18. Y. Kashiwaya, M.T. King, R.L. Veech, Substrate signaling by insulin: a ketone bodies ratio mimics insulin action in heart, Am. J. Cardiol. 80 (1997) 50A–64A.
19. D.H. Williamson, P. Lund, H.A. Krebs, The redox state of free nicotinamide-adenine dinucleotide in the cytoplasm and mitochondria of rat liver, Biochem. J. 103 (1967) 514–527.
20. C. Lema, A. Varela-Ramirez, R.J. Aguilera, Differential nuclear staining assay for high-throughput screening to identify cytotoxic compounds, Curr. Cell. Biochem. 1 (1) (2011) 1–14.
21. A. Varela-Ramirez, M. Costanzo, Y.P. Carrasco, K.H. Pannell, R. Aguilera, Cytotoxic effects of two organotin compounds and their mode of inflicting cell death on four mammalian cancer cells, Cell Biol. Toxicol. 27 (3) (2011) 469 159–168.
22. N. Li, K. Ragheb, G. Lawler, J. Sturgis, B. Rajwa, J.A. Melendez, J.P. Robinson, Mitochondrial complex I inhibitor rotenone induces apoptosis through enhancing mitochondrial reactive oxygen species production, J. Biol. Chem. 278 (2003) 8516–8525.

Chapter 3

1. Findley, L. J. (2007) The economic impact of Parkinson's disease. Parkinsonism & Relat. Disord. 13, Supplement, S8-S12.
2. Meek, P. D., McKeithan, E. K., Schumock, G. T. (1998) Economic Considerations in Alzheimer's Disease. Pharmacotherapy: The Journal of Human Pharmacology and Drug Therapy 18, 68-73.
3. Moretto, A., Colosio, C. (2013) The role of pesticide exposure in the genesis of Parkinson's disease: Epidemiological studies and experimental data. Toxicology 307, 24-34.
4. Pezzoli, G., Cereda E. (2013) Exposure to pesticides or solvents and risk of Parkinson disease. Neurology 80, 2035-2041.
5. Gilbert H. F. (1998) Protein disulfide isomerase. Methods Enzymol. 290, 26-50.
6. Narayan, M. (2012) Disulfide bonds: protein folding and subcellular protein trafficking. FEBS J. 279, 2272-2282.
7. Benham, A. M. (2012) The Protein Disulfide Isomerase (PDI) family: key players in health and disease. Antioxid. Redox Signal 16, 781-789.
8. Benhar, M., Forrester, M. T., Stamler, J. S. (2006) Nitrosative stress in the ER: a new role for S-nitrosylation in neurodegenerative diseases. ACS Chem. Biol. 1(6), 355-358.
9. Nakamura, T., Lipton, S. A. (2011) S-nitrosylation of critical protein thiols mediates protein misfolding and mitochondrial dysfunction in neurodegenerative diseases. Antioxid. Redox Signal 14, 1479-1492.

10. Uehara, T., Nakamura, T., Yao, D., Shi, Z. Q., Gu, Z., Ma, Y., Masliah, E., Nomura, Y., Lipton, S. A. (2006) S-nitrosylated protein-disulphide isomerase links protein misfolding to neurodegeneration. Nature 441, 513-517.
11. Uehara, T. (2007) Accumulation of misfolded protein through nitrosative stress linked to neurodegenerative disorders. Antioxid. Redox Signal. 9, 597-601.
12. Kieburtz, K. (2010) Discovering neuroprotection in Parkinson's disease, or getting to haphazard. Mt. Sinai J. Med. 77, 700-6.
13. Narayan, M. (2011) Factors impacting fold maturation of ER-processed proteins: The case of oxidative folding of ribonuclease A. In Folding of disulfide proteins (Chang, Rowen J. Y., Ventura, S.) Protein Reviews (Atassi, M. Z.), Vol. 14, pp 23-42, Springer.
14. Baba, M., Nakajo, S., Tu, P. H., Tomita, T., Nakaya, K., Lee, V. M., Trojanowski, J. Q., Iwatsubo, T. (1998) Aggregation of alpha-synuclein in lewy bodies of sporadic Parkinson’s disease and dementia with Lewy bodies. Am. J. Pathol. 152, 879-884.
15. Kawamata, H., McLean, P. J., Sharma, N., Hyman, B. T. (2001) Interaction of alpha-synuclein and synphilin-1: effect of Parkinson's disease-associated mutations. J. Neurochem. 77, 929-934.
16. Neystat, M., Rzhetskaya, M., Kholodilov, N., Burke, R. E. (2002) Analysis of synphilin-1 and synuclein interactions by yeast two-hybrid beta-galactosidase liquid assay. Neurosci. Lett. 325, 119-123
17. Spillantini, M. G., Schmidt, M. L., Lee, V. M., Trojanowski, J. Q., Jakes, R., Goedert, M. (1997) Alpha-synuclein in Lewy bodies. Nature 388, 839-840.
18. Hess, D. T., Matsumoto, A., Kim, S-O., Marshall, H. E., Stamler, J. S. (2005) Protein S-nitrosylation: purview and parameters. Nat. Rev. Mol. Cell Biol. 6, 150-166.

19. Mattson, M.P. (2006) Nitro-PDI incites toxic waste accumulation. Nat. Neurosci. 9, 865-867.
20. Walker, A. K. & Atkin, J. D. (2011) Mechanisms of neuroprotection by protein disulphide isomerase in amyotrophic lateral sclerosis. Neurology Res. Int. Published online Apr 11, 2011. DOI: 10.1155/2011/317340.
21. Walker, A. K., Farg, M. A., Bye, C. R., McLean, C. A., Horne, M. K., Atkin, J. D. (2010) Protein disulphide isomerase protects against protein aggregation and is S-nitrosylated in amyotrophic lateral sclerosis. Brain. 133, 105-116.
22. Haldar, S. M. & Stamler, J. S. (2011) S-Nitrosylation at the interface of autophagy and disease. Mol. Cell 43, 1-3.
23. Uys, J. D., Xiong, Y., Townsend, D. M. (2011) Nitrosative stress-induced S-glutathionylation of protein disulfide isomerase. Methods Enzymol. 490, 321-332.
24. Osawa, T., Ide, A., Su, J. D., Namiki, M. (1987) Inhibition of lipid peroxidation by ellagic acid. J. Agric. Food Chem. 35, 808-812.
25. Thresiamma, K. C., Kuttan, R. (1996) Inhibition of liver fibrosis by ellagic acid. Indian J. Physiol. Pharmacol. 40, 363-366.
26. Abou-Zied, O., Al-Shihi, O. (2008) Characterization of Subdomain IIA Binding Site of Human Serum Albumin in its Native, Unfolded, and Refolded States Using Small Molecular Probes. J. Am. Chem. Soc. 130, 10793-10801.
27. Dockal, M., Carter, D. C., Rüker, F. (1999) The Three Recombinant Domains of Human Serum Albumin: Structural Characterization and Ligand Binding Properties. J. Biol. Chem. 274, 29303-29310.

28. Borges, G., Roowi, S., Rouanet, J-M., Duthie, G. G., Lean, M. E. J., Crozier, A. (2007) The bioavailability of raspberry anthocyanins and ellagitannins in rats. Mol. Nutr. Food Res. 51, 714-725.

29. Pacher, P., Beckman, J. S., Liaudet, L. (2007) Nitric oxide and peroxynitrite in health and disease. Physiol. Rev. 87, 315-424.

30. Cimino, F., Anderson, W. B., Stadtman, E. R. (1970) Ability of Nonenzymic Nitration or Acetylation of E. coli Glutamine Synthetase to Produce Effects Analogous to Enzymic Adenylylation. Proc Natl Acad Sci USA. 66, 564–571.

31. Radi, R., Beckman, J. S., Bush, K. M., Freeman, B. A. (1991) Peroxynitrite oxidation of sulfhydryls. The cytotoxic potential of superoxide and nitric oxide. J. Biol. Chem. 266, 4244-4250.

32. Barbara, S. B., Rodney, L. L., Earl, R. S. (1998) Carbon dioxide stimulates peroxynitrite-mediated nitration of tyrosine residues and inhibits oxidation of methionine residues of glutamine synthetase: Both modifications mimic effects of adenylylation. Proc Natl Acad Sci USA. 95, 62784-2789.

33. Aranda, A., Sequedo, L., Tolosa, L., Quintas, G., Burello, E., Castell, J. V., Gombau, L. (2013) Dichloro-dihydro-fluorescein diacetate (DCFH-DA) assay: A quantitative method for oxidative stress assessment of nanoparticle-treated cells. Toxicology in Vitro 27(2), 954-963.

34. Eruslanov, E., Kusmartsev, S. (2010) Identification of ROS Using Oxidized DCFDA and Flow-Cytometry. Methods Mol. Biol. 594, 57-72.

35. Kojima, H., Urano, Y., Kilkuchi, K., Higuchi, K., Hirata, Y., Nagano, T. (1999) Fluorescent Indicators for Imaging Nitric Oxide Production. Angew. Chem. Int. Ed. Engl. 38(21), 3209-3212.
36. Tanner, C. M., Kamel, F., Ross, G. W., Hoppin, J. A., Goldman, S. M., Korell, M., Marras, C., Bhudhikanok, G. S., Kasten, M., Chade, A. R., Comyns, K., Richards, M. B., Meng, C., Priestley, B., Fernandez, H. H., Cambi, F., Umbach, D. M., Blair, A., Sandler, D. P., Langston, J. W. (2011) Rotenone, paraquat, and Parkinson's disease. Environ. Health Perspect. 119(6), 866-872.
37. Burkart, V., Wang, Z-Q., Radons, J., Heller, B., Herceg, Z., Stingl, L., Wagner, E. F., Kolb, H. (1999) Mice lacking the poly(ADP-ribose) polymerase gene are resistant to pancreatic beta-cell destruction and diabetes development induced by streptozocin. Nat. Med. 5, 314-319.
38. Oliver, F. J., de la Rubia, G., Rolli, V., Ruiz-Ruiz, M. C., Murcia, G., Murcia, J. M. (1998) Importance of poly(ADP-ribose) polymerase and its cleavage in apoptosis. Lesson From An Uncleavable Mutant. J. Biol. Chem. 273, 33533-33539.
39. Ryu, E. J., Harding, H. P., Angelastro, J. M., Vitolo, O. V., Ron, D., Greene, L. A. (2002) Endoplasmic Reticulum Stress and the Unfolded Protein Response in Cellular Models of Parkinson’s Disease. J. Neurosci. 22(24), 10690-10698.
40. Gruber, C. W., Čemažar, M., Heras, B., Martin, J. L., Craik, D. J. (2006) Protein disulfide isomerase: the structure of oxidative folding. Trends Biochem. Sci. 31(8), 455-464.
41. Glickman, M. H., Ciechanover, A. (2002) The ubiquitin-proteasome proteolytic pathway: destruction for the sake of construction. Physiol. Rev. 82(2), 373-428.

42. Adams, P. A., Berman, M. C. (1980) Kinetics and mechanism of the interaction between human serum albumin and monomeric haemin. Biochem. J. 192(1), 95-102.
43. Lakowicz, J. R. (1999) In Principles of Fluorescence Spectroscopy (Kluwer/Plenum), 2nd ed., New York.
44. Mandeville, J., Froehlich, E., Tajmir-Riahi, H. A. (2009) Study of curcumin and genistein interactions with human serum albumin. J. Pharm. Biomed. Anal. 49, 468-474.
45. N'soukpoé-Kossi, C. N., Sedaghat-Herati, R., Ragi, C., Hotchandani, S., Tajmir-Riahi, H. A. (2007) Retinol and retinoic acid bind human serum albumin: Stability and structural features. Int. J. Biol. Macromol. 40, 484-490.
46. Kabiraj, P., Pal, R., Varela, R. A., Miranda, M., Narayan, M. (2012) Nitrosative stress mediated misfolded protein aggregation mitigated by Na-D-β-hydroxybutyrate intervention. Biochem. Biophys. Res. Commun. 426(3): 438-44.
47. Wu, M., Katta, A., Gadde, M. K., Liu, H., Kakarla, S.K., Fannin, J., Paturi, S., Arvapalli, R. K., Rice, K. M., Wang, Y., Blough E. R. (2009) Aging-associated dysfunction of Akt/protein kinase B: S-nitrosylation and acetaminophen intervention. PLoS One 4(7): e6430.

Chapter 4

1. Plassman, B. L. *et al.* Prevalence of dementia in the United States: the aging, demographics, and memory study. Neuroepidemiology 29, 125–32 (2007).
2. Hebert, L. E., Scherr, P. A., Bienias, J. L., Bennett, D. A. & Evans, D. A. Alzheimer Disease in the US Population. 60, 1–4 (2003).
3. Alzheimer’s Association. Early-Onset Dementia: A National Challenge, A Future Crisis. Washington, D.C.: Alzheimer’s Association, 2006.

4. Davis, K. L. & Samuels, S. C. in Pharmacological Management of Neurological and Psychiatric Disorders (eds Enna, S. J. & Coyle, J. T.) 267–316 (McGraw-Hill, New York, 1998).
5. Ferrer I, Gomez-Isla T, Puig B, et al. Current advances on different kinases involved in tau phosphorylation, and implication in Alzheirmer's disease and tauopathies. Curr Alzheimer Res. 2(1), 3-18 (2005).
6. Chun W, Johnson GV. The role of tau phosphorylation and cleavage in neuronal cell death. Front Biosci. 12, 733-756 (2007).
7. Stockley JH, O'Neill C. The proteins BACE1 and BACE2 and beta-secretase activity in normal and Alzheimer's disease brain. Biochem Soc Trans. 35, 574-576 (2007).
8. Grundke-Iqbal, I. *et al.* Abnormal phosphorylation of the microtubule-associated protein τ (tau) in Alzheimer cytoskeletal pathology. Proc. Natl Acad. Sci. USA 83, 4913–4917 (1986).
9. Nathalie P, Jean-Noe O. Processing of amyloid precursor protein and amyloid peptide neurotoxicity. Curr Alzheimer Res. 5, 92-99 (2008).
10. Burdick, D., B. Soreghan, M. Kwon, J. Kosmoski, M. Knauer, A. Henschen, J. Yates, C. Cotman, and C. Glabe. 1992. Assembly and aggregation properties of synthetic Alzheimer's A4/b amyloid peptide analogs. J. Biol. Chem. 267:546–554.
11. Pike, C. J., A. J. Walencewicz-Wasserman, J. Kosmoski, D. H. Cribbs, C. G. Glabe, and C. W. Cotman. 1995. Structure-activity analyses of b-amyloid peptides: contributions of the b 25–35 region to aggregation and neurotoxicity. J. Neurochem. 64:253–265.

12. Halverson, K., P. E. Fraser, D. A. Kirschner, and P. T. Lansbury Jr. 1990. Molecular determinants of amyloid deposition in Alzheimer's disease: conformational studies of synthetic b-protein fragments. Biochemistry. 29:2639–2644.
13. J. Stöhr *et al*. Purified and synthetic Alzheimer's amyloid beta(Aβ) prions. Proceedings of the National Academy of Sciences. doi: 10.1073/pnas.1206555109.
14. Aguzzi A, Polymenidou M. Mammalian prion biology: one century of evolving concepts. Cell 116, 313-27 (2004).
15. Lundmark K, Westermark GT, Nystrom S, Murphy CL, Solomon A, Westermark P. Transmissibility of systemic amyloidosis by a prion-like mechanism. Proc Natl Acad Sci USA. 99, 6979-84 (2002).
16. Kane MD, Lipinski WJ, Callahan MJ, Bian F, Durham RA, Schwarz RD, *et al*. Evidence for seeding of beta-amyloid by intracerebral infusion of Alzheimer brain extracts in beta-amyloid precursor protein-transgenic mice. J Neurosci. 20, 3606- 11 (2000).
17. Meyer-Luehmann M, Coomaraswamy J, Bolmont T, Kaeser S, Schaefer C, Kilger E, *et al.* Exogenous induction of cerebral beta-amyloidogenesis is governed by agent and host. Science 313, 1781-4 (2006).
18. Glickman, M. H., Ciechanover, A. (2002) The ubiquitin-proteasome proteolytic pathway: destruction for the sake of construction. Physiol. Rev. 82(2), 373-428.
19. P. Kabiraj, J. Marin, A. Varela-Ramirez, E. Zubia, M. Narayan, Ellagic acid mitigates SNO-PDI induced aggregation of Parkinsonian biomarkers. ACS Chemical Neuroscience (2014). DOI: 10.1021/cn500214k
20. Kopito RR. Aggresomes, inclusion bodies and protein aggregation. Trends Cell Biol. 10, 524-30 (2000).

21. Baba, M., Nakajo, S., Tu, P. H., Tomita, T., Nakaya, K., Lee, V. M., Trojanowski, J. Q., Iwatsubo, T. (1998) Aggregation of alpha-synuclein in lewy bodies of sporadic Parkinson's disease and dementia with Lewy bodies. Am. J. Pathol. 152, 879-884.
22. McKeith IG, Dickson DW, Lowe J, Emre M, O'Brien JT, Feldman H, Cummings J, Duda JE, Lippa C, Perry EK, Aarsland D, Arai H, Ballard CG, Boeve B, Burn DJ, Costa D, Del Ser T, Dubois B, Galasko D, Gauthier S, Goetz CG, Gomez-Tortosa E, Halliday G, Hansen LA, Hardy J, Iwatsubo T, Kalaria RN, Kaufer D, Kenny RA, Korczyn A, et al.: Diagnosis and management of dementia with Lewy bodies: third report of the DLB Consortium. Neurology 2005, 65:1863-1872.
23. Lippa CF, Duda JE, Grossman M, Hurtig HI, Aarsland D, Boeve BF, Brooks DJ, Dickson DW, Dubois B, Emre M, Fahn S, Farmer JM, Galasko D, Galvin JE, Goetz CG, Growdon JH, Gwinn-Hardy KA, Hardy J, Heutink P, Iwatsubo T, Kosaka K, Lee VM, Leverenz JB, Masliah E, McKeith IG, Nussbaum RL, Olanow CW, Ravina BM, Singleton AB, Tanner CM, et al.: DLB and PDD boundary issues: diagnosis, treatment, molecular pathology, and biomarkers. Neurology 2007, 68:812-819.
24. Hamilton RL: Lewy bodies in Alzheimer's disease: a neuropathological review of 145 cases using alpha-synuclein immunohistochemistry. Brain Pathol 2000, 10:378-384.
25. P. Kabiraj, R. Pal, A.V. Ramirez, M. Miranda, M. Narayan, Nitrosative stress mediated misfolded protein aggregation mitigated by Na-D-β-hydroxybutyrate intervention, BBRC. 426, 438-444 (2012).
26. Hensley, K., Carney, J.M., Mattson, M.P., Aksenova, M., Harris, M., Wu, J.F., Floyd, R.A., Butterfield, D.A., 1994. A model for beta-amyloid aggregation and neurotoxicity

based on free radical generation by the peptide: relevance to Alzheimer disease. Proc. Natl. Acad. Sci. U. S. A. 91, 3270–3274.

27. Conn KJ1, Gao W, McKee A, Lan MS, Ullman MD, Eisenhauer PB, Fine RE, Wells JM.. Identification of the protein disulfide isomerase family member PDIp in experimental Parkinson's disease and Lewy body pathology. Brain Res. 1022(1-2):164-72 (2004).
28. Honjo Y, Ito H, Horibe T, Takahashi R, Kawakami K. Protein disulfide isomerase immunopositive inclusions in patients with Alzheimer disease. Brain Res; 1349:90–96 (2010)
29. Lee SJ, Lim HS, Masliah E, Lee HJ: Protein aggregate spreading in neurodegenerative diseases: problems and perspectives. Neurosci Res, 70:339-348 (2011).
30. P Bernardoni, B Fazi, A Costanzi, R Nardacci, C Montagna, G Filomeni, MR Ciriolo, M Piacentini and F Di Sano, Reticulon1-C modulates protein disulphide isomerase function Cell Death and Disease (2013) 4, e581; doi:10.1038/cddis.2013.113
31. Kelly J. Conna,b, Wenwu Gaoa,c,1, Ann McKeea,d, Michael S. Lane, M. David Ullmana,f, Patricia B. Eisenhauera, Richard E. Finea, John M. Wells, Identification of the protein disulfide isomerase family member PDIp in experimental Parkinson’s disease and Lewy body pathology. Brain Research 1022 (2004) 164–172
32. Han Cheng & Lei Wang & Chih-chen Wang, Domain a’ of protein disulfide isomerase plays key role in inhibiting α-synuclein fibril formation. Cell Stress and Chaperones (2010) 15:415–421
33. Wang S-B, Shi Q, Xu Y, Xie W-L, Zhang J, et al. (2012) Protein Disulfide Isomerase Regulates Endoplasmic Reticulum Stress and the Apoptotic Process during Prion

Infection and PrP Mutant-Induced Cytotoxicity. PLoS ONE 7(6): e38221. doi:10.1371/journal.pone.0038221

34. Xu L-R, Liu X-L, Chen J, Liang Y (2013) Protein Disulfide Isomerase Interacts with Tau Protein and Inhibits Its Fibrillization. PLoS ONE 8(10): e76657. doi:10.1371/journal.pone.0076657
35. Sridhar Varadarajan, Jaroslaw Kanski, Marina Aksenova, Christopher Lauderback, and D. Allan Butterfield, Different Mechanisms of Oxidative Stress and Neurotoxicity for Alzheimer¢s Aβ (1-42) and Aβ (25-35). J. Am. Chem. Soc. 2001, 123, 5625-5631.
36. A.M. Swomley, Sarah Förster, Jierel T. Keeney, Judy Triplett, Zhaoshu Zhang, Rukhsana Sultana, D. Allan Butterfield., Abeta, oxidative stress in Alzheimer disease: Evidence based on proteomics studies, Biochim. Biophys. Acta (2013), http://dx.doi.org/10.1016/j.bbadis.2013.09.015
37. Mark S. Sherman*, C. Ian Ragan, and Leslie L. Iversen, Inhibition of PC12 cell redox activity is a specific, early indicator of the mechanism of 1-amyloid-mediated cell death Proc. Natl. Acad. Sci. USA, Vol. 91, pp. 1470-1474, February 1994.
38. R. G. Perez,J. C. Waymire, E. Lin, J. J. Liu, F. Guo, M. J. Zigmond, A Role for α-Synuclein in the Regulation of Dopamine Biosynthesis. The Journal of Neuroscience, April 15, 2002, 22(8):3090–3099.
39. Uehara, T., Nakamura, T., Yao, D., Shi, Z. Q., Gu, Z., Ma, Y., Masliah, E., Nomura, Y., Lipton, S. A. (2006) S-nitrosylated protein-disulphide isomerase links protein misfolding to neurodegeneration. Nature 441, 513-517.
40. Giasson BI1, Lee VM, Trojanowski JQ. Interactions of amyloidogenic proteins. Neuromolecular Med. (2003); 4(1-2):49-58.

41. Shults CW. Lewy bodies. Proc. Natl. Acad. Sci. USA. (2006); 103:1661–1668.
42. Jaskolski F, Mulle C, Manzoni OJ. An automated method to quantify and visualize colocalized fluorescent signals. J Neurosci Methods. 2005;146:42–49.
43. Wenxia Li, Yifen Tang, Zhiqin Fan, Ya Meng, Guang Yang, Jia Luo, Zun-Ji Ke1, Autophagy is involved in oligodendroglial precursor-mediated clearance of amyloid peptide Molecular Neurodegeneration (2013), 8:27
44. Abosch A1, Kapur S, Lang AE, Hussey D, Sime E, Miyasaki J, Houle S, Lozano AM. Stimulation of the subthalamic nucleus in Parkinson's disease does not produce striatal dopamine release. Neurosurgery. (2003);53(5):1095-102.

Chapter 5

1. Jordi Bové, Delphine Prou, Céline Perier, and Serge Przedborski, Toxin-Induced Models of Parkinson's Disease, NeuroRx. 2(3): 484–494(2005); Lee SJ, Lim HS, Masliah E, Lee HJ: Protein aggregate spreading in neurodegenerative diseases: problems and perspectives. Neurosci Res 2011, 70:339-348.
2. McKeith IG, Dickson DW, Lowe J, Emre M, O'Brien JT, Feldman H, Cummings J, Duda JE, Lippa C, Perry EK, Aarsland D, Arai H, Ballard CG, Boeve B, Burn DJ, Costa D, Del Ser T, Dubois B, Galasko D, Gauthier S, Goetz CG, Gomez-Tortosa E, Halliday G, Hansen LA, Hardy J, Iwatsubo T, Kalaria RN, Kaufer D, Kenny RA, Korczyn A, et al.: Diagnosis and management of dementia with Lewy bodies: third report of the DLB Consortium. Neurology 2005, 65:1863-1872.
3. Lippa CF, Duda JE, Grossman M, Hurtig HI, Aarsland D, Boeve BF, Brooks DJ, Dickson DW, Dubois B, Emre M, Fahn S, Farmer JM, Galasko D, Galvin JE, Goetz CG, Growdon JH, Gwinn-Hardy KA, Hardy J, Heutink P, Iwatsubo T, Kosaka K, Lee VM,

Leverenz JB, Masliah E, McKeith IG, Nussbaum RL, Olanow CW, Ravina BM, Singleton AB, Tanner CM, et al.: DLB and PDD boundary issues: diagnosis, treatment, molecular pathology, and biomarkers. Neurology 2007, 68:812-819.

4. Hamilton RL: Lewy bodies in Alzheimer's disease: a neuropathological review of 145 cases using alpha-synuclein immunohistochemistry. Brain Pathol 2000, 10:378-384

Vitae

Parijat Kabiraj earned his Bachelor of degree in Veterinary Medicine (DVM) from West Bengal University of Animal and Fishery Science, India in 2006. He received his Master of Science degree in Veterinary Public Health in 2009 from the West Bengal University of Animal and Fishery Science, India. In 2010 he joined the doctoral program in Chemistry.While pursuing his degree, Dr. Kabiraj worked as a research associate and teaching assistant for the department of Chemistry. Dr. Kabiraj has presented his research at many conferences and workshops such as; at Gordon Research Conference, ACS national meeting, University of California San Diego, Sanford-Burnham Medical Research Institute in 2014. Dr. Kabiraj has been the recipient of numerous honors and awards such as the Dodson Travel Grant from College of Science, Student Travel Grant from Graduate School of University of Texas at El Paso. He was also a recipient of poster award at Gordon Research Conference, New London, NH. Dr. Kabiraj's dissertation entitled, "Mechanisms to mitigate neurodegeneration by maintaining mitochondrial health," was supervised by Dr. Mahesh Narayan. He has done excellent collaborative research with the faculties of Department of Biological Sciences and Department of Psychology. Dr. Kabiraj's research led 3 research articles published and many are submitted and under-preparation till date. He is also passionate about travelling, sketching and his lucky number is three. After finishing his Doctoral study, Dr. Kabiraj is going to pursue his postdoctoral experiences at Yale School of Medicine.

Education

Doctor of Philosophy (PhD) in Chemistry ……..... December, 2014(GPA- 3.91/4.00)

The University of Texas at El Paso, El Paso, Texas

Master's (MS) in Vet. Public Health (M.V.Sc.).....2006-2008 (OGPA-8.25/10.00)

West Bengal University of Animal & Fishery Sciences (W.B.U.A.F.Sc), India

Bachelor of Veterinary Science and Animal Husbandry (BVSc & AH) (equivalent to DVM).....2001-2006 (OGPA-7.14/10.00)

West Bengal University of Animal & Fishery Sciences (W.B.U.A.F.Sc), India

Awards and felloships

- Poster got selected for the "*Sci-Mix*" at 248th ACS National Meeting and awarded as the most exceptional abstract in bioinorganic chemistry division held at San Francisco, CA- 10th-14th August 2014
- Selected for the "*Poster Award*" at Gordon Research Conference on "Protein Processing, Trafficking and Secretion" at New London, NH - 19th-25th July 2014
- Recipient of "*Travel Grant Funding*", Graduate School, UTEP - July 2014
- Twice the recipient of "*Dodson Travel Grant*", College of Science, UTEP - June & August 2014
- Two times recipient of "*Travel Award*", Student Government Association, UTEP- July & August 2014
- Cover page story in UTEP Prospector - 9th April, 2013 (http://www.utepprospector.com/news/kitchen-cures-1.3023695#.UWs_EMqNAg8)
- My PhD research work was highlighted by UTEP and Local News channel - 15th Feb, 2013 (http://newsuc.utep.edu/index.php/research-news/877-common-kitchen-items-may-help-protect-your-brain)
- Graduate Research Fund ($9000), UTEP - 2010, 2011, 2012 summer
- Recipient of University Merit Scholarship in the Graduate Program - (2006 – 2008)

- Recipient of University Merit Scholarship in the Under Graduate Program – (2001 – 2006)
- Recipient of National Merit Scholarship in Secondary Level Board Examination, Govt. of West Bengal, India - 1998

Publications

- **P. Kabiraj**, J. Marin, A. Varela-Ramirez, E. Zubia, M. Narayan, Ellagic acid mitigates SNO-PDI induced aggregation of Parkinsonian biomarkers. **ACS Chemical Neuroscience** (2014). **DOI:** 10.1021/cn500214k
- D. Roy, **P. Kabiraj**, R. Pal, EF24 prevents rotenone-induced estrogenic status alteration in breast cancer. **Cell Biology International**, 38: 4, 511-519 (2013).
- **P. Kabiraj**, R. Pal, A. Varela-Ramirez, M. Miranda, M. Narayan, Nitrosative stress mediated misfolded protein aggregation mitigated by Na-d-β-hydroxybutyrate intervention, **BBRC**, 426: 3, 438-444 (2012).
- **Kabiraj P**., Samanta I., Dutta T.K., Debnath C., Pramanik A.K., Characterization of bacteria with special reference to Escherichia coli isolated from ready-to-eat beef products in Kolkata, **IJCMIID**,2008, 29:1&2, 65-66 (2008).
- R. Pal*, A. Varela-Ramirez*, **P. Kabiraj***, S. Sirimulla, M. Romero, M. Miranda, M. Narayan, Prophylactic effect of EF24 against nitrosative stress induced apoptotic cell death and its binding affinity with human serum albumin. ****contributed equally***. (*Manuscript submitted*)
- **P. Kabiraj**, A. Varela-Ramirez, M. Narayan, Beta amyloid (25-35) induced Lewy body-like inclusions formation mediated by S-nitrosylation of PDI in SHSY-5Y cell line. (*Manuscript under preparation*)

- **P. Kabiraj**, D. Ramirez, L. Mendez, J. Marin, A. Varela, M. Narayan, R. Skouta, Fer-1 analogues inhibit apoptotic activation through intervention in α-synuclein aggregation. (*Manuscript under preparation*)

Abstracts/ Poster

- **Parijat Kabiraj**, Jose Marin, Armando Varela, Emmanuel Zubia, Mahesh Narayan, "Prevention of nitrosative stress mediated Lewy body formation through ellagic acid intervention in PC12 cell line". **248th ACS National Meeting**, San Francisco, CA 2014.
- **Parijat Kabiraj**, Emmanuel Zubia, Armando Varela, Mahesh Narayan, "SNO-PDI mediated accumulation of LB-like inclusions in SHSY-5Y cell as a function of Aβ(25-35) treatment". In **Gordon Research Conference**, Protein Processing, Trafficking and Secretion", New London, NH 2014.
- Skonieczki, Shane; **Kabiraj, Parijat**; Rivera-Hernández, Josué; Otaño-Vega, Myrna R.; Montes-González, Ingrid; Narayan, Mahesh, "Determination of the possible use of 1-ferrocenyl-3-(4-hydroxy-3-methoxyphenyl)prop-2-ene-1-one as a neurological antioxidant". **Summer Mentoring & Research Training: Methods in Neuroscience of Drug-Abuse**, El Paso, TX, Summer 2014.
- J. Marin, **P. Kabiraj**, M. Narayan, "Mechanism of Na-D-β-hydroxybutyrate neuroprotection and combo therapy with ellagic acid." In COURI symposium, El Paso, TX, Spring 2014.
- David A. Ramirez, **Parijat Kabiraj**, Jose Marin, Rachid Skouta, Mahesh Narayan, "Preventive treatment of Alzheimer's and Parkinson's diseases". In COURI symposium, El Paso, TX, Spring 2014.

- Jose Marin, **Parijat Kabiraj**, Juan Noveron, Mahesh Narayan, "Novel neuroprotective curcumin metallo-vessicles" in COURI symposium, El Paso, TX, Spring 2013.
- **Parijat Kabiraj**, A. Varela-Ramirez, Mahesh Narayan, “Prion-like propagation features of aggregated beta-amyloid (25-35) on synphilin-1 and α-synuclein expressed by dopaminergic cells”. Chemistry Research Day, **American Chemical Society** Local Chapter, 2013.
- G. Negron, J. Marin, **P. Kabiraj**, A. V. Ramirez, M. Narayan, “Nitrosative stress-induced neurodegenerative disorders prevented by psoralidin intervention.” **Summer Mentoring & Research Training: Methods in Neuroscience of Drug-Abuse**, El Paso, TX, Summer 2013.
- Brittany N. Talamantes, **Parijat Kabiraj** and Mahesh Narayan, "Mitigating ROS Induced Neurodegenerative Pathogenesis through Polyphenolic Phytochemicals". **Summer Mentoring & Research Training: Methods in Neuroscience of Drug-Abuse**, El Paso, TX, Summer 2012.
- **Parijat Kabiraj**, Manuel Miranda and Mahesh Narayan, “Nitrosative stress mediated misfolded protein aggregation mitigated by intrinsic metabolite”. Chemistry Research Day, **American Chemical Society** Local Chapter, 2012.
- **Parijat Kabiraj,** A.K. Pramanik, “Bluetongue Menace of Sheep Husbandry”. **17th West Bengal State Science & Technology Congress** organized by West Bengal Council of Science & Technology and WBUAFSc, Kolkata, India 2010.
- **P. Kabiraj**, C. Debnath, A.K. Pramanik, “Characterization of bacteria with special emphasis on shiga toxin producing E.coli from ready to eat beef product”. West Bengal Univ. of Animal & Fish. Sc, Kolkata, India 2008.

Permanent address: Patiram

Dakshin Dinajpur,

West Bengal,

India – 733133

This dissertation was conceptualize and written by Parijat Kabiraj.